DEPARTMENT OF PHYSICS
UNIVERSITY OF JYVÄSKYLÄ
RESEARCH REPORT No. 5/2005

ALPHA-DECAY AND DECAY-TAGGING STUDIES OF HEAVY ELEMENTS USING THE RITU SEPARATOR

BY
ARI-PEKKA LEPPÄNEN

Academic Dissertation
for the Degree of
Doctor of Philosophy

Jyväskylä, Finland
August 2005

ISBN 978-951-39-3162-9
URN:ISBN:978-951-39-3162-9

Preface

The work in this thesis has been carried out at the Department of Physics of the University of Jyväskylä during the years of 2000-2005.

I started my work at the University of Jyväskylä in August 2000. I was new to the business and the field of experimental nuclear physics presented a whole variety of challenges for me. Over the years several different parties, foreign and domestic, have contributed to my knowledge and introduced some of the secrets of experimental nuclear physics. These persons have also influenced the outcome of this thesis and I wish to thank them all for their tips and comments.

I wish to thank for all the present and former members of the RITU and Gamma groups and the professors Matti Leino and Rauno Julin. Their support and help all through these years has been essential. Especially important persons, without whom I could not have finished this thesis, deserve to be thanked. Dr. Juha Uusitalo who provided answers when needed, Dr. Pasi Kuusiniemi who was the inspiration for me to study the subjects of this thesis, Dr. Heikki Kettunen who provided invaluable help when in analyzing the experimental data and Mr. Janne Pakarinen for fruitful comments and cheerful moments in summer schools and conferences.

The financial support from the Department of Physics of the University of Jyväskylä and from the Rector of the University of Jyväskylä are gratefully acknowledged. I wish to thank the Emil Aaltonen foundation, the Magnus Ehrnrooth foundation and the Graduate School for Particle and Nuclear Physics (GRASPANP) for providing the means to attend summer schools and conferences.

Last but not least I wish to thank the persons closest to me. My wife Katja who stood by me all the time, my parents, Kaija and Risto, and my brother Toni and sister Anniina, who have encouraged and supported me for over 30 years.

Jyväskylä, May 2005

Ari-Pekka Leppänen

Abstract

The gas-filled recoil separator RITU was utilized in conjunction with different supplemental radiation detection devices to study nuclei under extreme conditions. The neutron deficient isotopes ^{218}U, ^{252}No and ^{255}Db were produced in fusion evaporation reactions. Each experiment used different experimental setups. Spectroscopic information was obtained via the detection of α and γ radiation. In the cases of ^{252}No and ^{255}Db the spontaneous fission decays of the nucleus were also observed.

The first study in this thesis addresses the issue of average charge of ions in dilute helium and also magnetic rigidities, or Bρ values of different heavy isotopes. The RITU separator separates beam from fusion products according to their magnetic rigidity. In heavy element studies, where production cross sections are low, the correct tuning of the RITU magnetic fields is essential in order to maximize the collection of the fusion recoils. The magnetic rigidity of a fusion recoil is dependent on the average charge of the ion. There are several models that predict the average charge of ions in dilute helium. These models were used to calculate theoretical magnetic rigidities which could be compared with experimental values.

In the ^{218}U experiment, the ground state properties were measured with improved statistics and a new α decaying isomer was detected. Some theoretical models predict a sub-shell closure at Z=92. These models partly rely on the single-particle shell model energies. However, these models do not take into account the octupole (L=3) correlation which is strong in the light uranium isotopes. The octupole correlation can distort the orbitals significantly. The detection of this isomer impugns the existence of the sub-shell closure at Z=92 and thus enforces the significance of the octupole correlations.

In the ^{252}No experiment a proof-of-method for recoil-fission tagging was achieved. In addition it was proved that fission originates from the same initial as the characteristic α decay. The statistics were increased by combining recoil fission and recoil α tagging data. The improved statistics revealed new weak γ-ray transitions at high spin.

The ^{255}Db experiment was the first RITU test experiment in the very heavy and extremely low cross section region. Two statistically meaningful ^{255}Db fission events were seen in the experiment. Also one chain was observed where ^{255}Db decayed via α emission into an excited state of ^{251}Lr. The ^{251}Lr decayed subsequently via fission. The ^{255}Db α decay indicates an allowed transition which according to systematics would be a decay from the ground state of ^{255}Db to an excited state in ^{251}Lr. These findings possibly mark a discovery of a new isotope.

Contents

1 Introduction

Nuclear physics studies have been going on for close to 100 years. Rutherford's discovery of a gold atom having a heavy tightly packed nucleus and an electron cloud opened up a whole new field of science. Many scientists started studying the nuclear structure and during the next 20 years a lot of progress was made. In 1929 E. Lawrence invented the cyclotron which allowed new elements and isotopes to be synthesized in nuclear reactions. The first transuranium elements synthesized in artificial nuclear fusion, neptunium and plutonium, were discovered in 1940. In 1938 O. Hahn discovered nuclear fission, new facilities and experimental methods were devised for synthesing new elements and isotopes. In the heavy element region many new isotopes were discovered.

Today 116 elements and some 3500 different isotopes of these elements are known to science. A lot of progress has been made in the study of the atomic nucleus yet it remains enigmatic and continues to surprise scientists. Many questions are still open which were asked almost 100 years ago, like *"How big can a nucleus be ?"* or *"Where are the limits of nuclear stability ?"* or *"What does a nucleus look like ?"* etc. In order to answer these questions scientists have studied the atomic nucleus extensively. Some of the results of these studies can be seen today in our daily lives in good and in bad. Many of us first think of the atomic bomb or nuclear power but one should not forget the many medical applications e.g. radiotherapy, Nuclear magnetic resonance imaging (NMRI) or Boron Neutron Capture Therapy (BNCT).

In nuclear physics the stability of the heaviest and superheavy elements has been a longstanding fundamental question. Theoretically, the mere existence of the heaviest elements with Z>102 is entirely due to quantal shell effects. Indeed, for these nuclei the shape of the classical nuclear droplet, governed by surface tension and Coulomb repulsion, is unstable to surface distortions driving these nuclei to spontaneous fission. That is, if the heaviest nuclei were governed by the classical liquid drop model, they would fission immediately from their ground states due to the large electric charge. However, in the mid-sixties, with the invention of the shell-correction method, it was realized that long-lived super-heavy elements (SHE) with very large atomic numbers could exist due to the strong shell stabilization [Mye66].

The shell model has proven to be fairly accurate when predicting the properties of many unknown nuclei. For example, the shell model predicts correctly the major shell closures or so called magic numbers. The question concerning the location of the next

major proton shell closure after Z=82 is a debate which has been going on for decades. The predictions for the next closed proton shell vary between different nuclear models. One of the important tasks which can shed light on this debate is to synthesize the heavy elements and test the validity of the shell model predictions with experimental data.

Nuclei far from stability are an important testing ground for the predictive power of nuclear models. The collected decay data establish a means of comparison with theoretical data. When searching for super-heavy elements (SHE) the island of stability beyond the magic Z=82 shell plays a crucial role. In order to understand shell stabilization in super-heavy systems one must have a clear understanding of nuclear structure. Unfortunately the super heavy elements are produced in fusion evaporation reactions at pico- or even at femtobarn level [Oga02]. This means that structure information is limited to α decay energies, branching ratios or decay half-lives. Transfermium elements with $100<Z\leq104$ are produced with much higher cross sections, in the sub-microbarn level and detailed nuclear spectroscopy can be performed even up to spins 22 $\hbar$. In recent studies new interesting information has also been obtained concerning the non-yrast states [Eec05], [Pri05].

In this thesis I will focus on three different heavy isotopes: ^{218}U, ^{252}No and ^{255}Db. All three experiments probe different parts of the nuclear chart. Each nucleus was studied for a different purpose using different experimental methods and thus different setups of detectors and target systems were needed. All of the experiments discussed in this work were made at the Accelerator Laboratory of the University of Jyväskylä. The ECR ion sources were used to produce the stable heavy ions which were accelerated with the K-130 cyclotron [Hei95]. The beams were accelerated to an energy of roughly 5 MeV/nucleon and used to bombard stable targets at the target position of the RITU recoil separator. The main instrument in these studies was the RITU gas-filled recoil separator which separated the fusion products from the unreacted beam and target-like particles. Different detectors were used to detect the radiation emitted by the fusion recoil. The detector setups used were the JUROSPHERE II γ-ray array to detect the prompt γ rays at the target position and various focal plane detector systems including the GREAT spectrometer. Different target and beam compositions were used to synthesize different isotopes. The uranium isotope was synthesized with the reaction of ^{182}W(^{40}Ar,4n)^{218}U, the nobelium isotope with the reaction of ^{206}Pb(^{48}Ca,2n)^{252}No and the dubnium isotope with the reaction of ^{209}Bi(^{48}Ti,2n)^{255}Db. All of these isotopes are relatively heavy and unstable. In these studies the α- and γ-ray spectroscopy were used to obtain nuclear structure information. The structure information was compared with theoretical predictions and conclusions of the structure of the nucleus of interest were made.

2 Physics background

2.1 The atomic nucleus

The atomic nucleus is very small compared to the size of the atom. The nucleus is only 1/10 000 of the size of the atom. The nucleus is composed of positively charged protons and neutral neutrons. The protons and neutrons are packed closely into a sphere or ellipsoidal object where protons repel each other. The force holding the nucleus together is called the strong interaction which is an attractive force. The strong interaction is a short range force with a range of only 10^{-15} m. The strong interaction is transmitted via particles called gluons.

Equation 2.1 shows that the nucleus grows in size as more protons or neutrons are added. Geometrically, the size of the nucleus follows the relation as if the protons and neutrons were billiard ball-like objects which are packed together. The nuclear radius R follows the relation

$$R = R_0 \, A^{1/3} \,, \tag{2.1}$$

where R_0 is the radius parameter and is approximately 1.4 fm for nuclear matter and roughly 1.25 fm for nuclear charge.

The most compact shape for a nucleus is spherical. The nuclei close to the closed shells are spherical, but the nuclei located between the magic numbers are deformed. There are several different shapes of nuclear deformation such as prolate, oblate, octupole and even tetrahedron. The first three shapes of the nucleus have been observed experimentally but the tetrahedron is only predicted from the theory [Dud02].

2.2 Fusion of two nuclei

The only transuranium nuclei that exist in nature are radioactive with long half-lives and nuclei arising from their subsequent radioactive decay. In order to study nuclei far from stability with half-lives of seconds or even milliseconds they have to be produced in nuclear reactions in a laboratory. The preferred method is the heavy-ion

fusion evaporation reaction where an accelerated heavy ion beam is used to bombard a heavy target. The ion and target fuse together forming a compound nucleus. The idea of compound nucleus formation was first suggested by Niels Bohr in 1936. By combining suitable target, beam and bombardment energy, a variety of new nuclei can be synthesized.

Two nuclei can be fused together by accelerating the projectile to an energy which is sufficient to overcome the Coulomb repulsion between the beam and target nuclei. This repulsion is more commonly known as the Coulomb barrier and it describes the energy which is needed in order to bring the two nuclei into contact. The height of the Coulomb barrier B_C can be described as

$$B_C = \frac{e^2}{4\pi\epsilon_0}\frac{Z_p Z_t}{R_p + R_t}\,, \tag{2.2}$$

where Z_p and Z_t are the proton numbers of the projectile and target, respectively. R_p and R_t are the nuclear radii of the projectile and target, respectively.

Typical energies needed to overcome the Coulomb barrier are around 5 MeV/nucleon which corresponds to 10 % of the speed of light. The energy equal to the Coulomb barrier height is only enough to bring the two nuclei into contact but it is not enough to initiate nuclear reactions. Additional energy is needed for two nuclei to fuse together. This additional energy is sometimes called extra push. For heavy systems the Bass barrier is used to model the Coulomb barrier [Bas74]. The Bass barrier takes into account the friction between nucleons and the energy needed to reorganize nucleons in the nucleus.

After the fusion the compound nucleus is "hot" i.e. having a lot of excess energy and angular momentum. The compound nucleus cools down by emitting particles. Depending on the excitation energy neutrons, protons, α-particles or combinations can be evaporated. In the cooling process of very heavy systems neutron emission is the preferred evaporation channel due to the frailty of the system. The final nucleus, when no more particles can be emitted, is called an evaporation residue.

The disadvantage of using fusion evaporation reactions for studying heavy neutron-deficient nuclei is the relatively low production cross section which sets high requirements for selectivity on separators and detector systems.

In addition to the fusion or interaction barrier, other important parameters in fusion evaporation reactions are the excitation energy of the compound nucleus and the reaction Q-value. The reaction Q value can be determined as the mass difference between the initial target and projectile and the final compound nucleus. This mass, or energy, difference is the binding energy difference in each nucleus. Many of the fusion

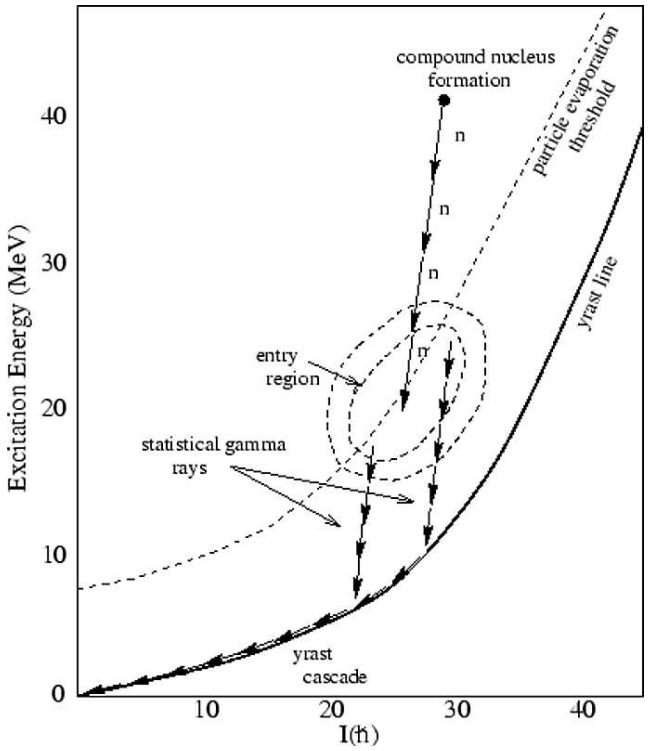

Figure **2.1**: A schematic of the decay of the compound nucleus.

reactions are endothermic or the fusion product is less bound than the projectile and the target. In such cases the Q value is negative and an energy input is needed for a fusion to occur. The reaction Q value is defined as

$$Q = (m_{initial} - m_{final})c^2 = (m_t + m_p - m_{CN})c^2 \,, \tag{2.3}$$

where m_t is the mass of the target, m_p is the mass of the projectile and m_{CN} is the mass of the compound nucleus.

The excitation energy E* determines the final product in the fusion evaporation reaction. Typically, the excitation energies are around 30-40 MeV and the typical energy removed by the evaporation of a neutron is approximately 12 MeV where 10 MeV can be accounted for by neutron separation and 2 MeV by neutron kinetic energy. The excitation energy can be expressed as the sum of center-of-mass bombardment energy and the reaction Q value.

$$E^* = E_{CM} + Q \,, \tag{2.4}$$

where E_{CM} is the bombardment energy in center-of-mass frame and Q is the reaction

Q value.

When synthesizing heavy elements the excitation energy has to be minimized due to the high fissility of the compound nucleus. This can be realized by choosing projectile and target nuclei with magic numbers of protons and/or neutrons. In a fusion evaporation reaction the excitation energy is important but it is not the only parameter which determines the success of the fusion of the target and the projectile. The angular momentum transfer in the fusion evaporation reaction should be small. The centrifugal repulsion caused by the rapid rotation of the hot nucleus can overcome the short-range attraction of the nuclear force which leads to a fission of the compound nucleus. The angular momentum transfer can be minimized by using asymmetric reactions where the target nucleus is heavy and the bombarding ion is light.

The measure of the successful fusion can be defined with a cross section and thus the cross section is one of the key parameters in nuclear physics. The cross section describes the probability for a nuclear reaction to occur. More commonly the cross section is the measure of the size of the nucleus from the point of view of the bombarding ion. The unit for cross section is the barn, which corresponds to the size of a typical atom, which is 10^{-24} cm^2. For different reactions the cross section can vary significantly. The highest known cross section is 3.1×10^6 barns for the thermal neutron capture cross section of the well known nuclear reactor poison ^{135}Xe. The fusion cross sections for the new super heavy elements are of the order few hundred femtobarns (10^{-15} barns) thus making the range 19 orders of magnitude wide [Oga02]. Fusion cross sections in RITU experiments are typically in the range of a few hundreds of microbarns down to few tens of picobarns.

The general equation for the cross section σ can be written as

$$\sigma = \frac{R_p A}{R_b N_A L \rho}\,, \tag{2.5}$$

where R_p is the production rate of the nuclei under interest, R_b is the rate of the bombarding ion, N_A is the number density of the target, A is the area of the target, L is the thickness of the target and ρ the density of the target.

A more useful form of equation 2.5 can be written as

$$\sigma = \frac{n}{I_b N_t T}\,, \tag{2.6}$$

where n is the number of produced ions, I_b is the beam intensity, N_t is the number density of the target and T is the duration of the experiment.

2.3 Different decay modes

Following the fusion the nucleus is "hot" and must cool down. The nucleus has a lot of excitation energy, typically of the order of a few tens of MeVs, and angular momentum. The easiest way for the nucleus to lose energy rapidly is to emit light particles like neutrons, protons, α-particles or some combination of these simultaneously. When synthesizing very heavy neutron-deficient nuclei, particle emission after fusion is less favored compared with fission which is usually the dominant decay mode. Indeed, the fusion-fission cross section can be several orders of magnitude higher than the fusion evaporation cross sections.

When the excess energy in the nucleus has fallen below the neutron or proton separation energy, no more particles can be emitted to cool down the nucleus. The evaporation residue has fairly low excitation energy but high angular momentum. The further cooling occurs via electromagnetic radiation by the emission of high energy E1 γ-rays. When the nucleus is near the yrast line the emission of γ rays slows down the rapid rotation of the nucleus as well as losing the excess energy. At this stage fission still competes with the γ-ray emission as a cooling down process. If the nucleus survives fission, a cascade of γ-rays are emitted until the ground state is reached. At ground state the nucleus does not have any excitation energy left yet it is unstable and must decay towards the valley of stability. This can be achieved via radioactive decay processes by emitting charged particles such as α- or β-particles or by spontaneous fission. In the heavy element region where the nuclei discussed in this work are located, spontaneous fission and α-decay are common decay modes.

2.3.1 Gamma decay

Most nuclear reactions and α or β decays leave the nucleus in an excited state. When the excitation of the nucleus has dropped below the particle separation energy the nucleus cools down towards the ground state by emitting γ rays. The γ rays are photons of electromagnetic radiation. The γ rays have characteristic energies according to the energy difference between quantum nuclear states. Our knowledge of nuclear structure can be extended by investigating the excited states in the nucleus. Thus the study of γ-ray emission is a standard technique in nuclear spectroscopy. By studying γ emission, and the rival process internal conversion, we may deduce the spins and parities of the excited states. Also collective phenomena such as vibrations and rotations can be studied via γ spectroscopy.

The motion of protons in the nucleus gives rise to charge and current distributions. The charge distributions can be described by electric multipole moments and current distributions by magnetic multipole moments. The electromagnetic radiation field

produced, when the nucleus emits radiation in the form of γ rays, can be described in terms of a multipole expansion. The index L can be defined so that 2^L is the multipole order of the radiation. One of the key properties of the 2^L-pole radiation is the angular distribution which is governed by the Legendre polynomials such as P_2=1/2(3cos$^2\theta$-1) for dipole and P_4=1/8(35cos$^4\theta$-30cos$^2\theta$+3) for quadrupole transitions. If the electric field is labelled with E and the magnetic field with M then the parity of the radiation field can be written as

$$\begin{aligned} \pi(ML) &= (-1)^{L+1} \\ \pi(EL) &= (-1)^{L}\,, \end{aligned} \tag{2.7}$$

where the electric and magnetic multipoles of the same order have opposite parity [Kra88].

After quantization of the radiation field the transition probabilities of the different multipole orders can be deduced assuming the nuclear radius follows the relation given in equation 2.1. Table 2.1 shows the simplified equations used to calculate the transition probability for the lowest 4 electric and magnetic multipoles [Kra88]. The unit of λ is s^{-1} when E is in MeV.

Table **2.1**: Simplified equation to calculate transition probabilities for electric and magnetic multipoles.

Multipole	1	2	3	4
λ(E)	$1.0\times10^{14}A^{2/3}E^3$	$7.3\times10^{7}A^{4/3}E^5$	$34A^2E^7$	$1.1\times10^{-5}A^{8/3}E^9$
λ(M)	$5.6\times10^{13}E^3$	$3.5\times10^{7}A^{2/3}E^5$	$16A^{4/3}E^7$	$4.5\times10^{-6}A^2E^9$

Internal conversion

Internal conversion is an electromagnetic process that competes with γ emission in heavy nuclei. In this case the electromagnetic multipole fields of the nucleus do not result in the emission of a photon. Instead, the fields interact with the atomic electrons and cause one of the electrons to be emitted from the atom. In contrast to β decay, the electron is not created in the decay process but rather is a previously existing electron in an atomic orbit. Thus the transition energy is the sum of the kinetic energy and the binding energy of the electron which must be supplied to knock out an electron from an atomic shell. The internal conversion has a threshold energy equal to the electron binding energy in a particular shell. As a result, the conversion electrons are labelled according to the electronic shell from which they originate: K, L, M etc. When a conversion electron is ejected the atomic shell is left with a vacancy. This vacancy

is quickly filled with an electron from a higher orbit. In the process characteristic X-rays are emitted and associated with the conversion electron. The strength of the conversion is measured with the conversion coefficient α, the conversion coefficient gives the probability of electron emission relative to γ emission,

$$\alpha = \frac{\lambda_e}{\lambda_\gamma} \quad , \tag{2.8}$$

where λ_e is the decay constant for conversion electron emission and λ_γ is the decay constant of γ emission.

Some of the general features of the conversion process can be stated. The conversion increases as Z^3 and thus is more important for heavy nuclei. The conversion coefficients decrease rapidly with increasing transition energy i.e. low energy transitions are more likely to be converted. Also the conversion coefficients increases as the multipole order of the transition increases. For high spin (I) values the conversion electron emission may be far more probable than the emission of γ ray. The conversion coefficients decrease for higher atomic shells as $1/n^3$, where n=1,2,3... corresponding to the principal atomic quantum numbers, or alternatively the electronic shells K,L,M....

2.3.2 Alpha decay

The nucleus has survived through the cooling process to the ground state or to an isomeric state. At this stage the immediate cooling has stopped. The nucleus is still unstable and the heavy nuclei on the neutron-deficient side of the valley of stability gain stability via α decay. In heavy systems the disruptive Coulomb force increases with size at a faster rate than does the specific nuclear binding force. The nucleus can spontaneously emit an α-particle carrying away disruptive positive charge. An α particle is an ideal particle to be emitted because it is a light, stable and tightly bound. The emission of an α particle can be represented as:

$$^{A}_{Z}X_N \rightarrow ^{A-4}_{Z-2}X'_{N-2} + \alpha$$

The driving force in the α decay is the Coulomb interaction where the positively charged daughter and the α particle, having a 2+ charge state, are repelled from each other.

The energy release is dependent on the energy level in the nucleus from which the α-particle originates, the higher the energy level the higher the Q-value. There is a

striking connection between the Q-value and the half-life of the nucleus that was discovered in 1911 by Geiger and Nuttall. Geiger and Nuttall discovered that α emitters with large decay energies had short half-lives and vice versa. For example a factor of two in energy corresponds to a factor of 10^{24} in half-life.

The α-particle emission can be treated as a barrier penetration problem. The one-body model of α decay assumes a preformed α particle confined inside the nucleus by the Coulomb barrier. In this theory the α particle is assumed to move in a potential well, determined by the daughter nucleus. The α particle vibrates inside the nucleus hitting the Coulomb barrier, classically the α particle cannot escape from the nucleus unless the energy of the particle is higher than the potential well where the particle is confined in. The Coulomb barrier height at the distance of R_i, the surface of the nucleus or the inner radius of the potential, can be defined as

$$B_C = \frac{1}{4\pi\epsilon_0}\frac{zZ'e^2}{R_i}\,, \tag{2.9}$$

where z is the charge of the α particle, Z' is the proton number of the daughter nucleus and e is the unit charge.

Classically, an α particle cannot escape from the nucleus but in quantum mechanics there is a finite probability that the α particle can penetrate, or "tunnel", through the barrier and escape from the nucleus [Gur29], [Gam28]. The α particle vibrates in a certain energy state inside the nucleus hitting the Coulomb barrier. At this level the Coulomb barrier depth is determined by the inner and outer radii of the barrier.

The α-decay constant can be written as a product of the frequency of collisions with the barrier, or "knocking frequency" f, and the barrier penetration probability P, as

$$\lambda = \left(\frac{v_\alpha}{2R_i}\right)P = fP\,, \tag{2.10}$$

where λ is the decay constant, v_α is the velocity of the α-particle and R_i is the inner radius of the Coulomb potential. When a typical potential well depth of 35 MeV is considered and the Q-value is 5 MeV the knocking frequency is of the order of 10^{21} Hz.

The barrier penetration probability P can be written as

$$P = e^{-2G}\,, \tag{2.11}$$

where the Gamow factor G is

$$G = \sqrt{\frac{2m}{\hbar^2}} \int_{R_i}^{R_o} [V(r) - Q]^{1/2}\, dr = \sqrt{\frac{2m}{\hbar^2 Q}} \frac{zZ'e^2}{4\pi\epsilon_0} \left[arccos\sqrt{x} - \sqrt{x(1-x)} \right], \quad (2.12)$$

where $x = Q/B$. Here Q is the Q value of the α decay process and m is the mass of the α particle. R_i and R_o are the inner and outer radius of the Coulomb barrier, respectively.

One of the main features in α decay is that a given initial state can populate different final states in the daughter nucleus. This property is known as fine structure of α decay. Similarly, in the mother nucleus there can be different states where the α decay can originate from. Thus, α-decay spectroscopy is a sensitive probe of nuclear structure.

Spectroscopic tools

In α decay the α particle has to penetrate through the total barrier which is composed of the Coulomb and the angular momentum barriers. The spin of the α particle is zero and thus the total angular momentum carried away by the α particle is purely orbital in character. If the spin of the final state (I_f) is different from the the spin of the initial state (I_i), the α particle must carry this difference in angular momentum. The allowed angular momentum l carried by the α particle is limited to the range $|\, I_i - I_f \,| \leq l \leq (I_i + I_f)$. The parity follows the rule $(-1)^l$. If the initial and final parities are the same then l must be even and if the parities are different then l must be odd. The addition of the centrifugal barrier can add a significant portion to the total barrier thus hindering the decay process and prolonging the half-life significantly.

The previous models assume a preformed α particle inside the nucleus. The preformation of α particle is dependent on the nuclear structure. The preformation probability may result in a reduction in the α-decay probability. More commonly the preformation probability is referred to as the reduced α-decay width, or simply the reduced width. In the late 1950's J.O. Rasmussen defined the reduced α-decay width (δ^2) using the decay constant and barrier penetration factor. The Rasmussen method simplified the calculation of the reduced α-decay width. The method became popular and widely used as a spectroscopic tool in the α decay studies. The reduced width defined according to the Rasmussen method is given by

$$\delta^2 = \frac{\lambda_{exp}\, h}{P}\ [\mathrm{eV}], \quad (2.13)$$

where λ_{exp} is the experimental decay constant, h is the Planck's constant and P the barrier penetration factor. The δ^2 values calculated with the Rasmussen method are normally around 40 keV or greater for a favoured decay and around 1 keV for a hindered α decay.

A widely used spectroscopic tool is the concept of hindrance factor (HF) which can be defined as

$$HF = \frac{\delta^2_{even-even}}{\delta^2_{exp}}$$

where $\delta^2_{even-even}$ is the reduced width of the closest even-even nucleus representing the general nuclear structure in that particular region of nuclear chart and δ^2_{exp} is the reduced width of the nucleus of interest.

An alternative way to calculate the hindrance factor is

$$HF = \frac{T^{meas}_{1/2}}{T^{Rasm}_{1/2}}\,, \tag{2.14}$$

where $\mathrm{T}^{meas}_{1/2}$ is the measured half-life and $\mathrm{T}^{Rasm}_{1/2}$ is the Rasmussen half-life.

This alternative method calculates the hindrance factor using the half-lives instead of reduced widths. The $\mathrm{T}^{meas}_{1/2}$ is the measured half-life and $\mathrm{T}^{Rasm}_{1/2}$ is the half-life relative to the unhindered decay of ^{212}Po [Ras59]. In a one-body model the ^{212}Po is an ideal example where the α particle is vibrating in a spherical region formed by the doubly magic ^{208}Pb nucleus.

The Rasmussen method is an approximate method to determine spins and parities of different states. A hindrance factor less than 4 implies a favored α decay among states of equal spin, parity and configuration [Nuc75]. The hindered transitions usually have hindrance factors from few tens up to hundreds of thousands of units. There is no upper limit for hindrance factor but if the transition is very hindered other competing decay processes are more likely to occur.

The Rasmussen method is an approximate method and it does not take into account any structural changes between initial and final states. Thus the Rasmussen method is only used in decay studies where α decay is the only viable method to obtain any nuclear structure information.

2.3.3 Spontaneous fission

The energetic preference for nuclei to fission can be understood from the binding energy per nucleon. A heavy nucleus in the uranium region has a binding energy of 7.6 MeV/nucleon, if the nucleus is divided into two equal fragments with A≈119 the binding energy per nucleon would be 8.5 MeV/nucleon. A full range of approximately 800 different fragment nuclei may be formed in fission decay with each fragment being very neutron rich. A peculiarity of low-energy fission, thermal neutron induced or spontaneous fission, is the asymmetry of the mass division. In the lighter actinides from thorium to einsteinium, nuclei disintegrate asymmetrically into a heavier and a lighter fragment. For example, in a fissioning nucleus such as ^{236}U, a typical ratio of heavy/light fragment mass numbers is 140/96. The mass A=132 is singled out due to the extra stability of the ^{132}Sn nucleus with a magic Z=50 proton number and with a magic N=82 neutron number. The shell-stabilization of ^{132}Sn is understood to be one of the roots for the preference of asymmetric mass splits in the actinides. Similarly, in the light mass group one may anticipate the influence of the magic proton number Z=28 (Ni) and the magic neutron number N=50.

In a spontaneous fission process the fission fragments are "hot" and they cool down by evaporating neutrons. For example in the spontaneous fission of ^{252}Cf on the average 3.77 neutrons are evaporated.

The fission process itself can be treated as a barrier penetration problem where the fission fragments have to penetrate through the fission barrier. The fragments lie in a mean-field potential, the fission decay is analogous to the α decay with the difference in particle mass and energy.

The two fragments are pushed away by Coulomb repulsion and a neck region is formed between the fragments. As the Coulomb repulsion gets stronger the fragments are pushed apart and the neck region collapses. The fragments share the fission energy according to their masses as kinetic energy and the angle between the fragments is determined by conservation of momentum. Usually the fragments are ejected in 180° angle in respect to each other. This holds true if the nucleus is scissioned into two fission fragments. In some rare cases the neck region may form ternary or quarternary fission fragments. In these cases the fission energy is divided between three or four fragments causing deviation in the fragments relative emission angles. Figure 2.2 shows a schematic drawing of a spontaneous fission process.

The energy release in fission is much higher than in other forms of radioactive decays, of the order of 200 MeV. The total kinetic energy release (TKE) is a measure of the fission energy. It has been found that the fission energy can be described by a simple model based on Coulomb repulsion between prolate spheroids. Such a model predicts that the most probable total kinetic energy release $\langle E_K \rangle$ depends linearly on

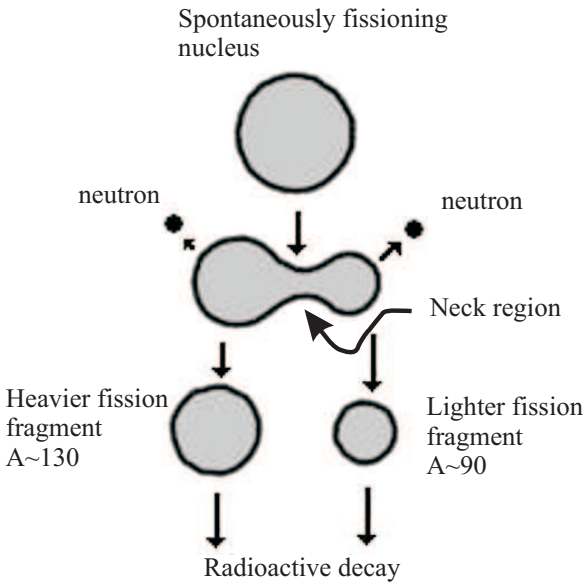

Figure **2.2**: Schematic drawing of a spontaneous fission process.

the Coulomb parameter $Z^2/A^{1/3}$ of the fissioning nucleus [Vio85]. This is also known as the Viola systematics which can be written as

$$\langle E_K \rangle = 0.1189 \frac{Z^2}{A^{1/3}} + 7.3 MeV \, . \tag{2.15}$$

A single fission event has a well-determined energy but for a large group of fission events an energy distribution is formed. This is due to the fact that fission fragments have a mass distribution instead of the nucleus always scissioning into the same particles.

2.3.4 Beta decay

The β decay is a weak interaction process. There are three different decay paths which the β decay can proceed through: β^+ decay, β^- decay and electron capture. In β^+ decay a proton is converted into a neutron, in β^- decay a neutron is converted into a proton and in electron capture (ϵ) an orbital electron is captured by a proton in the nucleus. These decay processes are are described below.

$$n \rightarrow p + e^- + \overline{\nu} \quad \text{negative beta decay } (\beta^-)$$
$$p \rightarrow n + e^+ + \nu \quad \text{positive beta decay } (\beta^+)$$

$$p + e^- \rightarrow n + \nu \quad \text{orbital electron capture } (\epsilon)$$

In a nucleus, β decay changes both Z and N by one unit so that the mass number A of the nucleus remains constant. In the decay process one electron or positron and one neutrino or antineutrino are created. The neutrino is an electrically neutral particle with a spin of $\frac{1}{2}$. The emission of a neutrino and an electron results in a continuous electron energy spectrum where the decay energy is divided between the neutrino and the electron. The maximum energy of the electron corresponds to the energy of the transition in the nucleus.

Beta decay is the most common decay mode among the different isotopes. The β^- decay occurs in neutron-rich nuclei while the β^+ decay and the electron capture are decay processes of proton-rich nuclei. The β decay differs from the α decay significantly. The β particle and the neutrino are not preformed but have to be created in the decay process and in β^- decay there is no barrier to be penetrate. Even in β^+ decay the exponential factor in the barrier penetration factor is of the order of unity [Kra88].

2.3.5 Nuclear excitations

The timescale of nuclear phenomena has an enormous range. The shortest lived nuclei break apart in 10^{-21} s. Many nuclear reactions take place in this time scale which is roughly the length of time which the reacting nuclei are in range of each other's nuclear force. Electromagnetic decays of nuclei occur with lifetimes of 10^{-15} s and even up to years.

The fundamental excitations of atomic nuclei fall into two classes; single particle excitations in which individual nucleons change orbits and collective excitations involving the coherent motion of many nucleons. The latter can be pictured as rotations and vibrations of the nucleus. Several different types of vibrational excitations have been discovered but the nature of the vibrational excitations is not well understood

A fundamental issue for any many-body system of strongly-interacting fermions is the interplay of collective and single-particle degrees of freedom. Collective vibrational (phonon) modes are constructed from excitations of nucleons from one orbit to another. Each type of phonon will be different in structure depending on the characteristic orbits involved and will evolve differently in energy and excitation strength with neutron and proton number. But the Pauli Principle limits the number of fermions in a given orbit. In nuclear states consisting of superpositions of many phonons, there is a continuous struggle between the Pauli Principle and the survival of collectivity in these states. This strikes at the heart of the issue of understanding the coherent motion of nucleons in the nucleus.

By studying the γ radiation emitted by the nucleus structural information about different nuclear excitations can be obtained. For example, indications of vibrational states in ^{252}No (detailed in Chapter 6) were observed in addition to the rotational ground state band.

3 Experimental devices & methods

In order to acquire a broad experimental knowledge of exotic nuclear properties different experimental techniques must be employed. The exotic nuclei can be synthesized in a fusion evaporation reaction by bombarding a target with projectile ions. The flux of the beam is enormous compared to the flux of synthesized nuclei. The nuclei of interest have to be isolated from the large background of the unwanted nuclei in order to study the radiation which they emit and thus get structure information. The experimental techniques together with an advanced data acquisition system allow us to separate "the needle from a haystack".

3.1 The RITU separator

The RITU (Recoil Ion Transport Unit) separator is designed to separate fusion recoils from the beam particles, prompt fission and transfer products [Lei95]. RITU is a gas-filled separator with QDQQ configuration where Q stands for quadrupole magnet and D for dipole magnet. RITU was designed for the study of heavy elements with maximum dipole magnetic field of 1.2 T. The separator is filled with dilute helium gas, normally at 0.5-1.0 mbar pressure. Following formation at the target position, the nuclei of interest recoil into the first quadrupole magnet. The first quadrupole magnet is vertically focusing and matches the recoil cone to the acceptance of the RITU dipole chamber. The dipole magnet separates fusion products from the primary beam according to their magnetic rigidities. The fusion products recoil through the dipole chamber into the final set of quadrupole magnets where they are focused and implanted into an implantation detector located at the magnetic focal point. A schematic drawing of RITU can be seen in figure 3.1.

The original projectiles, or beam particles, are bent in a magnetic field to a trajectory with a smaller radius of curvature than the evaporation residues and eventually dumped into a beam stopper made of tantalum. The trajectory of the evaporation residues can be calculated and thus the magnetic field can be tuned in each case. In the case of lighter mass regions, where more symmetric reactions with beam and projectile mass of A$\approx$40-50 are used, RITU has difficulties in separating the beam from the fusion products.

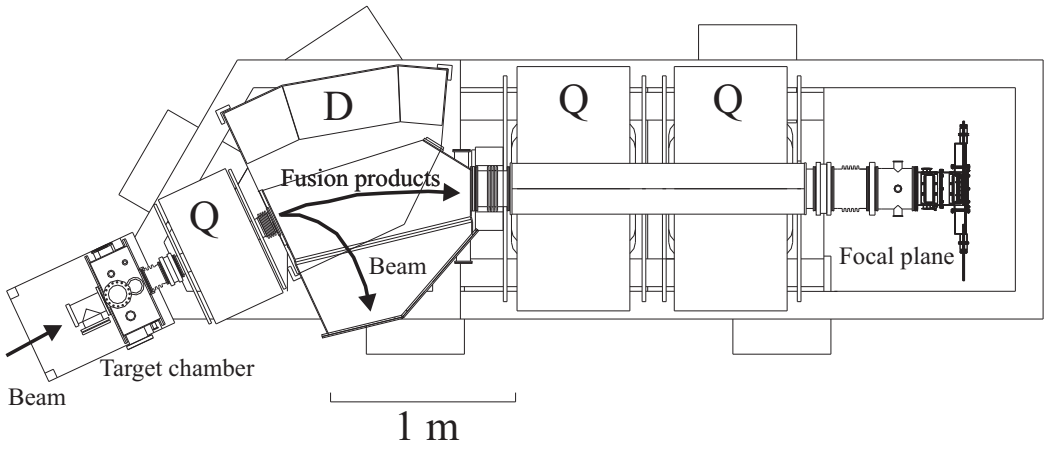

Figure **3.1**: Schematic view of the RITU gas-filled separator.

3.1.1 Working principle

The working principle of RITU relies heavily on understanding the mechanism of separation of ions in a magnetic field. Soon after the discovery of fission there was a need to develop a theory concerning heavy ions moving with high velocity in a gaseous medium. The following separation method was first developed by Cohen and Fulmer in 1958 for fission products [Coh58].

Like fission fragments, fusion products inside the target are formed with high velocity and a variety of high charge states. When entering RITU the ions are in 20-30 different charge states. In a magnetic field the radii of curvature of the ions are determined by their momentum and charge. In vacuum this would mean 20-30 different trajectories even for constant momentum. Focusing of such a large number of trajectories into a small spot at the focal plane is virtually impossible. The transmission can be improved by filling RITU with dilute helium. In helium the different charge states are "focused" to an average charge state. The fusion recoils close to the average charge can be focused into to the focal plane of RITU. In vacuum separators an additional carbon recharging foil is used to reduce the number of different charge states thus improving the transmission.

The RITU separator is filled with dilute helium gas, normally under 0.5-1 mbar pressure. In dilute helium the collisions between recoiling nuclei and the gas atoms continuously change the charge state of the recoils thus making charge fluctuate around an average charge state. The trajectory of each particle is determined by its average charge state $\overline{q}$. This average charge is found to be independent of the initial charge distribution and roughly proportional to the velocity of the particles. The mechanism results in charge and velocity focusing so that a gas-filled separator acts as a mass separator. The RITU transmission is dependent on the target and projectile. The

transmission of fusion products formed with heavy beams and heavy targets can be as high as approximately 40 %. For slower recoils, for the combination of a light beam (A≈20-30) and a heavy target (A>200), the transmission drops and can be as low as 10 %.

3.2 The 1999 setup and JUROSPHERE II

At the time of the experiment described in Chapter 6, the JUROSPHERE II detector array was mounted at the target area of RITU to detect prompt γ rays. This can be seen in figure 3.2. The JUROSPHERE II array consisted of 27 Compton suppressed HPGe detectors (15 Eurogam Phase I, 5 Nordball and 7 Tessa) with a total photopeak efficiency of 1.7 % at 1.3 MeV [Bea92], [Her85], [Nol85].

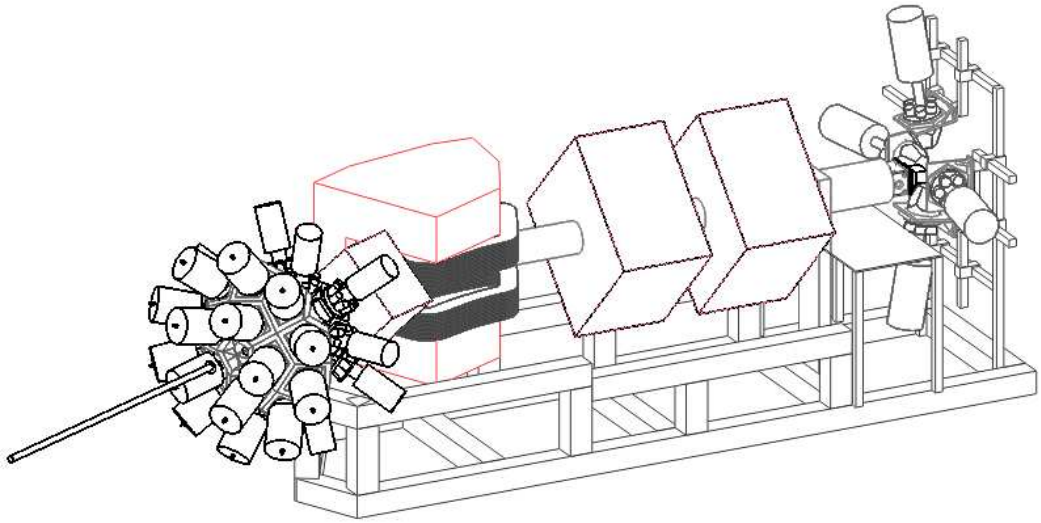

Figure **3.2**: RITU coupled with JUROSPHERE II array.

The recoiling ions were implanted in a focal plane detector setup comprising a Passivated Implanted Planar Silicon (PIPS) detector and a multiwire proportional counter (MWPC). The PIPS-type silicon detector has 16 individual strips. This detector was used to collect energy and position signals from fusion implants and decay products. The MWPC was placed 10 cm upstream from the main detector and it was used to measure the energy loss of the ion (ΔE). A time-to-amplitude converter (TAC) unit was placed between the PIPS and the MWPC to measure the Time-Of-Flight (TOF) of the fusion products. The PIPS had a lower counting rate thus the start signal for the TOF measurement was taken from the PIPS. The stop signal for the TOF measurement was taken from the MWPC signal which was delayed. The whole system had one master trigger which was a high energy signal from the PIPS detector. If

triggered, all the detectors were read simultaneously. Thus all the signals collected within a certain time window after the trigger signal are considered to belong to that particular event which triggered the master trigger. Figure 3.3 shows a block chart of the JUROSPHERE II electronics.

3.2.1 The focal plane detector system

The PIPS detector was used to measure the implantation of the fusion products and the subsequent decay (α or fission) energy of the implanted nuclei. The detector was 305 μm thick and measured 80×35 mm^2 and consisted of sixteen 5 mm wide individual strips. Each strip was position-sensitive with a boron implanted resistive layer. The vertical position resolution was typically around 700 μm (the full width of the position window).

Top and bottom signals were taken from each strip. The signal was divided to either the high or low amplification channel depending on the detected energy. This allowed different amplifications for low energy α decays and high energy recoils. The two amplification channels overlapped and high energy α decays could be seen in the recoil side also. In addition, there were sum amplifiers on either amplification channel which took the sum of the top and bottom signals indicating the total energy. The signal from the sum amplifier saturated before the individual top and bottom signals saturated. This is a problem when measuring energetic fission decays. This could be partly avoided if a new sum energy signal was created by summing the individual top and bottom signals in the offline analysis. The time limit for the focal plane measurements was set by the flight time of the fusion products through RITU and the electronics dead time. The flight time of the fusion products was approximately 500 ns and the electronics dead time was some tens of microseconds. A block diagram of the the PIPS electronics is shown in Figure 3.4.

3.3 RITU upgrades

RITU went through a series of upgrades during the years of 2000-2002. These upgrades improved the suppression of the scattered beam particles and the target-like products. The improvements affected the whole energy region but the most significant reduction in background was in the low-energy part of the recoil spectrum. The quality of the low-energy α spectrum was also improved by the second MWPC and two quadrant detectors behind the PIPS detector. Each quadrant detector was a silicon detector of thickness 450 μm and of area 60×60 mm^2. The quadrant detectors were used to veto high energy α particles and protons that punched through the main PIPS detector.

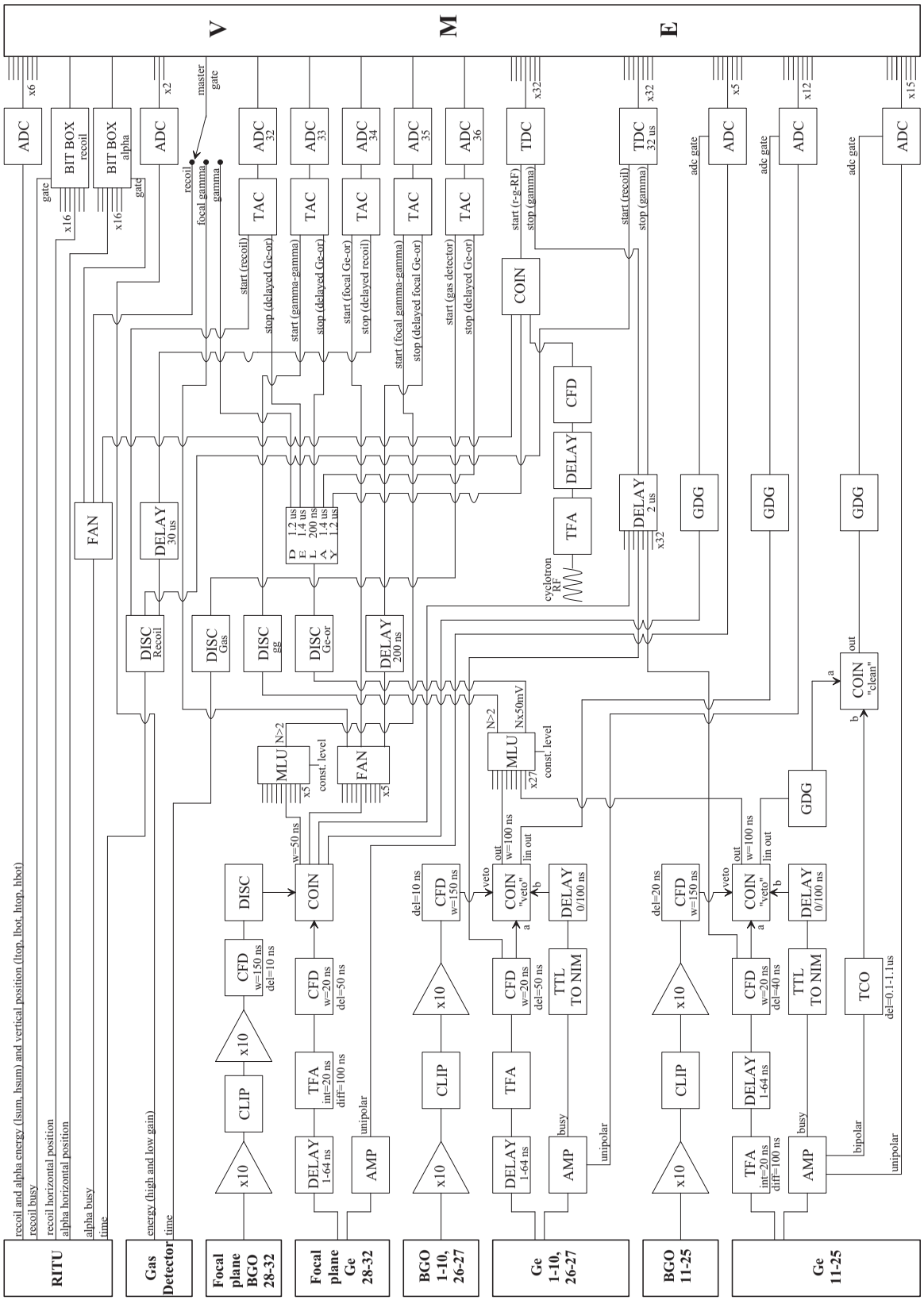

Figure **3.3**: Diagram of measurement electronics used in RITU and JUROSPHERE II setup

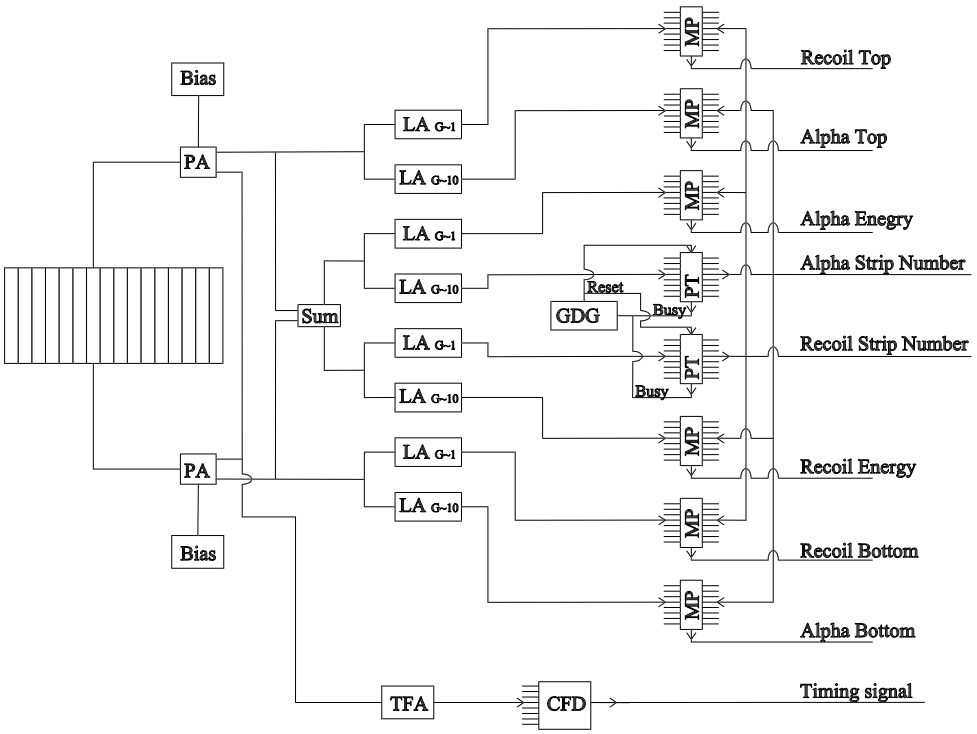

Figure **3.4**: A block chart of the main stop detector (PIPS detector) electronics. In the figure LA=linear amplifier, PA=preamplifier, TFA=timing filter amplifier, SUM=sum amplifier, CFD=constant fraction discriminator, GDG=gate and delay generator, PT=pattern trigger and MP=multiplexer.

3.3.1 The second focal plane setup

The first improvement to the RITU focal plane detector system was the inclusion of a new gas-counter system [Ket01]. The old MWPC was replaced by two new MWPCs where the first MWPC was placed only 1.5 cm from the PIPS detector. The second MWPC was placed 30 cm upstream allowing better discrimination of beam and recoils in the TOF spectrum compared with the preceding system. The MWPCs had a 20 μm thick wiring with 1 mm pitch. The wire was made of tungsten coated with gold. The filling gas in the MWPCs was isobutane at 3 mbar pressure. The system was isolated from the vacuum with 0.9 μm thick mylar windows. The TOF measurement was made between the two gas counters. The required start signal was taken from the first MWPC, closest to the PIPS detector, and the stop signal was taken from the second MWPC. The signal from the second MWPC was delayed with a delay circuit. The second MWPC was also used to veto escaped α particles thus reducing the background in the low energy part of the α spectrum. Two quadrant detectors were placed behind the main detector to act as a veto for punch through α particles and energetic protons. The main detector of this system was a PIPS detector as in the previous system.

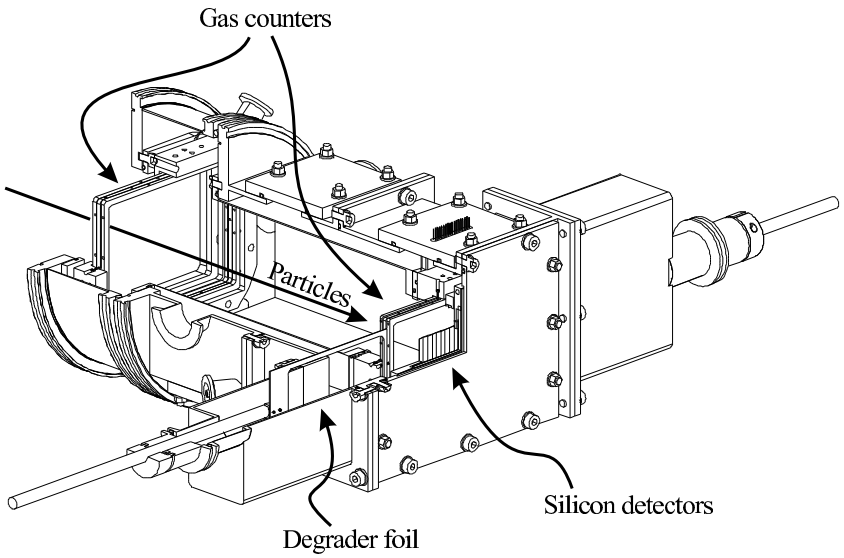

Figure **3.5**: A wireframe view of the new focal plane setup. The new gas counter (MWPC) systems are visible along with a partial view of the PIPS detector.

Figure 3.6 shows a block chart of the gas counter electronics.

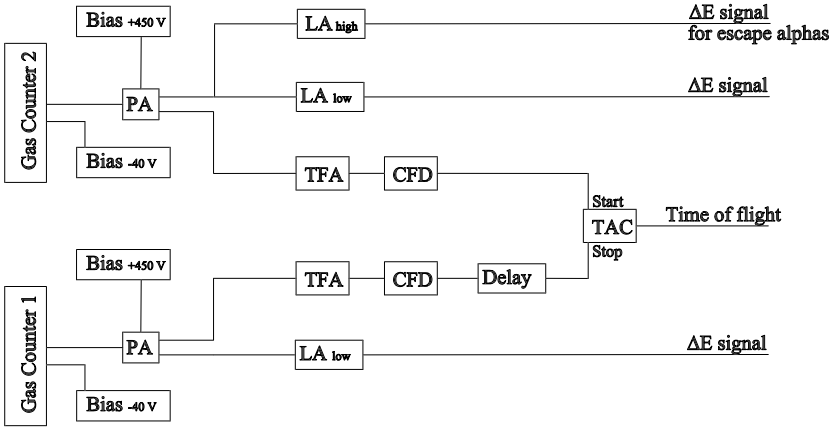

Figure **3.6**: A block chart of the MWPC electronics. In the figure PA=preamplifier, LA=linear amplifier, TFA=timing filter amplifier, CFD=constant fraction discriminator, TAC=time to amplitude converter.

3.3.2 The differential pumping system and the new dipole chamber

The differential pumping system was installed together with the new dipole chamber in October 2001. The upgrade was important since it reduced the background from scattered beam particles significantly. The beam dump was moved further away from the dipole magnet which reduced the amount of scattered beam reaching the focal plane. The new beam dump was modified to fit into the new chamber. The retractable beam delimiter was replaced with a new one. Figure 3.7 shows the improvements made to the dipole chamber.

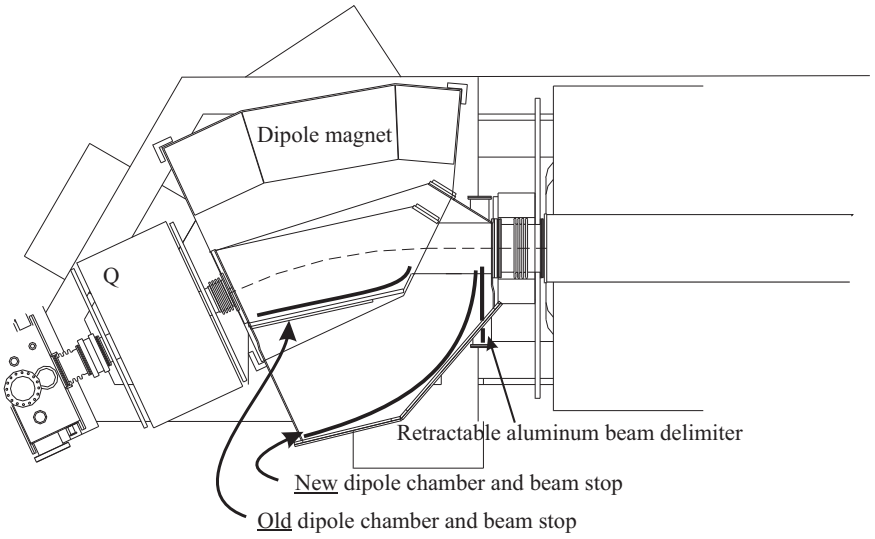

Figure **3.7**: Comparison of new and old RITU dipole chambers.

The differential pumping system replaced the carbon and nickel foils which were used as a gas window. The gas window was a limiting factor in experiments where very high beam intensities were used. The differential pumping reduced the scattering and energy straggling of the primary beam. A well-defined primary beam energy allows a more efficient production of the desired fusion products. The gas window also increased the background counting rate of the HPGe detectors at the target area. The reduction of the scattering was seen at the focal plane where less scattered light particles were detected.

The differential pumping system consists of a Roots pump station and a turbomolecular pump station. The Roots pump station has a 1020 m^3/h Roots pump which is prepumped with a two-stage rotating vane pumps. The Roots pump operates with a great volume flow thus evacuating most of the helium out of the system. Although the Roots is pumping most of the helium away it does not have the capability to reach pressures of the order of 10^{-5} mbar. The turbomolecular pump is located right next

to the Roots station. With the turbo station $10^{-5...-7}$ mbar pressures in the beam line can be achieved. The collimators are needed to reduce the volume flow of helium and maintain the required helium pressure inside RITU. Figure 3.8 shows a flow chart of the differential pumping system.

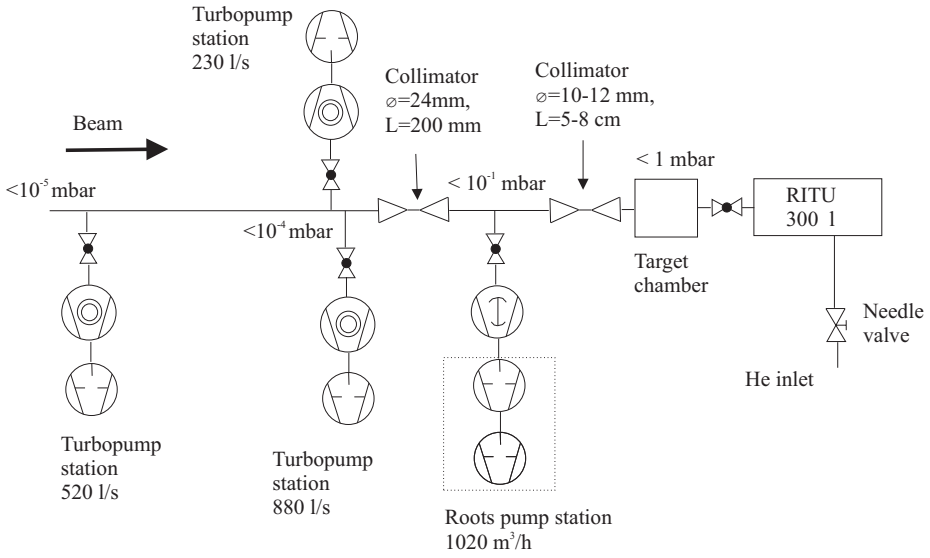

Figure **3.8**: Flow chart of the differential pumping system

3.4 The GREAT spectrometer and TDR data acquisition system

The GREAT (Gamma Recoil Electron Alpha Tagging) focal plane spectrometer [Pag03] and its associated Total Data Readout (TDR) [Laz01] data acquisition system were installed and combined with RITU in November 2002. The GREAT spectrometer replaced the second focal plane detector setup described in chapter 3.3.1. At the same time the data acquisition electronics were replaced by TDR. The most significant feature of the TDR data acquisition system is that it does not contain a hardware trigger. The heart of the TDR system is the 100 MHz clock, or metronome, where every event is time stamped. The time stamped data is eventually fed to event builder which constructs the events. Figure 3.9 shows a block diagram of the TDR data acquisition system.

The GREAT spectrometer is composed of two Double-sided Silicon Strip Detectors (DSSD), 28 PIN diodes, a planar High Purity Germanium (HPGe) strip detector, a Clover detector located outside the vacuum chamber and an MWPC. The DSSD acts as a main stop detector where fusion products are implanted. The DSSD also acts as

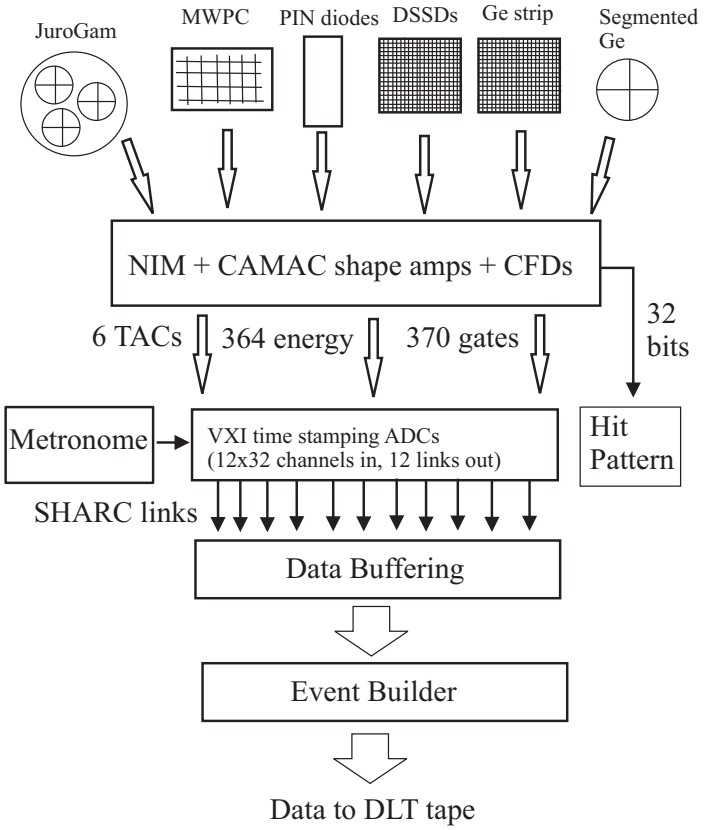

Figure **3.9**: Schematic diagram of TDR system's electronics and data acquisition. Figure adapted from [Laz01].

a start detector for Time-Of-Flight measurement between the DSSD and the MWPC. PIN diodes are placed in a box geometry around the DSSD pair to measure conversion electrons and escape α particles. A planar HPGe detector is located behind the DSSD pair to measure X-rays and low energy γ rays. The Clover detector is located outside the vacuum chamber above the DSSD pair. The Clover is used to measure delayed γ-rays. The MWPC is placed 40 cm upstream from the DSSD pair. Figure 3.10 shows a wireframe drawing of the GREAT setup. The quadrant detectors are not shown in figure 3.10 but the detectors can be installed as an add-on feature whenever needed.

Although the focal plane germanium detectors play an important role in many experiments and are crucial in the study of isomers, here only the DSSDs, PIN diodes and MWPC are discussed. The planar HPGe detector and the Clover detector were not included in any of the experiments discussed in this thesis.

Each DSSD is 300 μm thick and 60×40 mm^2 in size consisting of 60 individual strips in x-direction and 40 individual strips in y-direction. Thus one pixel measure approximately 1×1 mm^2 in size. The two detectors are adjacent to each other with only a small gap between them allowing majority of the Gaussian-like recoil distribution to

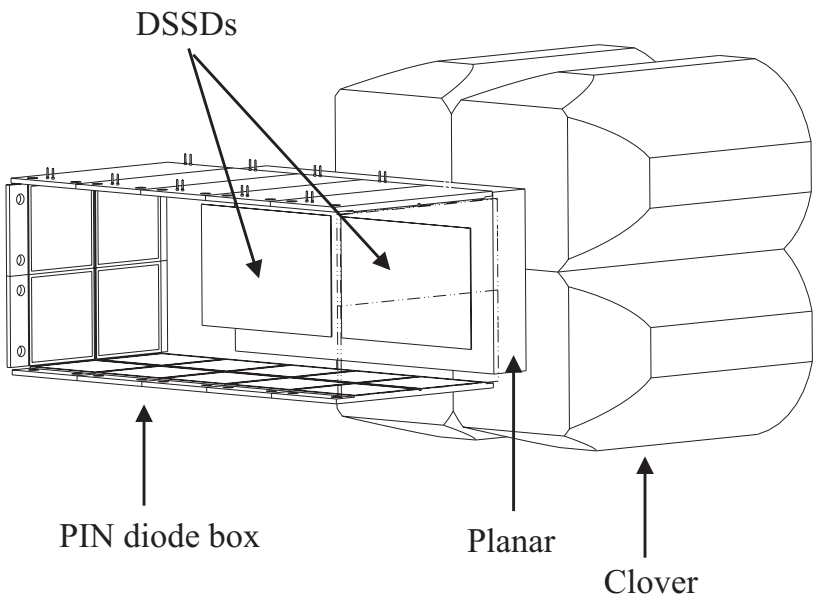

Figure **3.10**: A wireframe drawing of the GREAT focal plane detector setup excluding the MWPC.

be collected. The energy signals from the strips are read out with a hybrid preamplifier mounted on a motherboard which is directly connected to the DSSD. The DSSD and PIN detectors and the DSSD preamplifiers are mounted on a custom made cooling block which is cooled with circulating alcohol. The normal operating temperature is around -15 °C. Figure 3.11 shows a block diagram of the DSSD detector electronics.

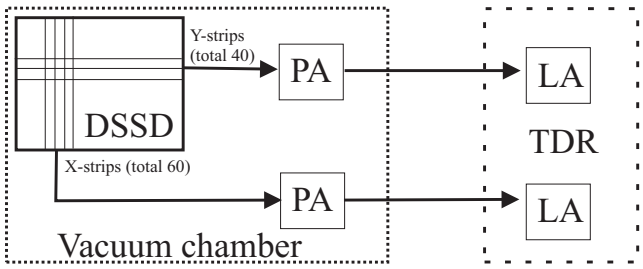

Figure **3.11**: A block diagram of the DSSD detector electronics. In figure PA=pre-amplifier and LA=linear amplifier.

A distinctive feature of GREAT is the array of 28 PIN photodiode detectors to measure conversion electrons and escape α-particles. Each PIN diode measures $28\times28\times0.5\text{mm}^3$. An implanted nucleus inside the DSSD can emit conversion electrons which will escape the DSSD detector since the thickness of the DSSD is not sufficient to stop conversion electrons from escaping. Similarly, the range of α particles in silicon is around 50-60 μm while the range of significantly heavier fusion recoils is only around 10 μm. The implantation depth of fusion products is not enough to stop α particles emitted backwards. Only 55 % of the α decays are detected with a full energy and 45 % of the α particles escape from the DSSD. The PIN diode array is placed upstream in respect

to DSSD. The PIN diode array is connected to the same cooling block as the DSSD pair.

The purpose of the MWPC is to detect and distinguish fusion recoils from the scattered beam and transfer products by the energy loss and time-of-flight. The MWPC is wired in X- and Y direction with 50 μm thick tungsten wire coated with gold with a 1 mm pitch. The MWPC is filled with isobutane gas at approximately 3.5 mbar pressure and the central cathode is biased with -470 V. The windows on either side of the MWPC are made of 0.9 μm thick mylar foil. The central cathode is made of 0.9 μm thick aluminized mylar foil where the aluminum coating is on both sides. Figure 3.12 shows a cross section of the GREAT spectrometer MWPC.

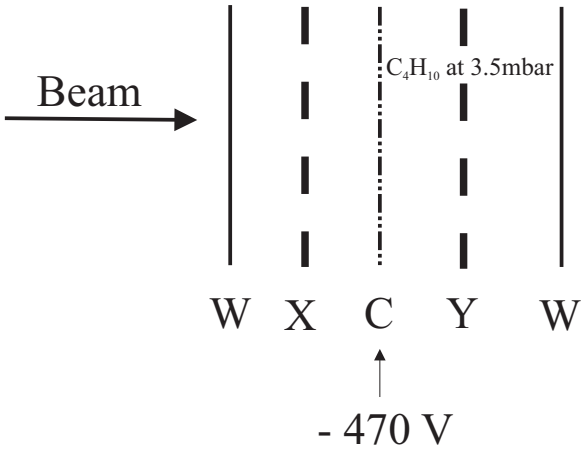

Figure **3.12**: Schematic drawing of the cross section of the MWPC. In the figure W= 0.9 μm mylar window, C= 0.9 μm aluminized mylar cathode, X= wiring to measure particles in X- direction, Y= wiring to measure particles in Y-direction.

3.5 Calibration of the detectors

The whole data analysis relies on the accuracy of the calibration. The detector systems measure only electrical signals and without a reference they have no significance. All the detectors have to be calibrated to match the energy region of the current measurement. The detectors have to be calibrated with a radioactive source with known α or γ-decay energies.

3.5.1 Source calibration

The sources used for the calibration of the main implantation detector contain isotopes with long half-lives like ^{239}Pu, ^{241}Am and ^{244}Cm. These isotopes are synthesized in

nuclear reactors in neutron capture processes. The α-decay energies of these nuclei are well known but since they have relatively long half-lives the α-particle energy is very low from 5.1 MeV to 5.8 MeV. This calibration is less reliable for the studied nuclei in which an α-particle energy is normally a few MeV higher than the energy of the calibration peaks. In source calibration some of the α-particle energy is lost in the dead layer of the detector thus introducing an additional error to the calibration. In addition, in experiment the Q-value of the decay is measured instead of the energy of α particle. Thus the source calibration does not take into account the effect of the recoil.

The γ-ray detectors are calibrated with a γ emitting source. The γ-ray detectors are calibrated in energy and efficiency. Standard calibration sources contain isotopes of ^{60}Co, ^{152}Eu and ^{133}Ba for energy calibration [Trz90].

3.5.2 Internal calibration

The uncertainties introduced in the source calibration of the implantation detector can be minimized with an additional internal calibration. The internal calibration uses the known α decays of fusion products that are implanted into the detector. The actual beam is used to bombard a target which produces fusion recoils with high cross sections. The decay energy of the fusion recoils is close to or at the α-decay energy range of the studied nucleus. The internal calibration measures the reaction Q-value instead of α-particle energy. This type of calibration is similar to the real situation and it eliminates the effect of the detector dead layer and the pulse height defect provided that the mass of the recoil in the calibration and in the experiment are reasonably similar. The calibration obtained is accurate and reliable. The problem associated with internal calibration is that the cross sections of the desired calibration nuclei might be low thus the calibration consumes valuable beam time. Also the finding of the right beam and target combination to produce isotopes with suitable decay properties in some cases may be difficult.

3.6 Data analysis

In data analysis the methods of recoil gating and recoil-decay tagging (RDT) were used to obtain clean γ-ray spectra [Pau95] [Sim86]. In recoil-decay tagging three stages of data collection can be defined; first the detection of prompt γ-rays at the target position, second the detection of the recoiling fusion product at the focal plane and third the detection of the subsequent radioactive decays or electromagnetic radiation. The data from these three stages will be reconstructed offline with the help of com-

puters to create the whole event chain. The offline analysis method is known as the correlation method where each event is related the to following event(s). The required correlations can be a certain time, position or energy window or a combination of different windows.

The decay lifetime is one of the key parameters when correlating implanted recoil events with their subsequent decays, in this work α or fission. The lifetime information can be turned into half-lives which is a key element in nuclear physics. The data acquisition system records time information on all the detected events. The lifetime of, for example an α-decay event is determined as the time difference between the entry of the recoil and the actual α decay.

The random background from scattered beam particles can pass the same gates as set for α-decay thus interfering with the lifetime measurements of the real events. The half-life of an α decay can be determined from the decay curve. When random background from scattered beam is present two components can be seen in this plot; one from the real events and one from random background from scattered beam particles. In order to obtain the half-life of the decaying nucleus the random background has to be accounted for. The background events obey a similar exponential decay law as the real events and thus the background events have an apparent half-life. Usually the half-life of the background events is significantly longer than the half-life of real events. The background half-life can be separated from the real data by doing a two component fit with a very long search time. The search time has to be long so that no real events are present towards the end of the search time. This can mean search times up to 100 or even 1000 times the half-life of the real events [Lei81].

3.6.1 Sorting the data

In order to analyze the experimental data a suitable program had to be written to perform decay correlations. The data acquisition system during the ^{252}No and ^{255}Db experiments used the old VME based TARDIS system. The sort code was written in the C-programming language to perform correlation analysis. The system output files were in ASCII-format and the detailed analysis had to be done with separate tools. Some earlier experiments were reanalyzed in order to benchmark the code.

The current data acquisition system is the Total Data Readout- system. The GRAIN package was designed to analyze the TDR data [Rah05]. The GRAIN package is coded with Java which allows it to run on every platform. The GRAIN package works as a standard method to sort online and offline data from JUROGAM and RITU experiments. The data from the ^{218}U experiment were analyzed with the GRAIN package. GRAIN gives the advantage of being able to perform correlations online.

3.6.2 Error analysis

For reliable analysis of the decay properties, error limits must be determined. Error analysis also provides a method to determine the statistical significance of the obtained results. In many heavy element studies production cross sections are very low. In these cases the number of interesting events is low and it can be questioned whether is a real event or produced by the random background. In these cases the error analysis plays an important role in determining the significance of the observed events.

Maximum likelihood method

The fitting of a decay curve is unreliable and quite often impossible due to low statistics. The regular methods of data analysis do not apply for low statistics cases. The low statistics cases require special analysis tools. One of the most utilized methods to analyze low statistics cases is the maximum likelihood method [Sch84]. With the maximum likelihood method the decay energy and the decay half-life can be determined with reasonable accuracy.

In this method the α decay half-life $T_{1/2}$ is based on the arithmetic mean of the individual lifetimes. A correction to the mean lifetime τ must be added due to the finite search time T, which can be calculated iteratively from the equation

$$\tau = \frac{1}{N}\sum_{n=1}^{N}\tau_n + \frac{T}{e^{T/\tau}-1}\,, \tag{3.1}$$

where N is the number of nuclei and τ_n is the lifetime of the n'th individual nucleus [Seg65].

Making this correction can be avoided by making the search time T long enough so that the second term in equation 3.1 approaches zero. Usually 7 half-lives is long enough so that all the nuclei can be considered to have decayed. This applies only if the counting rate of the detector is low enough and the number of accidental correlations is not significant.

The error limits for lifetimes are based on the method presented in Ref. [Sch84]. The lower and upper error limits for the lifetime measurement can be calculated for the case of N>2 from the equations

$$\tau_u \approx \frac{\tau}{1 - z/\sqrt{N}}$$

$$\tau_l \approx \frac{\tau}{1 + z/\sqrt{N}}\,, \tag{3.2}$$

where τ is the measured mean lifetime and N is the number of events and the quantity z is determined from the chosen confidence level. If the 68.3 % confidence level is chosen, the parameter z is equal to 1. For cases with N$\leq$2 the error limits are shown in table 3.1.

Table **3.1**: The error limits for unit half-life when N$\leq$2.

Number of counts	lower error limit	upper error limit
1	0.543	5.79
2	0.606	2.82

The α-particle energy can be obtained by fitting a Gaussian curve into a peak in the α-decay energy spectrum. The centroid of the fit corresponds to the α-decay energy. This is useful especially in the situation when several α-particle decay energies are close to each other and it is not possible to separate the decay energies. Hence, a multi-curve fit has to be performed. If the number of decay events is too low to fit a Gaussian in order to determine the decay energy, the α-decay energy E_α can be determined as an arithmetic mean of the individual α-particle energies. In equation 3.3, the α-particle energy is determined as an arithmetic mean

$$E_\alpha = \frac{1}{N}\sum_{n=1}^{N} E_{\alpha n}\,. \tag{3.3}$$

The error limits for the α-particle energy can be established from the quadratic sum of standard error of the mean and from the energy calibration error. Equation 3.4 gives the error of α-particle energy as

$$\Delta E = \sqrt{\left(\frac{FWHM}{2.35 \cdot n}\right)^2 + \Delta E_{cal}^2}\,, \tag{3.4}$$

where n is the number of events, *FWHM* is the full width at half maximum of the corresponding α-decay peak and ΔE_{cal} is the calibration error.

In cases of only a few events, the FWHM can be determined from an α peak close to the energy of interest. The typical FWHM for the GREAT DSSD detectors is 25 keV at 8000 keV.

The number of accidental correlations

In the case of low statistics the observed recoil-fission, recoil-α-α or any decay events observed after recoil implantation could have been produced by random correlation with background fluctuations. Before decay chains can be labelled as real chains, or statistically significant chains, produced by the nuclei of interest, the number of observed decay chains have to be compared with the number of accidental correlations produced by random events. Simply, the purpose is to "beat the odds". If the chance for a random chain is low enough compared to the observed decay chain, the chain can be considered as statistically significant. However, in a low statistics case there is always the danger to confuse a real decay chain originating from another reaction channel. In such a case the number of accidental correlations may be very low compared to the number of observed chains, and yet the decay chain is not a correct one.

The random events obey the Poisson statistics. The number of accidental recoil-α-α correlations can be estimated using the equation by Schmidt [Sch84]. The equation can be written as

$$N_{acc} = \sum_{i=1}^{n_{pixels}} N_{evaps}(i) \frac{\lambda_m(i)\lambda_d(i)}{\lambda_t(i)^2} [1 - e^{-\lambda_t(i)\Delta t_m}][1 - e^{-\lambda_t(i)\Delta t_d}] \,, \tag{3.5}$$

where N_{evaps} is the number of evaporation residues, $\lambda_m(i)$ is the counting rate of the mother α particles, $\lambda_d(i)$ is the counting rate of the daughter α particles, $\lambda_t(i)$ is the total counting rate (the sum of the average counting rates of evaporation residues, and mother and daughter α particle counting rates), Δt_m the search time for mother α particles and Δt_d the search time for daughter α particles.

The probability that the observed number of chains would have been produced by random correlations can be estimated with equation

$$P_{err} = \sum_{n=N_{obs}}^{\infty} \frac{N_{acc}^{n}}{n!} e^{-N_{acc}} \,, \tag{3.6}$$

where P_{err} is the error probability, N_{obs} is the number of observed decay chains and N_{acc} is the number of accidental correlations obtained from equation 3.5.

4 Bρ studies

The very heavy elements are produced with a cross section of the order of picobarns or even femtobarns. In practice this means one atom being produced in a day or even one in a year. In order to study these nuclei one cannot afford to lose even a single count. In the low cross section studies with RITU the cross sections are on the order of few tens of picobarns. In these experiments RITU must be tuned so that the maximum amount of fusion recoils hit the main detector. Due to the low counting rate of the fusion products RITU cannot always be tuned during the experiment. The correct magnetic rigidity of the fusion recoils must be calculated beforehand to optimize the implantation of the evaporation residues. The separation inside the RITU magnetic field obeys fairly simple electromagnetic law, but the equations contain parameters which are difficult to determine. Thus, the calculation of the correct magnetic field is difficult.

4.1 Theoretical background

RITU is a gas-filled magnetic separator where the ions are separated in-flight according to their magnetic rigidity. As the recoiling nuclei fly through RITU they will have a known mass and a fairly constant velocity. The charge state of the ions varies around an average charge state as they fly through RITU. The RITU dipole magnet bending radius ρ is fixed to 1.85 m. The magnetic rigidity Bρ of the ion can be determined as

$$B\rho = \frac{mv}{q} \approx \frac{mv}{\overline{q}}\,, \tag{4.1}$$

where $\overline{q}$ denotes the average charge state, B the magnetic field, ρ the bending radius, m the mass of the ion and v the velocity of the ion.

The velocity of the recoil can be calculated simply from the kinetic energy of the fusion recoil immediately after fusion. This can be approximated with the equation

$$E^{ER}_{lab} = \frac{m_B}{m_{CN}} \times \frac{m_{ER}}{m_{CN}} \times E^{B}_{lab} \tag{4.2}$$

where E_{lab} is the laboratory energy, B denotes beam, ER denotes evaporation residue and CN denotes the compound nucleus.

Since the velocities are well below relativistic values, normally ≈ 2 % of the speed of light, the energy and velocity of the ion can be related as

$$E = \frac{1}{2}mv^2 \tag{4.3}$$

In equation 4.1 the parameters B, ρ, m and v are known or can be calculated fairly easily. The unknown in the equation is the average charge $\overline{q}$. The determination of the average charge is rather complex containing many uncertainties. Right after the target recoiling fusion products have 20-30 different charge states. In vacuum this would mean 20-30 different trajectories when recoils pass through a magnetic field. RITU is filled with a dilute helium gas which is used to focus the different charge states to an average charge state. In gas the charge states of the recoiling nuclei vary around an average charge $\overline{q}$.

According to Bohr's stripping criterion for an ion moving in a gaseous medium, the ion loses those orbital electrons whose orbital velocity is less than the speed of the ion. In the Thomas-Fermi atomic model the average charge state of the ion, or the number of electrons whose speed is less than the speed of the moving ion, can be approximated as

$$\overline{q} \approx \frac{v}{v_0} Z^{1/3} \tag{4.4}$$

Equation 4.4 is valid if the ion velocity v satisfies the following condition

$$1 < \frac{v}{v_0} < Z^{2/3}\,, \tag{4.5}$$

where v_0=2.19×10^6 m/s which is the velocity of the 1s electron of hydrogen atom in Bohr's atomic model. In a typical RITU experiment equation 4.5 is well satisfied.

In 1982 Brandt and Kitagawa suggested that Bohr's stripping criterion should be modified to consider the ion's electron velocity only relative to the Fermi velocity of the solid [Bra82]. The Fermi velocity is defined as the velocity of atomic electrons at Fermi level. This modification to the stopping power theories has turned out to be quite accurate. The SRIM 2003 code uses the Thomas-Fermi model modified with Brandt and Kitagawa's approximation and is known to calculate stopping powers with the accuracy of 4.8 % [SRI03].

The recoiling nucleus is in a very high charge state as it exits the target and some of the primary ions can even be fully stripped. While recoiling through the helium volume, the collisions between the ion and helium atoms strip electrons from helium atoms transferring them to the moving ion. The degree of ionization is proportional to the ion velocity. An electron is stripped if the velocity of the orbital electron is smaller than the velocity of the ion. The velocity dependence of the average charge $\overline{q}$ can be seen from equation 4.4. At the focal plane the separated fusion recoils will have a Gaussian-like position distribution in the horizontal direction. The width of the distribution is case sensitive but it is normally several centimeters. The total width of the two GREAT DSSD detectors used at the focal plane of RITU is 120 mm while in the earlier system using the PIPS detector the total width was 80 mm.

The tails of the position distribution are normally lost since the detector width is smaller than the total size of the image. If the distribution is not well centered the reduction in transmission can be significant. This has been studied at the Dubna Gas-filled Separator (DGS) which is filled with hydrogen [Oga01]. Figure 4.1 shows how broad the fusion product distribution is at the focal plane of DGS. The width of the fusion distribution at the RITU focal plane is comparable to figure 4.1. The width of the distribution presented in figure 4.1 is often referred to as image size. The illustration of the effect of Bρ to the position of the focal point is presented in figure 4.1. This property is often referred to as dispersion.

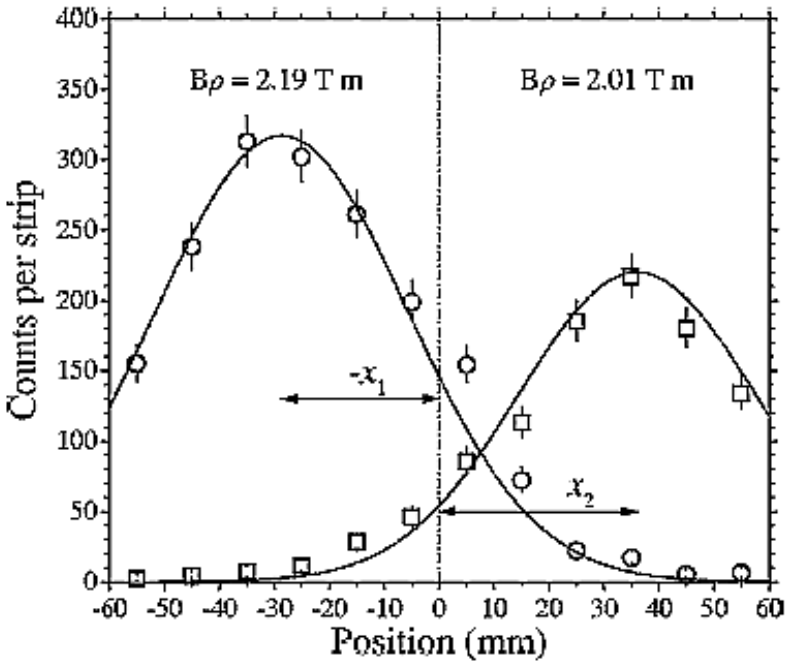

Figure **4.1**: Focal plane horizontal distribution of ^{252}No ions corresponding to 9 % change in magnetic rigidity in DGS. Figure is adapted from [Oga01].

RITU was never designed to use hydrogen as filling gas. The average charge state of the fusion recoils is dependent on the proton number of the gas. Thus use of hydrogen would require stronger magnetic fields since the average charge states of the recoils is lower in hydrogen than in helium. At present the maximum magnetic dipole field that can be achieved by RITU is 1.2 T and in the heavy element region (Z≥100) the required magnetic fields in helium mode are around 1.1-1.15 T. Thus for heavy and very asymmetric reactions the current RITU dipole magnet is not strong enough to operate in hydrogen mode. In addition hydrogen gas is highly explosive and the gas handling system would be more complex.

4.2 Empirical formulae

Empirical formulae have been used to calculate the average charge state of heavy ions passing through a dilute gas. In this work the emphasis has been on heavy ions in dilute helium gas since these are the working conditions for RITU. Dilute hydrogen is also being utilized as a filling gas in the DGS separator at Dubna. Empirical average charge state formulae have been constructed for ions in hydrogen by Yu. Oganessian et al. [Oga01]. The interactions between two colliding atoms involve many-body systems and the charge exchange between these systems is a very complex phenomenon. The process of the charge exchange is so complex that today there is no reliable theory for predicting the mean charge of heavy ions moving through a dilute gas. Practically all the available information has been obtained either experimentally or by very approximate models [Oga01]. Several formulae have been constructed over the years in various institutes. The first empirical formula was developed by Nikolaev in 1968 [Nik68]. Nikolaev studied the average charge state of Br, I, Ta and U passing through solids and constructed a semi-empirical formula for the average charge $\overline{q}$. This formula is valid for ions with Z≥20.

$$\overline{q} = Z\left[1 + \left(\frac{v}{Z^{\alpha}\, v'}\right)^{-\frac{1}{k}}\right]^{-k}, \tag{4.6}$$

where α, k and v' are experimentally determined parameters having values α=0.45, k=0.6 and v'=3.6×10^6 m/s.

In the early 1970's H.D. Betz made an extensive survey of the available theoretical and experimental data. As a result of this study a formula was constructed in order to determine the average charge of ions in dilute helium gas medium. The equation 4.7 is mainly valid for ions with atomic number 16≤Z≤92 with $v_o < v < Zv_o$, where v_0=2.19×10^6 m/s or Bohr's velocity [Bet72].

$$\overline{q} = Z\left[1 - C_0\, e^{-C_1\left(\frac{v}{v_0}\right)Z^{-2/3}}\right], \tag{4.7}$$

where C_0 and C_1 are determined by fitting the parameters into experimental data. For C_0=C_1=1 a first order expansion of the exponential gives the equation 4.4.

In the 1980's Ghiorso et al., took all the experimental data available at the time. Equation 4.7 was fitted to the data points and the parameters C_0 and C_1 were determined. The values for the parameters were found to be C_0=1.04 and C_1=0.91 [Ghi88]. The resulting equation, along with equation 4.9, is quite often used to calculate the average charge state $\overline{q}$ in RITU experiments.

$$\overline{q} = Z\left[1 - 1.04\, e^{-0.91\left(\frac{v}{v_0}\right)Z^{-2/3}}\right] \tag{4.8}$$

Meanwhile the research group at Dubna was actively studying the subject. Yu. Oganessian has studied the problem for several years and constructed empirical formulae for both filling gases, helium and hydrogen. The following formula is the most popular for determining the average charge state ($\overline{q}$) for RITU experiments. The equation can be used with an accuracy of about 5 % and it is valid for ions with 60<Z<101 [Oga91]. In table 4.2 this equation is labelled as Ogan. 1.

$$\begin{aligned} &\text{if} \quad vZ^{1/3} < 2\times 10^7; \qquad \overline{q} = 1.8\times 10^{-7}\, vZ^{1/3} + 1.65 \\ &\text{if} \quad vZ^{1/3} > 2\times 10^7; \qquad \overline{q} = 3.3\times 10^{-7}\, vZ^{1/3} - 1.18 \end{aligned} \tag{4.9}$$

After additional measurements with improved statistics Yu. Oganessian et al. constructed another mean charge state equation (equation 4.10). The data are from experiments performed with the DGS separator at Dubna. Equation 4.10 covers the whole velocity range while equation 4.9 has different forms for different velocity ranges. In table 4.2 the equation 4.10 is labelled as Ogan. 2.

$$\overline{q} = 0.00871\left(\frac{v}{v_0}\right)^{1.54} Z^{1.10} + 2.05\,, \tag{4.10}$$

where the Bohr velocity is v_0=2.19×10^6 m/s.

The latest work and probably the most general formula have been published by G. Schiwietz in 2001 [Sch01]. In this study a wide range of experimental charge distributions were analyzed and an empirical formula was fitted to the experimental data.

The empirical formula is valid for heavy ions in gaseous and in solid targets. The ions range from protons all the way up to uranium while the targets, or in RITU's case filling gases, cover all the gases [Sch01]. The equation for average charges in solid targets is not presented here. Equation 4.11 shows the method to determine the average charge in any of the gaseous targets

$$\overline{q} = Z\frac{376x + x^6}{1428 - 1206\,x^{0.5} + 690x + x^6}$$

with

$$x = \left[\left(\frac{v_p}{v_0}\right) Z_p^{-0.52} Z_t^{\left[0.03-0.017\, Z_p^{-0.52}\left(\frac{v_p}{v_0}\right)\right]}\right]^{1+0.4/Z_p}, \tag{4.11}$$

where the subscript t stands for gas (target) and p for ion (projectile). Equation 4.11 can be used with a relative uncertainty of $\Delta\overline{q}/Z_p = 2.6$ % which is comparable to the uncertainty of Bohr's stripping criterion $\Delta\overline{q}/Z_p = 4.7$ %.

4.3 Calculating the average charge

Calculating the average charge state is not as straightforward as it seems at first. The input data needed for the equations are not easily obtained. The average charge calculated with equations 4.6-4.11 is dependent on the fusion recoil velocity. The initial kinetic energy of the fusion recoil can be calculated with equation 4.2. The velocity of the recoil is reduced significantly by the target. In addition, there are energy losses in the helium volume before the RITU magnetic dipole where the actual separation takes place. By knowing the stopping powers of the target material and the helium volume the recoil velocity at the center of the dipole can be determined. Thus the average charge and finally the required Bρ value of the ion can be determined with the equation 4.1. The determination of the recoil velocity for heavy and slow ions is difficult since the stopping powers for elements heavier than uranium (Z=92) in various target materials are not well known. This is due to that at slow velocities the ionization energies of different electronic orbitals come into play. The determination of stopping powers for transuranium ions is challenging both experimentally and theoretically. The knowledge of ionization energies in the transuranium region is still sparse. One could neglect the ionization energies and estimate the stopping power from the Coulomb repulsion assuming a bare nucleus, but this method is not very accurate [Zie05].

4.3.1 Determining the stopping powers

The energy of the primary beam is known to an accuracy of ±1 MeV. The center of target energy can be calculated if the energy losses in helium and in the target are known. The stopping powers of different materials and elements (up to uranium (Z=92)) have been calculated with the help of SRIM 2003. The stopping powers for ions heavier than uranium cannot be found from SRIM. In the recent heavy element studies with RITU it has been necessary to determine the stopping powers of the heavy elements with Z≥100.

The stopping powers of transuranium (93≤Z≤103) ions are calculated and tabulated in Ref. [Nor70]. These values are obtained from different extrapolations of experimental stopping power data up to iodine (Z=53). The extrapolation of the stopping power curves around and below 0.1 MeV/amu were guided by the predictions from the LSS-theory [Lin63], [Nor70]. The typical energy of a fusion product at the middle of the target is approximately 0.15 MeV/u. All the experimentally measured stopping power tables end at 1 MeV/u. Below this energy the atomic shell effects start to play a crucial role.

Unfortunately none of the stopping power theories take atomic shell effects into account. Therefore only estimates of stopping powers can be made. In the present work the stopping powers have been calculated with the help of SRIM 2003 for recoils with Z=66-92. The stopping powers were plotted as a function of Z while the velocity of the recoiling ion was kept constant. Although the SRIM program is not ideal, since the ionization of electronic orbitals should be taken into account, it is the best available means of estimating stopping powers. Unfortunately, SRIM tends to underestimate the stopping powers [Zie05]. By plotting stopping powers as a function of Z the general trend of the stopping power at constant velocity of E≈0.15 MeV/u can be obtained. The stopping powers in the Z≥100 region can be estimated by extrapolation. The extrapolation of data points is difficult due to scattering effects from different electron shells. This is particularly well represented by the odd-even staggering in the heavier elements. The atomic structure of the transfermium elements has been studied and the atomic configurations are known, yet the energy losses in different materials are unknown. Intuitively the value of the stopping power should increase with increasing Z. In figure 4.2, two different stopping power curves are displayed. The SRIM curve is calculated by using SRIM 2003 code and shows an interpolation of different data points. The N-S curve represents tabulated Northcliffe-Schilling stopping power values (N-S) and interpolation of different data points [Nor70]. In both cases the velocity of an ion has been kept constant, in SRIM it was 0.15 MeV/u which corresponded to a real experimental value and in N-S the tabulated 0.16 MeV/u values were taken.

Different functions were fitted to the data points calculated with SRIM and the best fit was determined. The predictive power in this case is difficult to define since reliable

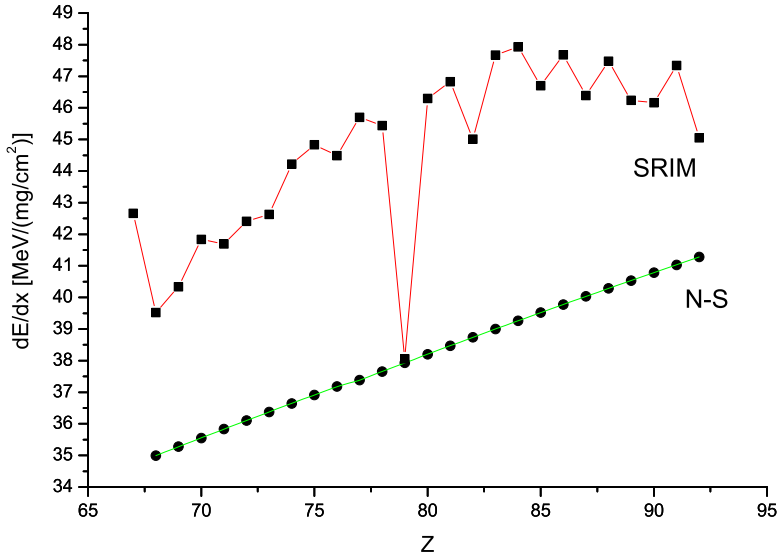

Figure **4.2**: Interpolation of the stopping power data points as a function of Z in helium calculated by using the SRIM 2003 and Ref. [Nor70]. The curves represent different models of stopping power. The SRIM values have been calculated at an energy of 0.15 MeV/u while the Northcliffe-Schilling (labeled as N-S) values are taken from tabulated values at 0.16 MeV/u.

experimental stopping power data are not available for heavy elements with Z>92 at low energies E≈0.1 MeV/u. The overall trend is increasing but starting from Z=83 the stopping powers decrease which contradicts with the overall trend. The fitted function tries to follow the overall trend and thus is a very crude approximation. The function can be written as

$$\frac{dE}{dx} = a \times ln(Z) - b \quad \left[\frac{MeV}{mg/cm^2}\right], \tag{4.12}$$

where a and b are adjustable parameters. The fitted values for a and b were 5.0 and 13.6 respectively.

The stopping powers calculated for transfermiums with the equation 4.12 contain large margins of error and the estimated values are not very accurate.

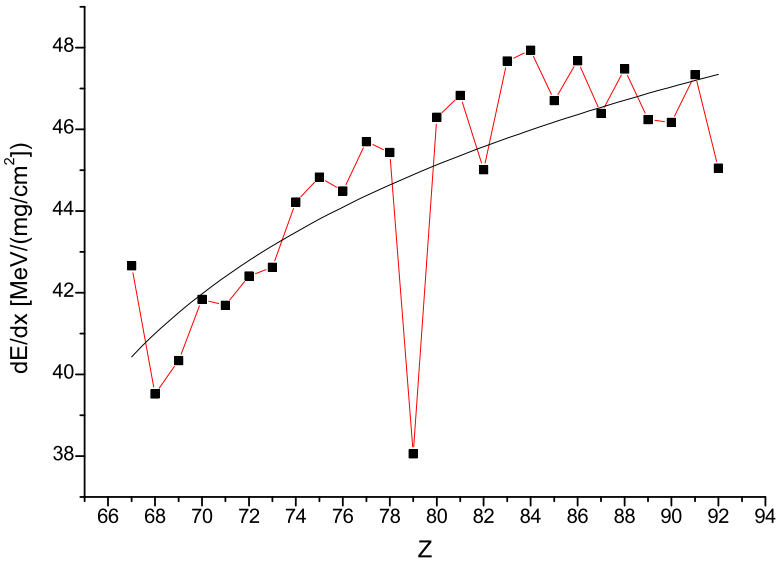

Figure **4.3**: Logarithm function fit to the stopping powers in helium obtained from SRIM 2003. The velocity of the ion was 0.15 MeV/amu.

4.4 Comparison between theoretical and experimental values

There are several empirical formulae available to calculate the average charge of an ion in helium gas. Each of them is tuned to match experimental data obtained from certain area of the chart of nuclides. A problem arises when one does experiments with heavy elements with Z>92. The formulae presented in Section 4.2 were fitted to the data points obtained from the lighter regions of the nuclear chart. The question is which of the formulae presented gives the most realistic result in the heavier region when the average charge ($\overline{q}$) is used in equation 4.1. The reference Bρ value can be obtained from the magnetic field values used in RITU heavy element studies. A comparison between the experimental magnetic field values and calculated magnetic field values, where the average charge have been calculated with equations 4.7-4.11, determines the most feasible average charge formula in the heavy element region.

In the average charge calculations the velocity of the ion plays a crucial role. With respect to RITU experiments one cannot use the E_{Lab} directly but several energy losses have to be taken into account as discussed in Section 4.3. Most of the energy loss takes place in the target but also different degraders change the energy of recoiling ion significantly. For example, an increase in beam energy increases the recoil velocity and since the average charge is velocity dependent, the average charge is increased. In

a magnetic field, such as the RITU dipole field, a higher charge state forces ions into a trajectory with smaller radius of curvature. Intuitively, one would easily think the increase in beam energy would force the ions into a trajectory with greater radius of curvature and thus higher magnetic fields would be required to focus the beam.

Table 4.1 shows quite a wide spread of the predicted average charge states calculated with different equations. The equation by Betz was developed in the 1960's when the experimental data in the heavy element region was sparse, thus the inaccuracy of the equation in the heavy element region. The rest of the equations show a fairly small spread of the average charge.

Table **4.1**: Average charge states in dilute helium calculated with equations presented in this chapter. The energies of the ions are taken from real experiments and the helium pressure corresponds to actual RITU helium pressure of 0.6 mbar. In the table Betz refers to equation 4.7, Ghiorso refers to equation 4.8, Ogan. 1 refers to equation 4.9, Ogan. 2 refers to equation 4.10 and Schiw. refers to equation 4.11.

Ion	Betz	Ghiorso	Ogan.1	Ogan.2	Schiw.
^{245}Fm	9.6	5.1	6.1	6.6	7.3
^{250}Fm	11.6	7.1	7.8	8.3	9.3
^{251}Md	10.9	6.3	7.2	7.7	8.6
^{252}No	10.8	6.2	7.0	7.6	8.4
^{253}No	10.7	6.1	7.0	7.6	8.4
^{254}No	10.8	6.2	7.0	7.6	8.4
^{255}No	10.6	6.0	6.9	7.5	8.3
^{255}Lr	10.7	6.1	7.0	7.6	8.4
^{257}Rf	10.0	5.3	6.4	7.0	7.7
^{255}Db	10.7	6.0	7.0	7.6	8.4

In table 4.2, the calculated magnetic field values are compared to those used in actual RITU experiments. The average charge states were taken from table 4.1. All of the equations 4.7-4.11 are used in the comparison. Over the years different helium pressures have been used in RITU. This affects the energy losses of the recoiling ion inside RITU gas volume which affects the average charge and thus the trajectory of the ion. The effect of helium pressure on the trajectory can be seen in table 4.2. Some of the experiments have been re-done due to the improvements in the RITU separator and in the detector performance. Lower helium pressures have been used especially in the experiments made after the installation of the new dipole chamber and differential pumping system in the fall of 2001. In table 4.2 the Experimental 1 values refer to magnetic field values when helium pressure of 1 mbar was used and Experimental 2 values refer to magnetic field values when He pressure of 0.6 mbar was used. The column Δ% shows the difference between the calculated value and the actual experimental value in percent. The difference to the experimental values was only calculated for equations 4.8 and 4.9 since they were the closest ones to the experimental ones.

Table **4.2**: Calculated magnetic field values compared with magnetic field values used in experiments. All the values are expressed in units of Tesla [T]. The column Exp. 1 refers to magnetic field values used with 1 mbar He pressure while Exp. 2 refers to magnetic field values used in 0.6 mbar He pressure. The column labelled with Δ% refers to the percentage difference between experimental and calculated values. The difference to experimental values is calculated from the experimental 2 value if available otherwise from the experimental 1 value.

Ion	Exp.1	Exp.2	Betz	Ghi.	Δ%	Ogan.1	Δ%	Ogan.2	Schiw.
^{245}Fm	1.083		0.680	1.277	17.9	1.070	-1.2	0.987	0.888
^{250}Fm	1.155	1.137	0.702	1.154	1.5	1.053	-7.4	0.984	0.882
^{251}Md		1.137	0.699	1.204	5.9	1.066	-6.3	0.991	0.890
^{252}No	1.121		0.699	1.220	7.4	1.069	-6.0	0.989	0.892
^{253}No	1.142	1.155	0.701	1.228	6.4	1.074	-7.0	0.993	0.896
^{254}No	1.131	1.149	0.704	1.231	7.1	1.078	-6.2	0.997	0.899
^{255}No		1.161	0.707	1.248	7.2	1.085	-6.6	1.003	0.905
^{255}Lr	1.149	1.167	0.704	1.241	6.4	1.079	-7.5	0.994	0.900
^{257}Rf		1.170	0.415	1.318	13.0	1.099	-5.9	1.003	0.913
^{255}Db		1.133	0.411	1.251	10.4	1.073	-5.3	0.980	0.894

The magnetic field value used in the ^{255}Db experiment was calculated before the experiment using the method and equation 4.9 described in this chapter. During the experiment only 3 events were observed and thus the magnetic field value tabulated in the table 4.2 may not represent the optimum.

4.5 Conclusions

Table 4.2 compares the calculated and measured magnetic field values. In this study the equations Ghi. (equation 4.8) and Ogan. 1 (equation 4.9) predicted the magnetic field values most accurately.

The difference between experimental and theoretical values is very reasonable considering all the uncertainties in the average charge state models, in beam energy and in the stopping powers of different media. The general trend is that equation 4.8 underestimates and the equation 4.9 over estimates the average charge. The most reliable equation in light of this study would be equation 4.9 since the relative difference to experimental values is fairly constant of 5-7 %. Empirically, equation 4.8 does not work well for light or medium mass ions but works quite well in the heavy element region. Equation 4.9 is the most universal one of all the formulae since it works fairly well in the mass regions A>100 [Uus05].

The measured RITU momentum dispersion is 12-13 mm/%(ΔB) [Kos05]. The differ-

ence of 5-7 % in RITU dipole field changes the image in horizontal direction 60-90 mm. When taking the detector size into consideration, 80 mm for PIPS detector and 120 mm for the DSSD, the 5 % error in RITU dipole field reduces the detection efficiency by more than 50 %. Thus the predetermined magnetic field value, calculated with equation 4.8 or with equation 4.9, must be corrected towards higher values on the average by 6 % to avoid the reduction in detection efficiency. This is especially important in heavy element experiments where production cross sections are small and where the tuning of RITU in the middle of the experiment is difficult. The difference of 1-2 % in magnetic field value to the optimum is within the acceptable limits since the reduction in detection efficiency is not significant.

5 Alpha decay study of ^{218}U

5.1 Motivation

The neutron-deficient uranium nucleus ^{218}U is suggested to be a doubly magic nucleus with Z=92 and N=126 by assuming a sub-shell gap at Z=92 between the $h_{9/2}$ and the $f_{7/2}$ proton orbitals. This is predicted by many recent theoretical calculations [Rut98], [Möl97]. The Nilsson diagram for the deformed nuclei has been quite successful in explaining the single-particle levels and the semi-magic numbers when the super-heavy elements have been studied. Since the Nilsson diagrams partly rely on the input of single-particle shell model energies also the magicity of Z=92 has an important role. This picture is in contradiction with the recent experimental results studying N=126 isotones [Hau01],[Heß02]. The standard mean field model does not take into account octupole correlations which can distort the orbitals significantly. The current detector system is not sensitive enough for in-beam γ spectroscopy at nanobarn level. At nanobarn level the ^{218}U nuclear structure can be probed with α spectroscopy. Thus detecting a relatively low energy shell-model isomer in ^{218}U would give some evidence against the sub-shell gap at Z=92.

5.1.1 Odd-even cases

The odd members of the N=126 isotones have been studied extensively. The states above the Z=82 magic shell gap are $h_{9/2}$, $f_{7/2}$ and $i_{13/2}$. By forming particle-hole excitations with the odd proton several different states with different spins and parities can be formed. The heavier odd N=126 isotopes, ^{215}Ac and ^{217}Pa, have been studied experimentally with α decay in the Refs. [Kuu04], [Iku98], [Heß02]. In the recent study no α-decaying isomers have been found in ^{215}Ac. The heavier odd-N=126 isotope ^{217}Pa has α-decaying isomers which are based on particle-hole excitations between proton $h_{9/2}$ and $f_{7/2}$ or $h_{9/2}$ and $i_{13/2}$ orbitals. The α decay from these isomeric states is hindered due to a large difference in angular momentum between the initial and final states. There is some dispute over the interpretations of the experimental results and the ordering of the single particle levels is uncertain. F. Heßberger in Ref. [Heß02] has concluded that the isomeric decay would come from a state with the configuration $\pi(h_{9/2}f_{7/2}i_{13/2})$ coupled to spin $29/2^+$. With this interpretation the lifetime of the state and the change of the angular momentum between the initial and final states does

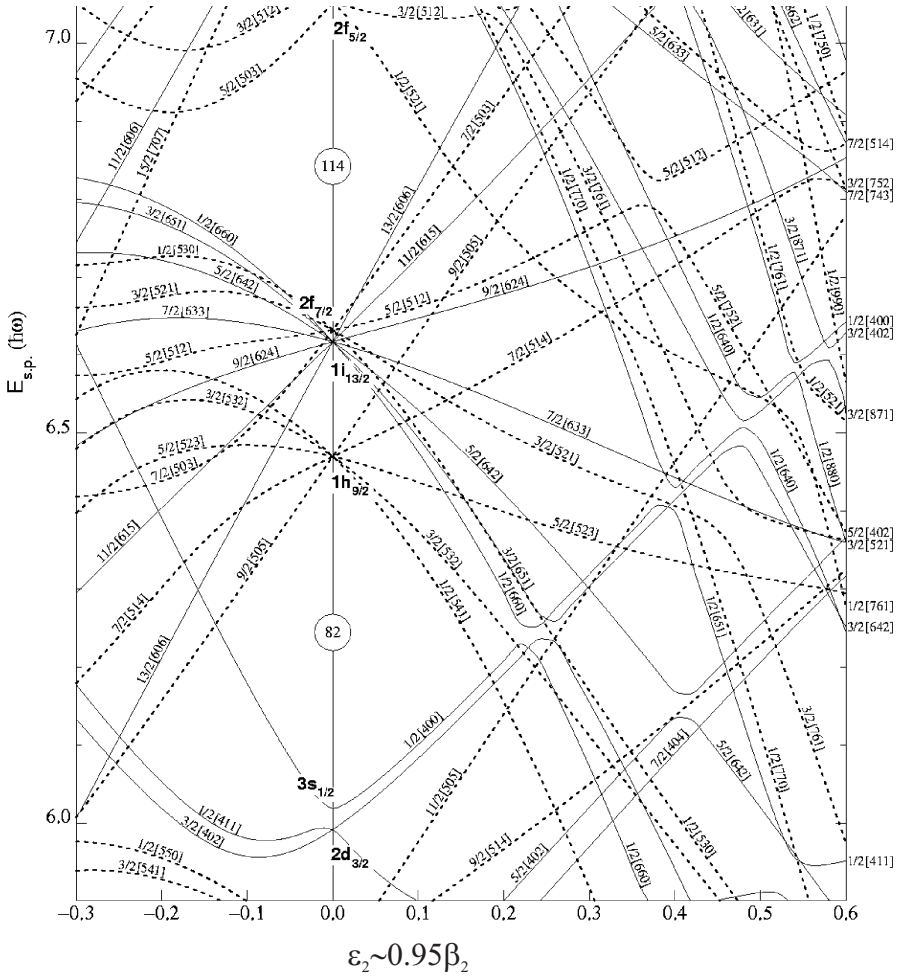

Figure **5.1**: Single particle levels above Z=82. The full $h_{9/2}$ orbital would correspond to the magic sub-shell Z=92. The figure is adapted from [Fir96].

not follow the systematics of Rasmussen. This is interpreted as an anomaly in ^{217}Pa [Heß02]. In addition this picture contradicts the recent shell model calculations by Caurier et al. [Cau03].

5.1.2 Even-even cases

The recent shell model calculations by Caurier et al. do not support the shell gap theory but rather a scenario where the shell gap is non-existent. The occurrence of a low-lying isomeric state in ^{216}Th is cited as evidence against the existence of a shell gap. In ^{216}Th an 8^+ state, with a $\pi h_{9/2}\pi f_{7/2}$ configuration, has been found to be closer in energy to the 6^+ state, forming an isomer with a 5 % α-decay branch [Hau01]. While several other N=126 isotones have been studied extensively, in ^{218}U only the

ground state properties were known with fairly poor statistics. The discovery of a low lying isomeric state in ^{218}U would speak against the existence of a sub-shell gap at Z=92 [Lep05]

The same orbitals play a role in the ^{218}U case as in the odd-even cases but with the exception that the $h_{9/2}$ proton orbital is now completely full. The nucleus can be excited by breaking a proton pair and exciting a proton to the $f_{7/2}$ or $i_{13/2}$ orbital. In the shell model calculations the 8^+ state is predicted to have a lower excitation energy than 6^+ state forming an yrast trap [Cau03]. Such an yrast trap would have a sufficiently long half-life to survive the flight time through RITU and to be detected at the RITU focal plane with the efficient GREAT spectrometer.

The light uranium isotopes have been studied previously but with rather poor statistics. Only 4 chains of ^{218}U have been synthesized before [And92]. The same applies for other light uranium isotopes, only 3 chains of ^{217}U and 6 chains of ^{219}U have been synthesized and thus more statistics were needed to determine decay properties accurately [Mal00], [And93a].

5.2 The experiments with ^{40}Ar beam

In this study two separate experiments were performed one year apart. Between the experiments the focal plane detector setup was upgraded from the setup of H. Kettunen presented in Section 3.3.1 to the new GREAT spectrometer presented in Section 3.4 [Ket01], [Pag03]. In addition, the data acquisition system was upgraded from the old VME based system to the TDR data acquisition. The experiments were carried out at the JYFL cyclotron laboratory with the RITU recoil separator. Both experiments were RITU "stand-alone" experiments where only MWPC, DSSD pair and PIN diodes of the GREAT spectrometer were used. This allowed the use of relatively intense beams on target e.g. the average beam intensity in the second experiment was 140 pnA. The data from these experiments were analyzed separately and the results were combined. The experimental data from the first experiment was analyzed with a separate sort code while the second set of experimental data was analyzed with the GRAIN package [Rah05]. Both sorting methods are described in Section 3.6.1.

A beam of ^{40}Ar at an energy of E_{lab}=186 MeV was used to bombard a ^{182}W target of 600 μg/cm^2 thickness. The desired reaction channel was ^{182}W(^{40}Ar,4n)^{218}U. This reaction was similar to the reaction of Hauschild et al. used in the ^{216}Th experiment [Hau01]. All the experimental details have been recorded in table 5.1. The other option was to use the reaction ^{174}Yb(^{48}Ti,4n)^{218}U. Since the ^{40}Ar beam has a significant advantage in beam intensity the former reaction was selected. The ^{40}Ar beam compared to ^{48}Ti beam can be produced 3-5 times higher in intensity [Koi05].

Table **5.1**: Summary of the experimental details

Beam	$^{40}Ar^{8+}$
Beam energy (E_{lab})	186 MeV
Excitation energy (E^*)	45 MeV
Target	^{182}W
Target thickness	600 μg/cm^2
Irradiation time	97 h
Total dose	3×10^{17} part.

5.2.1 Calibration

The DSSDs were calibrated with an internal calibration. The internal calibration allowed a more accurate calibration at higher α-decay energies than the standard α source. The internal calibration was performed with the beam of ^{40}Ar which was used to bombard a ^{175}Lu target. The compound nucleus was ^{215}Ac which is one of the N=126 isotones. The α-decay energies of the fusion products in the calibration runs range from 6900-7500 keV. The energies are only 1.5-2 MeV lower than the α-decay energy of the uranium isotopes of interest. Figure 5.2 shows the calibration spectrum after energy calibration and gain matching of the DSSD strips. The α-decay peaks were identified and 3 peaks were chosen for calibration. These peaks were chosen because they were single peaks which spread across the whole energy region used in the calibration runs. In figure 5.2 the peaks used in the calibration have been indicated with arrows.

5.2.2 The RITU-GREAT experiment

The same reaction and beam energy was used in the first experiment but with different detector equipment. The event chains were constructed offline with the GRAIN package [Rah05]. The major improvements in the second experiment were the reduction in accidental recoil-α correlations due to the higher granularity of the DSSD detector and the TDR data acquisition system eliminates common deadtime. Figure 5.3 shows the α-decay energy versus the lifetime of the decay events. The TDR electronics dead time can be estimated from the figure by looking at the individual lifetimes of ^{218}Pa. The dead time in the second experiment was around 15 μs while in the first experiment with the old data acquisition system the dead time was of the order of 200 μs.

The reduction in the background from the scattered beam particles was greatly enhanced due to the new dipole chamber. The separation of the beam and fusion products is very clear resulting in a high quality α spectrum and also reducing the number

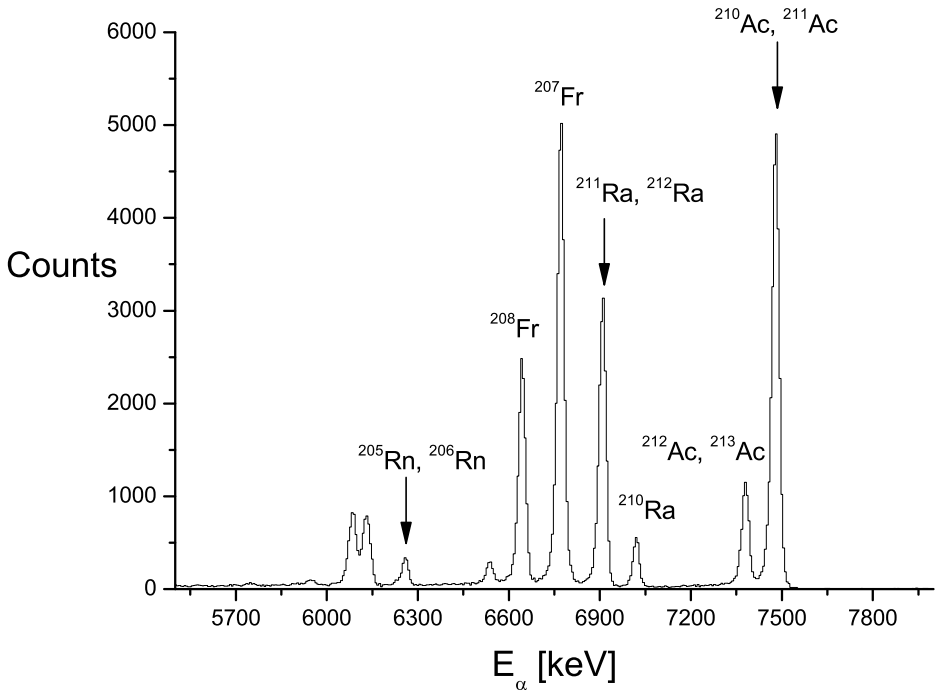

Figure **5.2**: Internal α calibration spectrum. The peaks used in the calibration are indicated with arrows.

of accidental correlations. Indeed, the recoil-gated α spectrum shows the very weak decay channels which are apparent above the background.

In order to select fusion recoils from the vast number of implantation events, the correlation method was used. The known α particles were correlated with recoil-like events with fully open gates. Figure 5.4 shows the online analysis plots of the uncorrelated TOF versus ΔE 2-D plot in top figure and on the bottom figure the correlated TOF versus ΔE. The bottom shows recoils correlated with the most intense α-decay peaks within 80 ms search time. The intensity of the spectrum b) has been enhanced compared to the spectrum a). The method picks out the real fusion recoils and thus the recoil TOF and recoil energy gates can be obtained to be used in the search for uranium recoil-α-α chains.

In the second experiment more statistics were collected and the new isomer in ^{218}U was measured with improved statistics. The energy of the isomer could be determined more precisely and moreover the improved precision in timing allowed a better determination of the decay half-life.

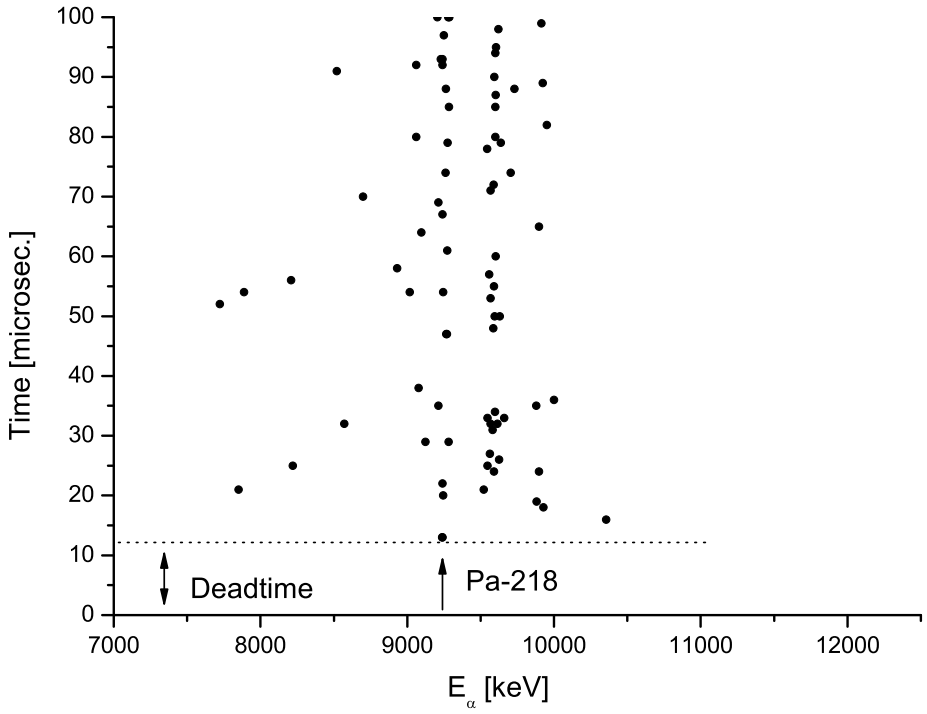

Figure **5.3**: Alpha decay energies versus the corresponding event lifetimes. The data acquisition dead time is the shortest lifetime detected in the experiment.

5.3 Data analysis

Both experiments were analyzed with their own sort code although the principles are the same. The data analysis from the second experiment with GREAT spectrometer is described here because it is the latest spectrometer development.

The gas vetoed α spectrum in the figure 5.5a shows only the strongest α-decay peaks. The interesting energy region suffers from a strong background from scattered beam particles and energetic α particles which punch through the DSSD detector. The MWPC cannot veto these energetic α particles since they are too fast to leave a detectable amount of energy in the MWPC. Figure 5.5b shows the gas vetoed and correlated α spectra with 100 ms search time. The strongest fusion evaporation channel in this experiment was not an xn-channel but an αxn-channel. In figure 5.5a the thorium isotopes ^{215}Th and ^{216}Th, are products from α3n and α2n evaporation channels, respectively, while the radium isotopes are daughters of thorium isotopes and the radon isotopes are produced in the decay process of radium.

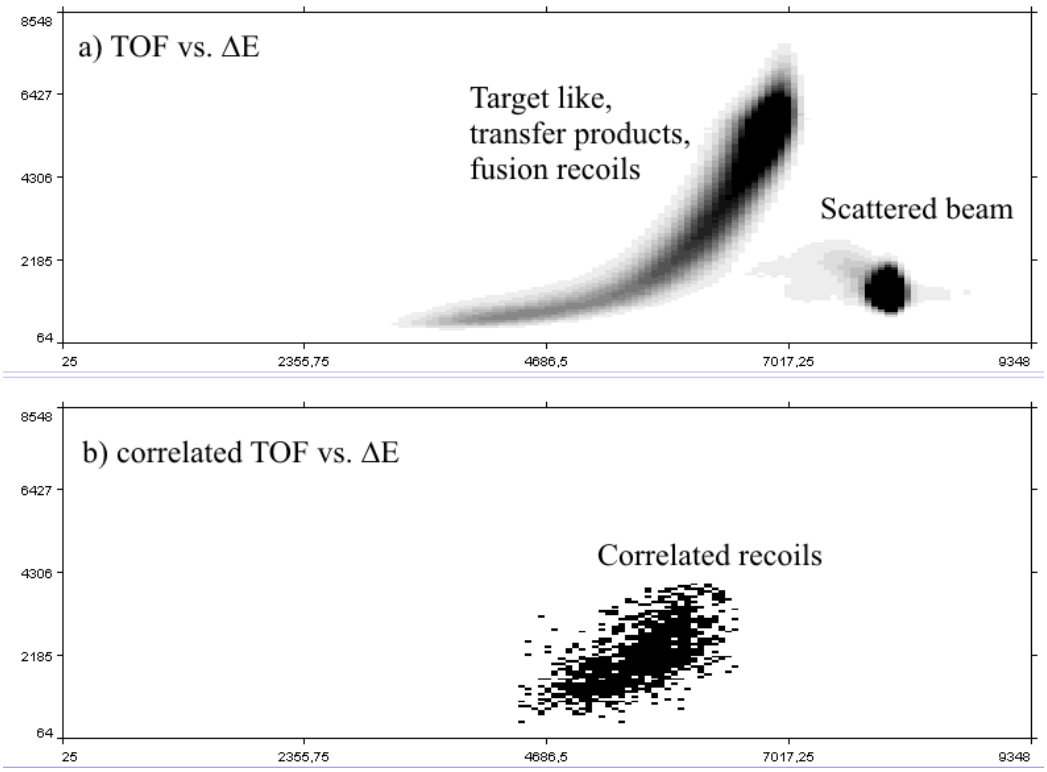

Figure **5.4**: Two GRAIN views; Time-Of-Flight versus energy loss (ΔE) in the MWPC in the figure a). The figure b) shows the location of the correlated fusion recoils within 80 ms search time, the intensity has been enhanced compared to the figure a). The units on the axes are arbitrary.

The recoil decay correlation method was used to identify decay chains. Each α decay was correlated back in time only with a recoil event within the same pixel and within a given time and position window. In some cases the decay events may be found in neighbouring pixels due to the current leakage and it would be justified to expand the search. This was not used because it increases the number of accidental correlations significantly compared with the number of additional real chains obtained. Thus only events within the same pixel were used in the correlation analysis. The recoil-α correlated spectrum is shown in the figure 5.5 b.

The spectrum quality is very good with little background. The peaks of different uranium isotopes are visible and they are indicated in the spectrum. Since the produced light uranium isotopes were measured earlier the observed decay energies could be compared with known decay energies [And92], [And93a]. The correlation method was used to correlate with the daughter and granddaughter α decays. The decay chain could not be extended further since the great-granddaughters of $^{217-219}$U isotopes decay via β^+-decay.

Figure 5.6 shows the observed mother-α daughter-α correlations. The uranium iso-

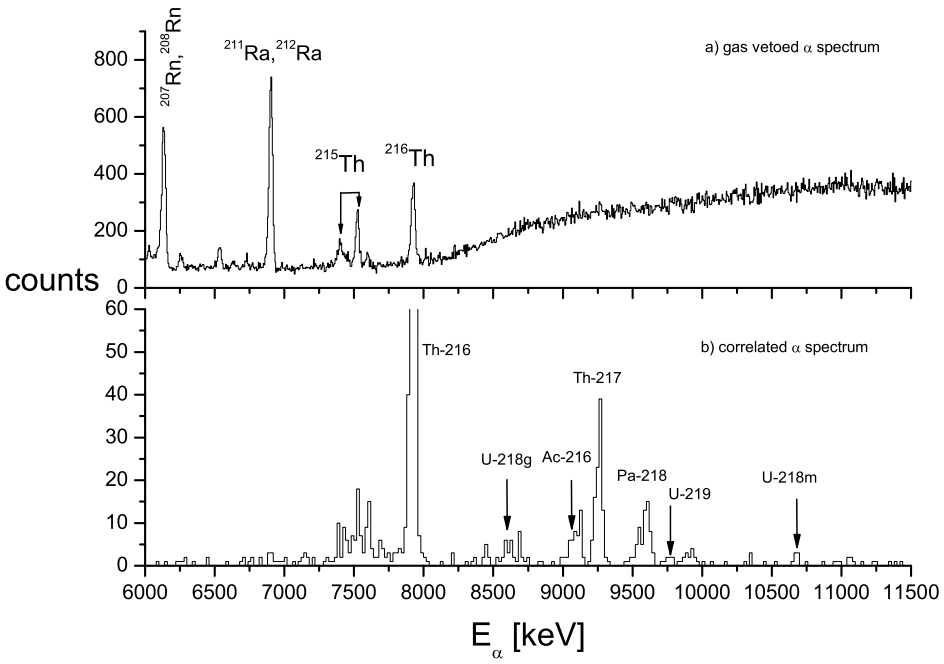

Figure **5.5**: a) shows the gas vetoed α spectrum. The decay peaks from the strongest reaction channel products are visible. b) shows the gas vetoed and recoil correlated α spectrum within the energy window of 6000-11500 keV and within the time window of 100 ms. Most of the background is suppressed allowing even the weakest α-decay peaks to be observed. Both of the figures are taken from the RITU-GREAT experiment.

topes are circled in this plot. If the daughter α has escaped and the search time is long enough, the correlation between the mother α and the granddaughter α can be observed. These types of correlations can be found directly below the mother-daughter correlations. A search time of 20 s. was used in the α-α correlations. The correlated ^{218}U and ^{219}U pairs are circled in figure 5.6.

In the second experiment the PIN diode box was also utilized. The PIN diodes can be used to clean the low-energy part of the α-decay spectrum by vetoing all the decay α particles detected in coincidence with an event in the PIN diodes. The α-particle range in silicon at these energies is 50-60 μm while the implantation depth of a recoil is only around 10 μm. Almost half of the α particles escape leaving only 1-2 MeV of energy in the detector.

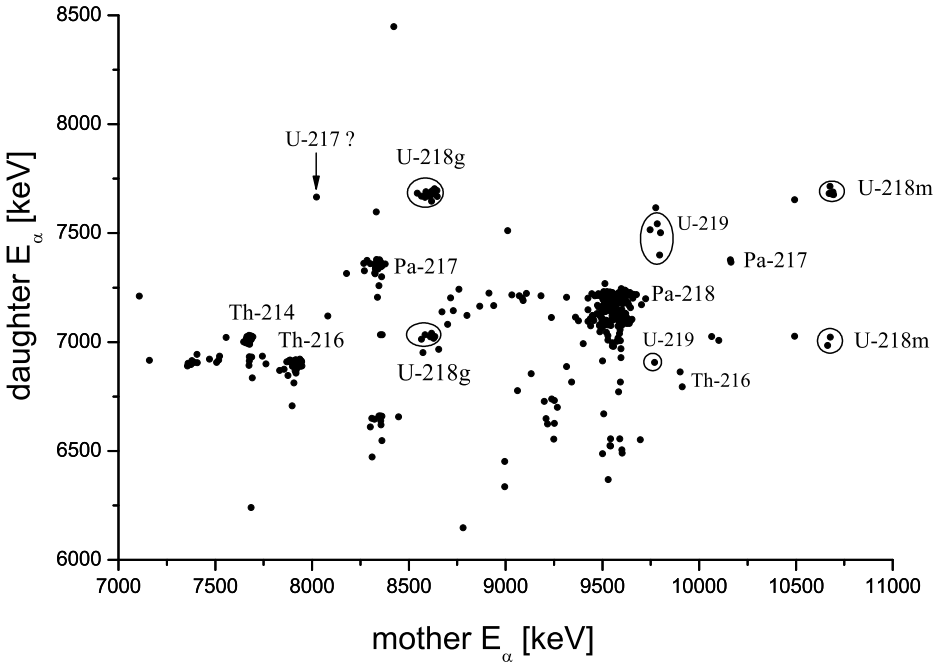

Figure **5.6**: Mother α energy versus daughter alpha energy from the irradiation of ^{40}Ar+^{182}W at E*= 45 MeV. The search time for recoil-α correlations was 100 ms, and the search time for α-α correlations was 20 s.

5.3.1 Observed decay chains

In figure 5.6 there are many correlations indicating decay chains of different isotopes. The 4n neutron evaporation channel is only a weak channel among many other open decay channels. The protactinium isotopes form broad blobs in the α-α correlated mother versus daughter α plot which is due to α-electron summing. The α decay is associated with a prompt emission of a conversion electron and the energies from two separate events are summed and the data acquisition only sees a single pulse from the DSSD. The energy of a conversion electron is well defined but the energy loss of an electron in the DSSD varies depending on the incident angle with respect to the DSSD. The result is a very broad distribution of decay energies.

The main interest lies in the uranium isotopes. The uranium decay chains were identified from figure 5.6 where the chains are labelled. The statistics were significantly improved compared to the previous experiments presented in Ref. [And92], [And93a]. This allowed the ground state properties of the ^{218}U and ^{219}U isotopes to be measured more accurately. The most interest in this experiment lies in the α-decaying isomeric

state in ^{218}U which was observed for the first time. The observed isomeric state in ^{218}U has a significant meaning in the debate of sub-shell closure at Z=92. A similar isomeric state has been observed in ^{216}Th which is an isotone of ^{218}U. The total number of recoil-α-α decay chains identified in the experiments were 20 of ^{218g}U, 12 of ^{218m}U, 5 of ^{219}U and in addition 1 candidate event of ^{217}U.

The half-lives of the isotopes were determined from the average of the individual lifetimes. Interestingly, in ^{218}U the half-life of the isomer seems to be longer than the half-life of the ground state. The high spin of the decaying state extends the total barrier to be penetrated by an α particle so that it compensates the difference in decay energy. Thus the decay energy and half-life do not follow the general Geiger-Nuttall systematics. Table 5.2 shows a summary of the data

Table **5.2**: Summary of the results

nucleus	E [keV]	half-life [ms]	cross section [nb]	number of chains	state
^{217}U	8024(14)	$0.19^{+1.13}_{-0.10}$	0.05	1	$(\frac{1}{2}^-)$
^{218g}U	8612(9)	$0.51^{+0.17}_{-0.10}$	0.9	20	0^+
^{218m}U	10 678(17)	$0.56^{+0.26}_{-0.14}$	0.5	12	8^+
^{219}U	9774(18)	$0.08^{+0.10}_{-0.03}$	0.2	5	$\frac{9}{2}^+$

The candidate event of ^{217}U requires careful inspection. If a recoil is implanted very close to the edge of a pixel, closer than the range of an α particle in silicon, the α particle might escape from the pixel to the neighbouring one. Thus some of the decay energy might be lost to the neighbouring pixel which is not included in the analysis. This is one type of escape α particle, the energy left in the pixel is fairly high, maybe even very close to the maximum energy of the decay. This type of an event is a real event but it looks like a random one. It can be seen as "ghost" events where only a partial amount of energy is collected and the α peak is shifted towards lower energies. The candidate chain for ^{217}U could be a such a ghost event. The decay energy matches the decay energy of ^{217}U presented in the Ref. [Mal00] but the lifetime of the event is too fast for ^{217}U. The lifetime matches better with the lifetime of ^{218}U. The daughters of ^{217}U and ^{218}U have almost identical decay properties and one cannot tell the difference by looking at other members of the decay chain. Another possibility is a decay from the isomeric or ground state of ^{218}U to an excited state in ^{214}Th. It is interesting to note that if the 8024 keV decay is assumed to occur between corresponding 8^+ states in ^{218}U and ^{214}Th, the decay becomes favored. The origin of the alleged ^{217}U cannot be confirmed and thus it cannot be labelled as ^{217}U. The measured fusion production cross section for ^{218}U was 1.4 nb. The fusion cross sections for all the uranium isotopes investigated in this work are presented in the table 5.2.

5.4 Discussion

The possible spin and parity assignment for the new isomeric state in ^{218}U is either 8^+ or 11^- based on references [Cau03], [Hau01]. These two assignments are the only ones which are consistent with the experimental α-decay data. If an isomeric α decay is observed at the focal plane of RITU, the decay out of the state must be hindered. The stronger the hindrance, the more likely it is that α decay can compete with γ decay. In the case of ^{218}U, 8^+ or 11^- states provide the necessary hindrance. The transitions from other levels do not have sufficient hindrance and thus they decay via γ decay which could not be observed at the focal plane of RITU. In order to determine the spin and parity of the new isomeric state the method of Rasmussen was applied [Ras59]. Tentatively the α decay branch from the new state was assumed to be very close to 100 %. The hindrance factor of the α decay from the new isomeric state was compared with that found for the 8^+ state in ^{216}Th assuming a 5 % α decay branch [Hau01]. The calculated hindrance factors of the isomeric state in ^{218}U seems to comply with the hindrance factors determined for the known 8^+ isomeric state in ^{216}Th. The values do not match exactly but are within acceptable limits. In the case of ^{216m}Th, the upper limit of four for an allowed transition is reached at Δl=10 while in the case of ^{218m}U the limit of allowed transition is reached at Δl=11. In addition, the hindrance factor with Δl=12 is already well below the allowed transition limit.

On the basis of this analysis the spin and parity of 11^- was ruled out and an 8^+ assignment was given for the new isomer in ^{218}U. The comparison can be reviewed from table 5.3.

Table **5.3**: Calculated hindrance factors

Δl	^{216m}Th	^{218m}U	^{219}U
0	14000	69000	130
4	3000	15000	24
6	500	2700	4.6
8	20	280	
9	13	73	
10	3	17	
11	0.5	3.4	
12	0.1	0.6	

Figure 5.7 compares the excitation energy of the new 8^+ isomer in ^{218}U with the calculations of Caurier et al. [Cau03]. The theoretical excitation energy of the lower 8^+ state is 2085 keV while the measured excitation energy of the isomeric state is 2105 keV, only 20 keV higher than the predicted value [Cau05]. This is another indication that the 8^+ assignment is correct.

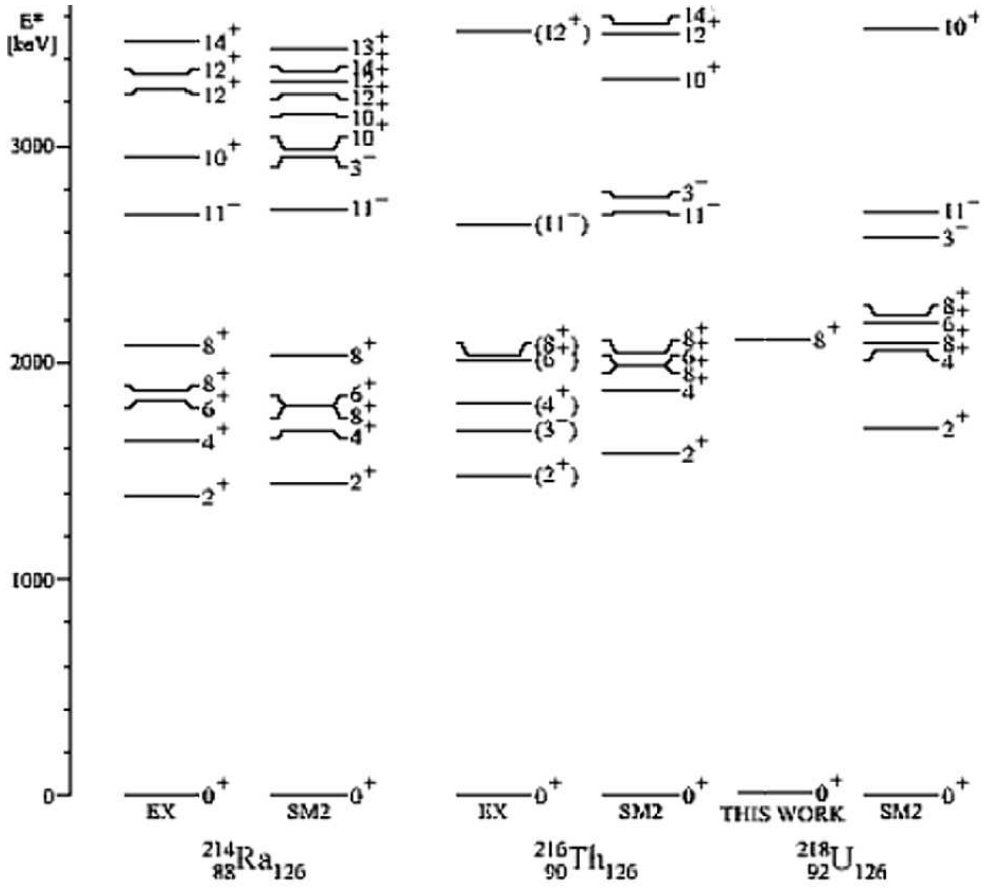

Figure **5.7**: Theoretical level schemes of different N=126 isotopes compared with experimental results. The new isomeric state found in ^{218}U has been added to the figure. Level scheme adopted from [Cau03].

The 8^+ state in ^{218}U was observed at the excitation energy of 2105 keV. The 8^+ state was formed with two quasi-particle excitation between the $h_{9/2}$ and $f_{7/2}$ proton orbitals. This excitation is possible only if the $h_{9/2}$ and $f_{7/2}$ proton orbitals are close enough in energy (which is not predicted by the relativistic mean field model). As a conclusion, the experimental results obtained in this study support the theory by Caurier et al. [Cau03] where the strong L=3 octupole correlations bring the $h_{9/2}$, $f_{7/2}$ and the $i_{13/2}$ proton orbitals closer in energy than predicted in the Ref. [Rut98]. The theoretical results made by Caurier et al. predicted the excitation energy and the spin and parity of the isomer correctly. The new isomer in ^{218}U supports the theoretical predictions where the sub-shell closure at Z=92 is non-existent.

5.5 Future experiments

The experimental result discussed in Section 5.4 gives only a glimpse of the single-particle structure in heavy neutron-deficient nuclei. The theoretical models predict many interesting phenomena in ^{218}U e.g. the locations of the 11^- and 3^- states. In theoretical models the 3^- state is predicted to lie high in energy but experiments show that the 3^- state comes lower in energy with increasing proton number in N=126 isotones. Based on systematics the 3^- state in ^{218}U should lie very low in energy, close to or even below the 2^+ state. If the 3^- state falls below the 2^+ state, the 3^- state decays via E3 γ decay which has a relatively long lifetime and may only be detected at the focal plane. Another interesting state is the 11^- state. In ^{216}Th there is a similar 11^- state which is an isomeric state with a 615 ns half-life. According to the Rasmussen method an unhindered α decay from this state, with decay energy around 11.2 MeV, would have a lifetime of about 5 ns. This type of α decay would be too fast to be detected at the focal plane of RITU since the flight time of a recoil through RITU is approximately 500 ns. Since the spin change in this case is 11, the increase of the barrier is significant and thus the decay is slow. In ^{218}U the α decay from the 11^- state is expected to be very hindered and the decay proceeds to the 8^+ state mainly via E3 γ decay. If this state has a lifetime longer than 500 ns, which is the flight time of the recoil through RITU, the detection of this γ transition should be possible at the focal plane of RITU.

Future ^{218}U experiments will require a lot of development on the hardware side. The low production cross section of 1 nb requires high beam intensities and high detection efficiencies so that the experiment could be performed in a reasonable amount of time. The intensity of the ^{40}Ar beam has to be increased by 5-10 times. The increased beam intensity requires further development of the ECR ion source. The ion source performance has already improved since January 2003 when the second experiment was performed. Even though tungsten has a very high melting point due to the increased beam intensity a rotating ^{183}W target system may be required. A very important requirement is the increase of the γ-ray detection efficiency at the focal plane of RITU. This might be realized sometime in 2006-2007 if three Cluster [Ebe97] detectors are installed with the GREAT Clover giving an estimated detection efficiency of approximately 4 %.

The RITU suppression for beam particles is very good, together with a well functioning MWPC, the quality of alpha, ΔE, TOF and recoil spectra is also very good. This allows clear discrimination and identification of the desired product thus making the α-gated γ-ray spectrum very clean. According to the systematics of the N=126 isotones, there should be only two dominating γ peaks in the focal plane spectrum. One strong peak could be the transitions from the 3^- state to 0^+ ground state which will be followed by the 8612 keV α decay to the ground state of ^{214}Th. The second strong

peak would be the decay from $11^- \rightarrow 8^+$ isomeric state which again will be followed by the 10 678 keV α decay to the ground state of ^{214}Th. These peaks are expected to dominate the spectrum and the construction of the level scheme should be fairly straightforward.

6 Recoil-decay tagging studies of ^{252}No

Nuclei far from stability are an important testing ground for the predictive power of nuclear models. The experimental decay data establish a means of comparison with theoretical data. Until recently studies of the super-heavy elements (SHE) have been generally limited to α-decay energies, decay half-lives and branching ratios. The transfermium elements with $100<Z\leq104$ are produced with cross sections at the submicrobarn level and detailed nuclear spectroscopy can be performed via in-beam experiments. Understanding the excited structure of the transfermium elements will allow us to begin to understand something about the structure of the super-heavy systems. Today the heaviest system for which in-beam structure data has been obtained is ^{255}Lr (Z=103) [Gre05].

6.1 Motivation

Many of the isotopes in the transfermium region have a significant spontaneous fission branch competing with α decay. This is due to the low fission barrier compared to the Coulomb barrier. After implantation into a silicon detector the evaporation residue decays via an emission of an α or β particle or undergoes fission. Generally the α-detection efficiency is around 55 % while the fission decay is detected with almost 100 % efficiency. The main technical problem in detecting both types of decay at the same time is the huge difference between the decay energies. The α-decay energies are of the order of 5-10 MeV while the total kinetic energy release (TKE) in fission is on the order of 200 MeV. The main physics problem is the nature of fission. When a nucleus undergoes fission it is scissioned into two massive nuclei with a certain mass distribution. The heavier part of the mass distribution is centered around mass A=130 and the lighter part around A=90 [Kra88]. A spontaneous fission event has a specific decay energy but for a large number of fission events only a wide energy distribution can be measured. The total kinetic energy release (TKE) is a measure of the fission energy. The TKE follows the Viola systematics which was presented in equation 2.16. In the case of ^{252}No fission the TKE would be 203 MeV according to equation 2.16. The experimental TKE value for the fission of ^{252}No is 194.3 MeV [Hul94]. As an accurate measurement of the TKE was not obtainable the expected energy distribution of ^{252}No

fission fragments is shown in figure 6.1 taken from [Bem77]. In figure 6.1 the ^{252}No (Z=102) fission study has been performed and the single fragment energy has been measured to range from 70 to 130 MeV [Yer04], [Bem77].

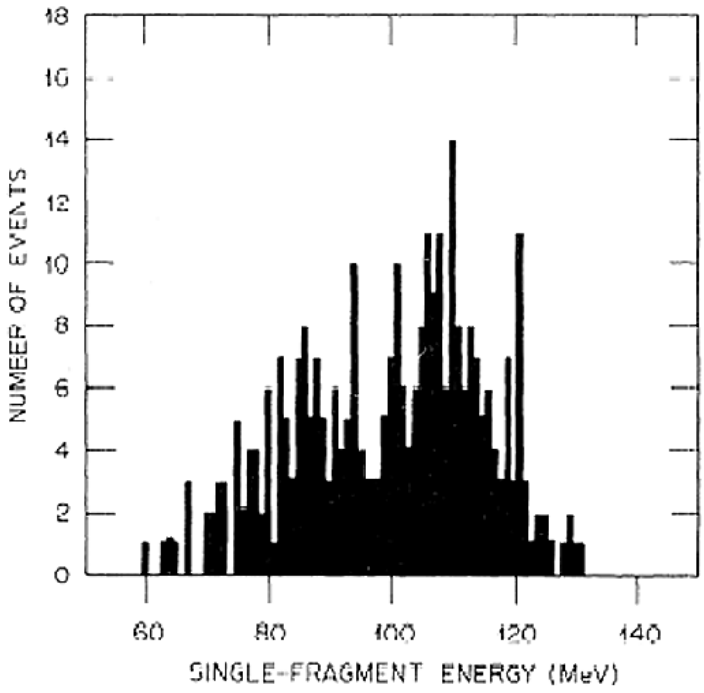

Figure **6.1**: Single-fragment energies in the ^{252}No fission. The figure shows the distribution of fission events that are expected to be seen in the focal plane detector. Figure adapted from [Bem77].

When studying weak reaction channels the fission events are distributed across several tens of MeV, thus making it almost impossible to distinguish them from scattered beam with high energy. At the time of the experiment the amplifiers and ADCs in the data acquisition system could not handle both α decay and fission simultaneously and still maintain good resolution for α particles throughout the whole energy range. Thus the system was normally tuned to get the α decays with a good energy resolution. The signals from the fission decays are too energetic, go over the range of the ADCs and are lost. In this work, a study of the ^{252}No nucleus was made with the RDT methods. The nucleus ^{252}No has a significant fission branch of 20-30 %, and a total production cross section of 220 nb using the reaction ^{206}Pb(^{48}Ca,2n)^{252}No at beam energy of E_{MOT}= 216 MeV. This makes it almost an ideal case for fission tagging because both α-decay events and fission events are obtained. At the time of the experiment the focal-plane electronics were composed of two different amplification channels thus enabling observation of the α-and fission-decay of ^{252}No.

The motivation for developing the fission tagging technique was to improve statistics, to prepare the way for in-beam spectroscopy of spontaneously fissioning heavy ele-

ments and to search for weak γ-ray transitions in ^{252}No. Such γ rays would represent transitions from possible low spin non-yrast states. These transitions have been observed in ^{246}Cm (N=150) and in ^{248}Cf (N=150) which is an isotone of ^{252}No [Mul76], [Yat75]. Recent in-beam studies of ^{250}Fm (N=150) show indications of similar structures as in ^{246}Cm and ^{248}Cf [Pri05]. Non-yrast states have also been observed in another nobelium isotope ^{254}No (N=152) [Eec05].

The statistics in the ^{252}No recoil-α tagged γ spectrum were insufficient to identify γ-ray transitions at higher energies but the combined recoil-α and recoil-fission tagged spectrum could have enough statistics to allow one to observe these transitions. The successful use of fission tagging proves the identification of fission events and the fact that fission originates from the same initial state as the α decay. This provides new opportunities in nuclear structure physics to do in-beam spectroscopy in the region of the nuclear chart where the nuclei have significant spontaneous fission branches.

6.2 The experiment

The experiment was carried out with the JUROSPHERE II array coupled to the gas-filled separator RITU at the University of Jyväskylä Accelerator Laboratory. The ^{252}No was produced in the reaction ^{206}Pb(^{48}Ca,2n)^{252}No, the beam energy at the center of the target being E_{MOT}=216 MeV. The targets were made of isotopically enriched ^{206}Pb as self-supporting foils of thickness 500 μg/cm^2. The total beam dose of ^{48}Ca to the target was 9.3×10^{16} particles. The experimental details are summarized in table 6.1.

Table **6.1**: Summary of the experimental details

Beam	$^{48}Ca^{9+}$
Beam energy (E_{lab})	216 MeV
Excitation energy (E^*)	22.5 MeV
Target	^{206}Pb
Target thickness	500 μg/cm^2
Irradiation time	238 h
Total dose	9.3×10^{16} part.

Two separate analysis were done. In the first analysis a total of 2800 α decays from the ground state of ^{252}No were identified and in the second analysis 1440 ^{252}No fission events were identified. The first analysis of the data was performed by Herzberg by using the recoil-gating and RDT method and the results were published in Ref. [Her01]. These results are presented in figure 6.2. The highest energy transitions are not defined unambiguously. Clearly more statistics would help identifying the highest energy transitions.

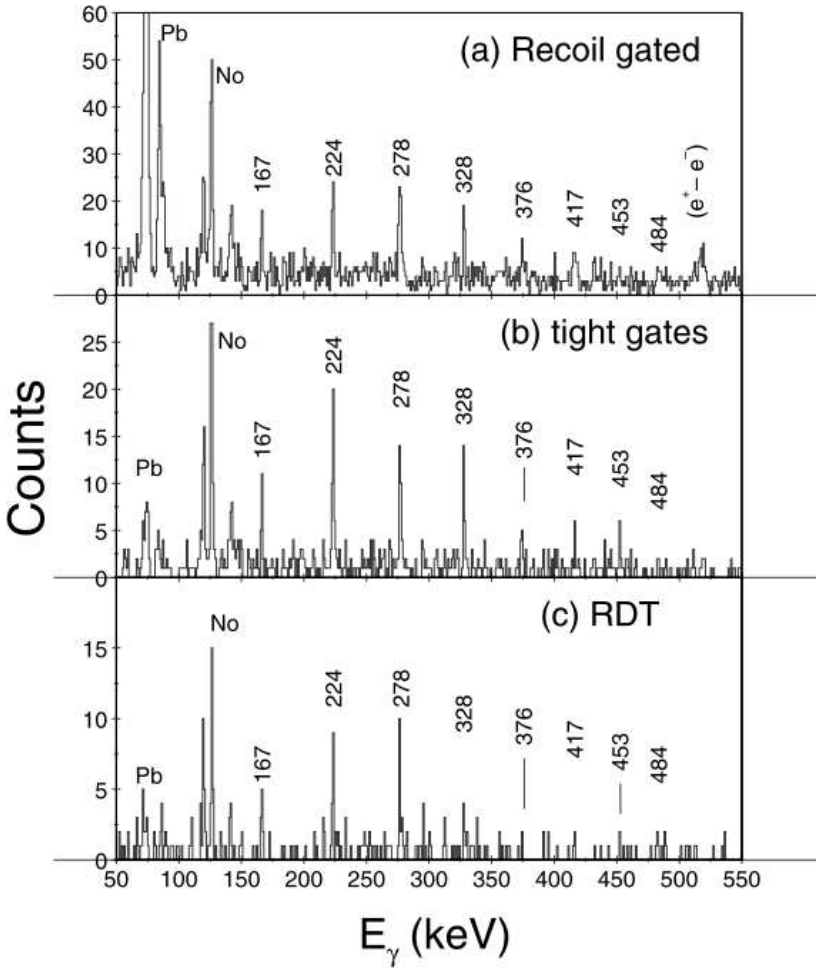

Figure **6.2**: Spectra from the initial analysis originally published by Herzberg et al. [Her01].

6.3 The analysis

The first step in the analysis was to reproduce the previously published results of ^{252}No. One of the most important things concerning the success of the analysis was the selection of ^{252}No recoils. This was done by setting certain gates or limits on spectra. The essential spectra were the recoil spectrum taken from the low amplification side of the PIPS detector, the TOF spectrum from the TAC which was set between the gas counter and the PIPS detector and the ΔE spectrum taken from the energy loss signal in the gas counter. By correlating these with ^{252}No α decays with all gates open with a long search time, the ^{252}No recoils were pinpointed. Accurate gates could then be set to limit the intrusion of the transfer products. The following 2-D plots show the gate limits found. The cluster shown in figure 6.3 represents ^{252}No recoils, this was confirmed by recoil-α correlations. The recoil gates were subsequently set around this cluster.

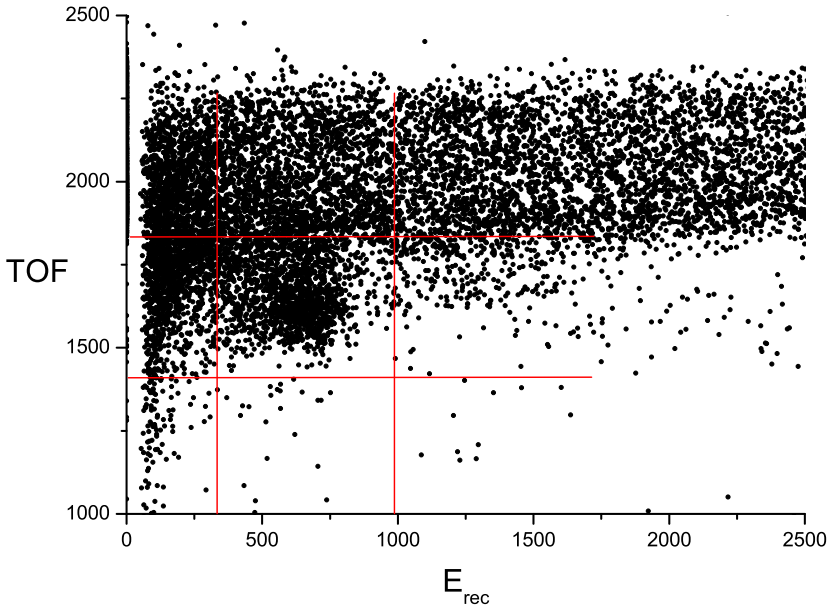

Figure **6.3**: Recoil energy vs. Time-Of-Flight. The axes are in arbitrary units.

The recoil energy versus the energy loss in the gas counter shown in figure 6.4 was a somewhat more difficult case. The gates for ΔE could be set following recoil-α correlations. It was found that there is no clear separation between the scattered beam and the fusion recoils. This is understandable because the MWPC is thin and a clear separation would require a thicker gas volume to be employed.

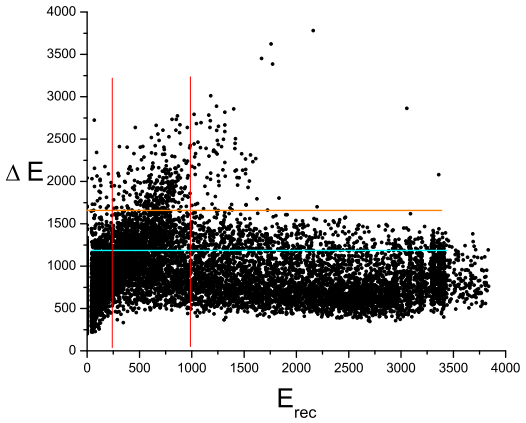

Figure **6.4**: Recoil energy vs. energy loss in the gas counter (ΔE). The axes are in arbitrary units.

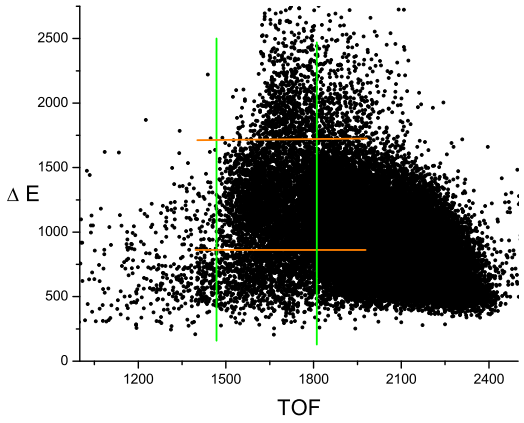

Figure **6.5**: Time-Of-Flight vs. energy loss in the gas counter (ΔE). The axes are in arbitrary units.

The Time-Of-Flight and ΔE gates are combined in figure 6.5.

6.3.1 Recoil-decay tagging

The correctness of the gates shown in figures 6.3, 6.4 and 6.5 can be tested. By making the recoil gated γ-ray spectrum the ^{252}No rotational band should be visible. Figure 6.6 shows the total recoil-gated singles γ-ray spectrum. Transitions in the ground state band of ^{252}No can clearly be seen, however the lead X-rays and random background is still present.

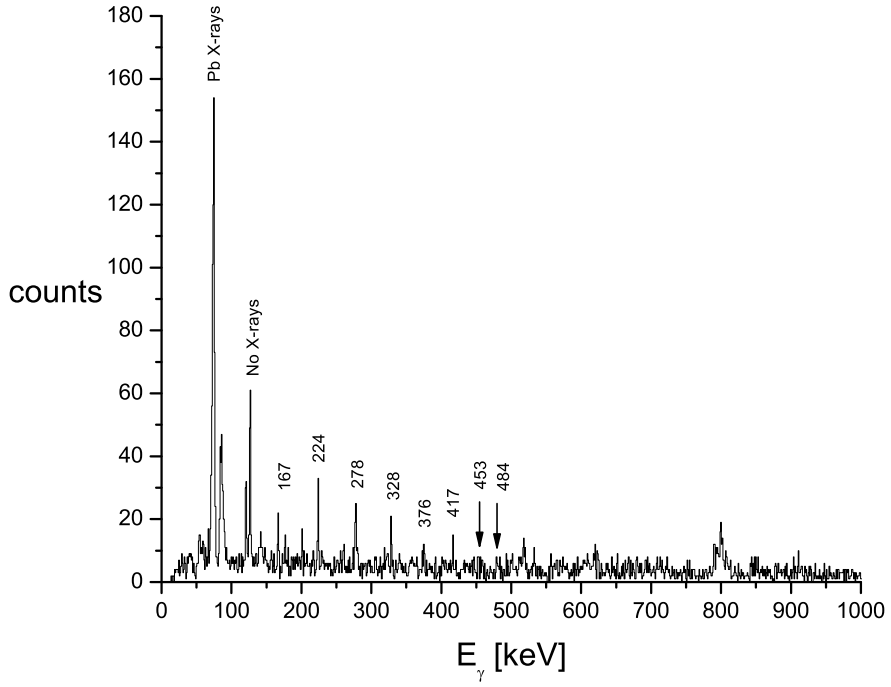

Figure **6.6**: Recoil gated γ-ray spectrum

The background in the recoil-gated γ-ray spectrum can be reduced and the quality of the spectra can be greatly enhanced by the recoil-decay-tagging method (RDT) [Pau95]. In RDT only those γ rays were accepted which were in coincidence with the recoil correlated with ^{252}No α decay. The condition for selecting a ^{252}No recoil was that it decayed via a characteristic ^{252}No α-decay within the same pixel within an appropriate search time. Usually the search time is selected to be a multiple of the decay half-life. This method is called recoil-decay tagging. The RDT method does not completely remove the random background but it enhances the spectrum quality significantly and it also allows selection of the weakest channels.

The nobelium recoils were correlated to α decay of ^{252}No. Similar results were obtained as Herzberg et al. found in the first analysis (figure 6.2). Approximately 2800 recoil-α chains were identified. In the recoil-gated α tagged (RDT) spectrum the ^{252}No rotational band is clearly visible with the correct transitions energies.

The singles α spectrum (figure 6.7) shows clearly how the two-neutron evaporation channel is dominant over all other channels. The α decay of ^{253}No is visible in the spectrum thus indicating the presence of the one neutron evaporation channel. But it can be stated that essentially only one strong channel is open in this fusion evaporation reaction. The daughter and grand-daughter and great-grand-daughter of ^{252}No can also be seen in the spectrum. The decay chain and the elements are labelled in the spectrum.

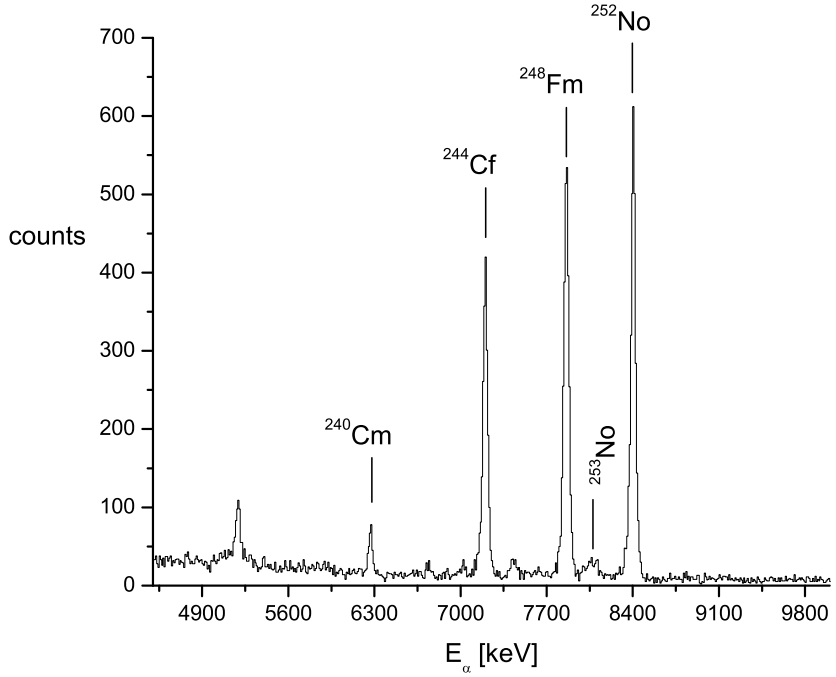

Figure **6.7**: Alpha decay spectrum obtained in the experiment.

One cannot state with 100 % certainty that the rotational band seen in the recoil gated spectrum belongs to ^{252}No. It is possible that it belongs to e.g. a transfer product. In an ideal case by tagging the recoil-gated spectrum with the characteristic α decay one should only be left with γ-rays belonging to the nucleus of interest.

By tagging with α decays the background is greatly reduced which can be seen in figure 6.8 with the reduction in intensity of the lead X-rays. In figure 6.6, the lead

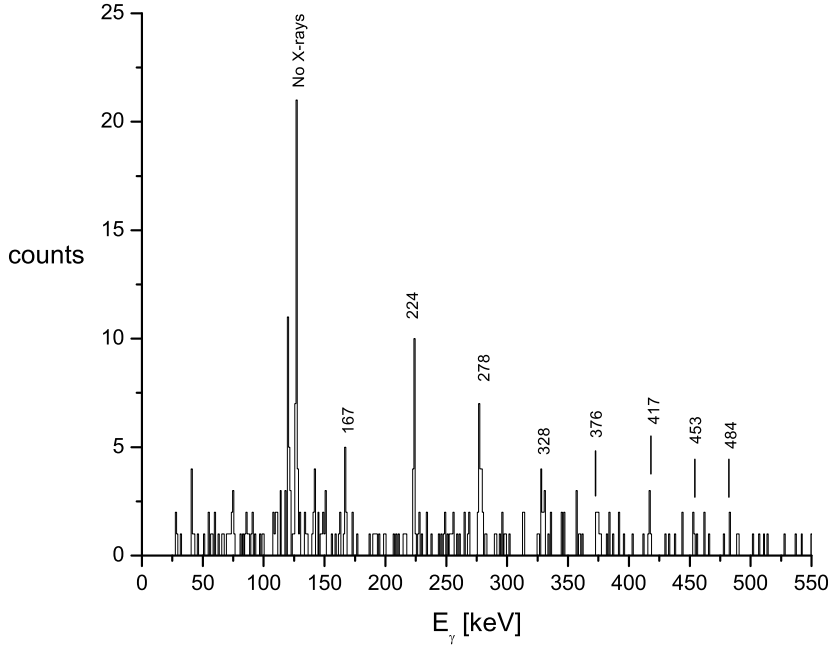

Figure **6.8**: ^{252}No α-tagged γ-ray spectrum. The same γ peaks are visible as in figure 6.2

X-rays are the strongest peaks while in figure 6.8 they have almost vanished. In the recoil-gated spectrum the rotational band is visible up to the $16^+ \rightarrow 14^+$ transition corresponding to the 417 keV γ-ray energy. There are higher energy peaks in the RDT spectrum, however it is impossible to extend the ground state band to high spin due to the low intensity of these peaks. Probably the most significant difference between the recoil-gated and RDT spectra is the reduction of not only background but also the intensities of the peaks. This is due to the fact that only 55 % of the α decays are detected while 45 % of the α particles escape from the PIPS detector leaving some fraction of the full energy in the detector.

6.3.2 Recoil-fission tagging

The first step in recoil-fission tagging was to define the possible fission events. This was the first time in RITU's history when fission events were studied. The major problem is the huge difference in decay energy between α and fission decay as discussed in section 6.1. A fission event would be identified as an energetic event detected solely on the low amplification side of the PIPS amplifiers, or in the so called "recoil-side", in the high channel numbers. An additional requirement is a simultaneous anti-coincidence (veto) with the MWPC. Figure 6.9 shows the low amplification side spectrum with

and without the MWPC veto.

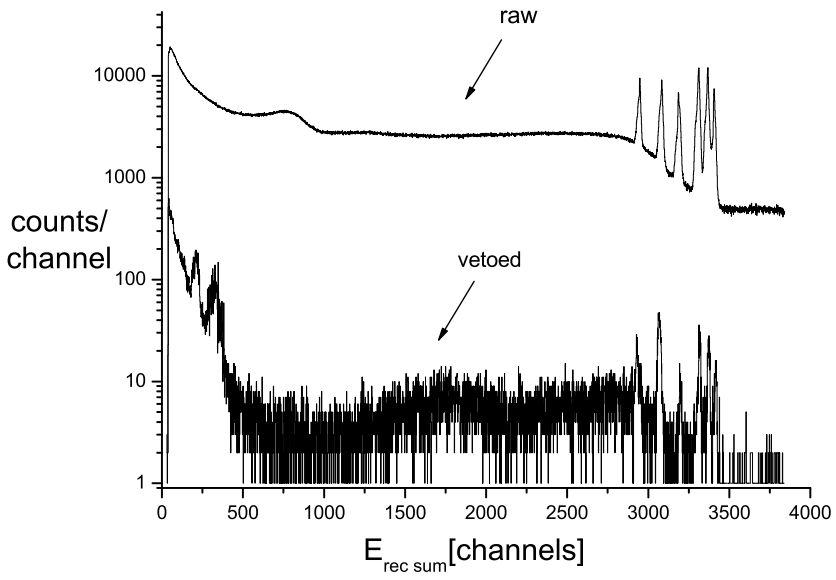

Figure **6.9**: Partial data from the recoil side spectrum with and without MWPC veto.

It can be seen from figure 6.9 that the most energetic signals are saturated. The high peaks at the end of the spectrum represent saturation from different strips since each strip has an individual sum amplifier. In the spectrum all the strips are summed together. This saturation effect poses a major problem in detecting the high-energy fission events. It can be seen from the vetoed spectrum that there is no clear indication of fission events in the high energy part.

This problem can be overcome by summing the individual top and bottom signals from the PIPS detector and thus creating a new sum signal which does not saturate as easily [Ket02]. This method increases the maximum energy by almost a factor of two. The following figure 6.10 shows the same spectrum as figure 6.9 but this time the individual top and bottom signals are used to create a separate sum signal which in this work has been labelled as "recoil sum plus".

The most interesting part lies at the top of the spectrum where no saturation of signals can be seen. Instead the spectrum gradually "dies" out towards the end of the spectrum. One should also pay attention to the two broad distributions seen on both sides of channel number 2000. The same broad distributions can be seen in the figure 6.9 from channel numbers 1500 to 3500. At the highest energies the signals starts to saturate while in the figure 6.10 the scale has been extended and no clear saturation can be seen. This demonstrates quite well the power of this method.

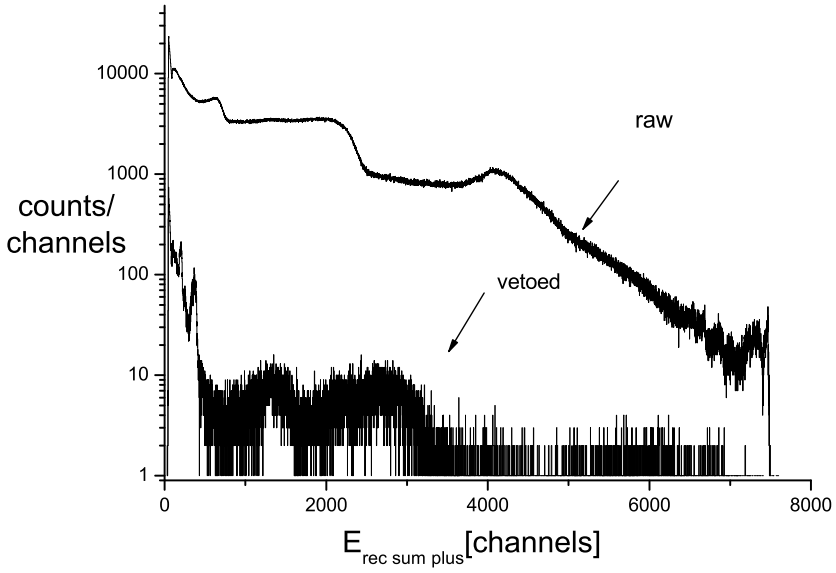

Figure **6.10**: Partial data from the recoil side with and without MWPC veto. Individual top and bottom signals were summed to create a new total energy signal.

There is an interesting feature in the high channel numbers. The smaller distribution around channel number 2700 represents target-like transfer products with mass around A=210 which have angle of approximately 0° with respect to beam direction. Simple kinematics calculations show that the energy of the transfer products can be estimated to be around 70-80 MeV when all the energy losses have been taken into account. The energy calibration on the recoil side can be performed by using these transfer products. If the channel 2700 corresponds to 70 MeV, the expected fission energy region should lie at channels 5000 and above. In fission the energy of the one fragment is collected fully while the energy of the other fragment may only be collected partially. Typical implantation depths of the fusion product are around 10 μm while the approximate range of fission fragments in silicon is 15-20 μm. The second fragment might escape the detector if the angle, with respect to the normal to the detector surface, is low enough. If the angle is greater than this "critical angle" the full energy of fission event is collected. With fission fragment ranges of 15-20 μm, the critical angle is around 45-60°. In all the cases the collected energy is higher than the energy of a single fission fragment. Figure 6.11 shows an illustration of the angles. The events which are ejected at angles smaller than α will escape while events ejected at angles smaller than β will trigger the MWPC. The shaded area corresponds to the area of the PIPS detector where full energy fission is collected, the white area corresponds to the area where only a partial amount of the fission energy is collected. The dark spot indicates the place where fission occurs.

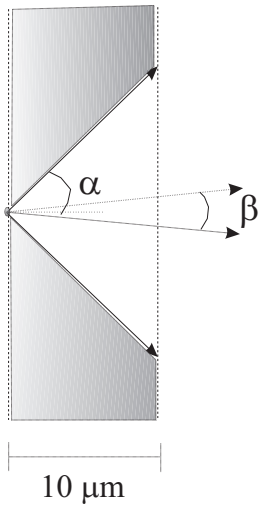

Figure **6.11**: The angle α corresponds to the "critical angle", fission fragments with a smaller angle than α will escape. From the escaped fragments the ones emitted at angles smaller than β will trigger the gas counter. When the range of fission fragments in silicon is 15-20 μm, the angle α is around 45-60°.

Figure 6.12 shows a gas vetoed and ^{252}No recoil correlated spectrum from the low amplification side, or the "recoil-side", when the total energy signal was created by summing individual top and bottom signals. As it can be seen from figure 6.12 there is a broad distribution in higher channel numbers than transfer products. If this distribution corresponds to real ^{252}No fission events the decay half-life of the broad distribution should be the same as the ^{252}No α decay half-life assuming that the fission occurs from the same state. The decay curves of the ^{252}No α decay and the assumed fission events are plotted in figure 6.13.

After taking background into account the half-life of the assumed fission events was determined as $T_{1/2}$= 2.54±0.07 s while the half-life of the ^{252}No α decays was $T_{1/2}$= 2.46±0.05 s. Within the error limits the half-lives are identical. The observed fission half-life agrees well with the ^{252}No spontaneous fission half-life of $T_{1/2}= (2.38^{+0.26}_{-0.22})$ s. reported in Ref. [Bel03] and with the half-life of $T_{1/2}$= 2.44±0.12 s reported in Ref. [Hul94]. This strongly supports the assumption that the broad distribution at high energy represents true ^{252}No fission events and that fission decay and α-decay originate from the same initial state. Further support can be obtained from the recoil-fission tagged γ-ray spectrum, if it shows identical structure as the recoil-α tagged spectrum. Both of the RDT spectra are presented in figure 6.14 where the top panel shows the recoil-fission tagged spectrum and the bottom panel shows the recoil-α tagged spectrum.

Both recoil-α tagged spectrum and recoil-fission tagged spectrum show the suppression of the lead X-rays and the ground state band of ^{252}No. This confirms that the assumed fission events are real ^{252}No fission events.

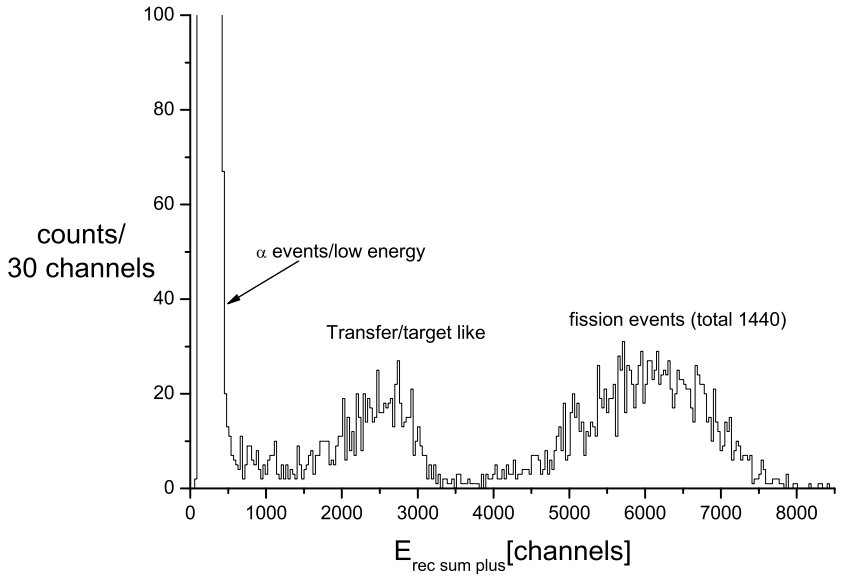

Figure **6.12**: Recoil correlated fission spectrum within 15 s search time. A total of 1440 fission events can be found when fission gates were from channels 4500 to 7500. The energy scale is in arbitrary units.

6.3.3 Combined recoil-α and fission tagged spectrum

The spectra from the recoil-α tagging and from the recoil-fission tagging methods can be combined to improve statistics by approximately 50 %. This allows an excellent opportunity to extend the known level scheme to higher spin and excitation energy. Figure 6.15 shows the combined spectrum. The γ-ray transitions of E_γ=453 keV ($16^+ \rightarrow 14^+$) and E_γ= 484 keV ($18^+ \rightarrow 16^+$) can be discerned above the background.

6.3.4 Spontaneous fission and α-decay branching ratios

The implantation depth in silicon is not enough to stop fission fragments emitted at smaller angles than α (see Fig. 6.11). The escaped fission fragments may hit the MWPC triggering it and thus making a fission event look like scattered beam reducing the fission detection efficiency. A geometric efficiency correction must be applied to the detected fission events. The correction can be calculated from the MWPC's solid angle coverage. The correction was found to be approximately 11 %. A total of 1440 fission events were identified in the experiment, following the geometrical correction the number of fission events is 1620. The total number of ^{252}No α decays was 2890

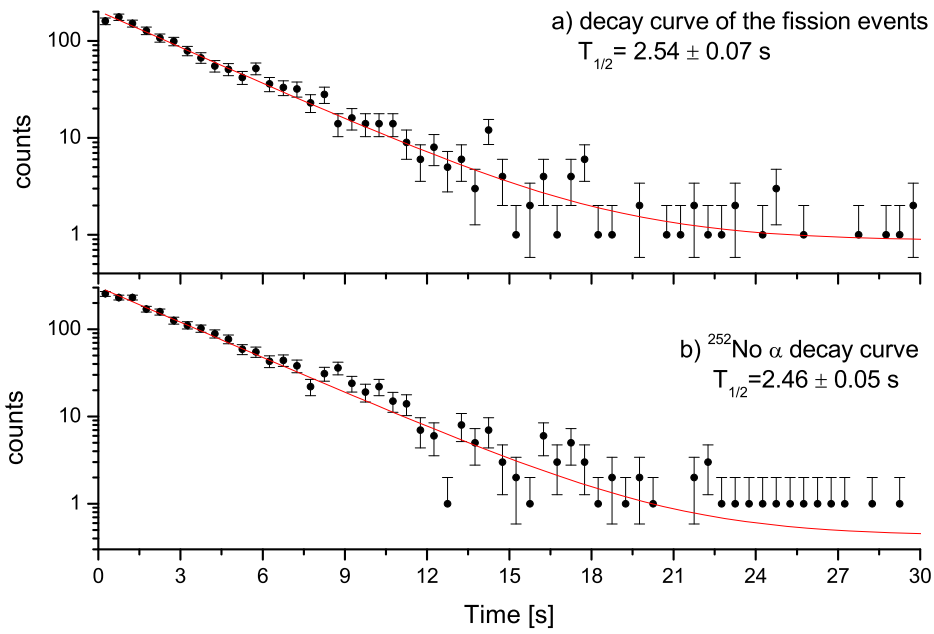

Figure **6.13**: The decay curve of the possible fission events (a). Decay curve of the ^{252}No α decay (b). A two component fit was made to the data, the second component is due to the random background. Identical decay rates can be observed in both cases.

after taking random background into account. This value has to be corrected with the number of escape α particles. Comparing these two numbers the ratio of α decay to spontaneous fission can be determined to be $\alpha/\mathrm{SF} = 76/24$. The obtained value agrees quite well with the accepted ratios of $\alpha/\mathrm{SF} = 73.1/26.9$ reported in Ref. [Bem77] and with the ratio of $\alpha/\mathrm{SF} = 78.4/21.6$ reported in Ref. [And93b]. The most recent study on the spontaneous fission of ^{252}No by Belozerov et al. reports a fission branch of b_{SF}=32±3 % [Bel03].

6.4 Transitions lying high in energy

An interesting question arises when the scale in the combined recoil-α and recoil-fission spectrum (figure 6.15) is broadened up to 1000 keV. Unfortunately, the in-beam γ data is very sparse in this region and thus a thorough level systematics study is difficult. Recently identified non-yrast states in ^{254}No and ^{250}Fm [Eec05],[Pri05] raised the question whether similar non-yrast states could also be present in ^{252}No. Transitions from these states show up in the γ-ray spectrum at 800-900 keV range. The recoil-fission tagging improved the statistics of the ^{252}No γ-decay spectrum thus

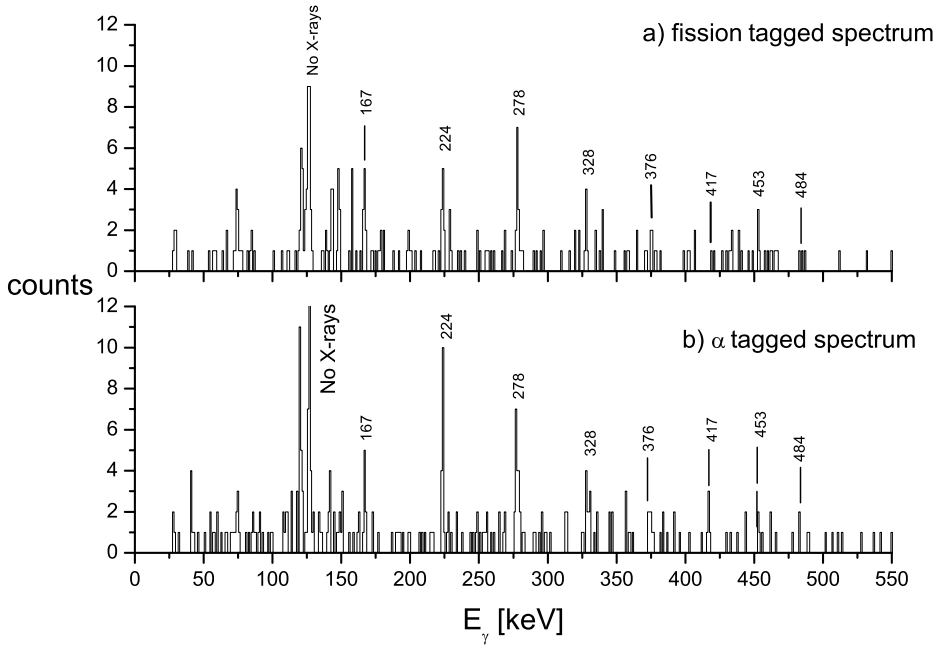

Figure **6.14**: Comparison between recoil-α and recoil-fission tagged spectrum.

a search for analogous transitions was made.

The comparison between ^{250}Fm, ^{254}No and ^{252}No γ-ray spectra is presented in figure 6.16. The non-yrast peaks found are marked with arrows and the areas where an intense cluster of peaks was found are indicated by the dashed lines. The spectra and peak identification for ^{250}Fm and ^{254}No has been adopted from Refs. [Pri05] and [Eec05] respectively. In the case of ^{252}No γ-γ coincidences are not available due to low statistics, thus only tentative conclusions can be made.

Similar behaviour can be observed in all three nuclei, i.e. a comb-like intense cluster of peaks at the 600 keV region and few peaks in the 800 keV to 1000 keV region. In the case of ^{252}No there are only a few counts in the high energy peaks. By comparing the number of counts in the peaks to the general background it can stated the high energy peaks are from real transitions. An enlarged view of the areas of the interest can be seen in the figure 6.17. For example, there are 9 counts in the region from 550 keV to 595 keV, an average of 0.2 counts/keV. Assuming that the random counts are distributed evenly the expected number of random counts in the region of 596 keV to 615 keV is 3.8, the measured number of counts in this window is 12. Thus it can be stated that all these counts cannot be produced by random background.

There are two types of structure in these spectra. Firstly, there is a dense comb-like

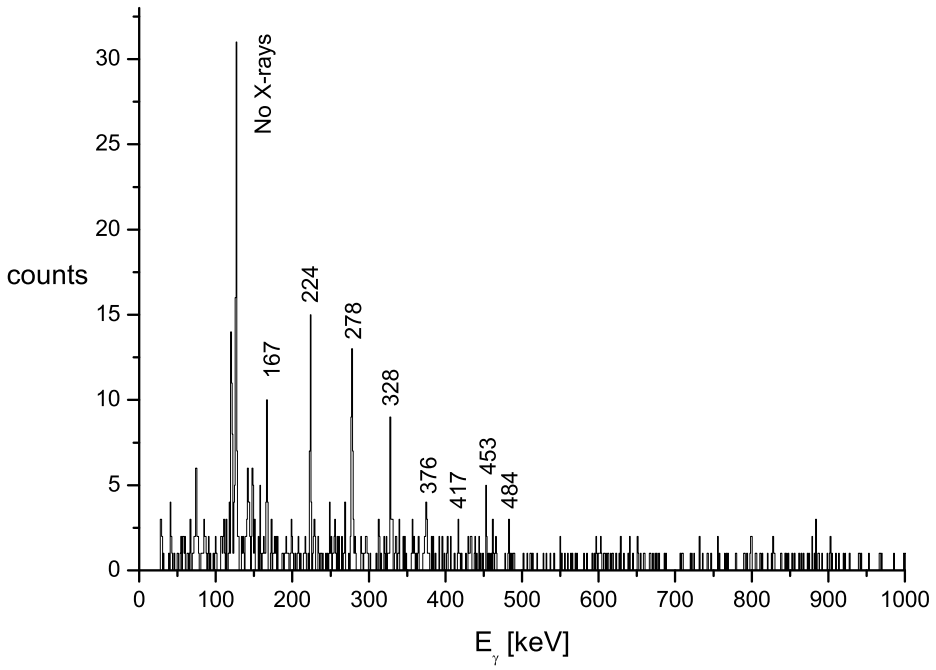

Figure **6.15**: Combined recoil α and recoil fission tagged spectrum.

structure at 600 keV, and secondly there are peaks with wider spacing up to 1000 keV.

The new peaks may belong to non-yrast states decaying to the lower members of the ground state band. Interestingly, the energy difference between the 607 keV and the 651 keV candidate peaks is 44±2 keV, or the energy difference between the 603 keV and the 651 keV peaks is 48±2 keV. The predicted energy difference in the ground state band between the 2^+ and 0^+ states is 46 keV, only a 2 keV difference. Similarly, the energy difference between the 627 keV and 732 keV peaks is 105±2 keV. The predicted energy difference between the 4^+ and 2^+ states of the ground state band is 107 keV, again only a 2 keV difference.

The peaks at 600 keV form an intense group. One could speculate that this structure is due to inter-band decays from a β-vibrational band. The β vibrations can only be found in quadrupole deformed nucleus [Cas00]. In the study by Herzberg et al. the measured quadrupole deformation of ^{252}No was β_2=0.27 [Her01]. In a β-vibrational band the energy spacing between the levels mimic the energy spacing of the ground state band. Obviously, the spacings between the ground state band and the β-vibrational band are not equal but fairly close. The β vibration couples with a rotation to form a rotational band with $I^\pi=2^+,4^+,6^+\ldots$.

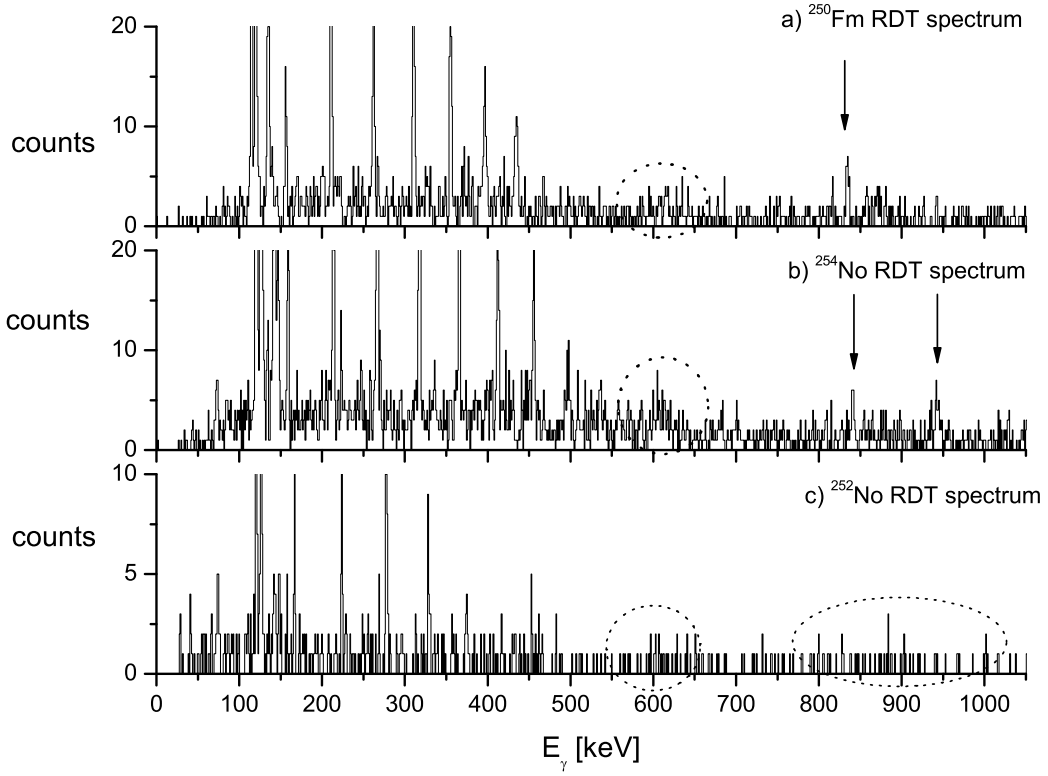

Figure **6.16**: A ^{252}No RDT spectrum compared with closest and relatively well studied ^{254}No and the N=150 isotone ^{250}Fm [Pri05], [Eec05]. The interesting areas and peaks have been indicated. The structure of ^{252}No seems to be very similar that of ^{254}No and ^{250}Fm.

Experimentally β-vibrational bands are difficult to detect and not many are known. The in-band transitions in β-vibrational bands are experimentally difficult to see since the high energy transition from β-vibrational band to the ground state band is preferred. In addition, in heavy elements the low-energy in-band E2 transitions are highly converted. Thus the only experimentally detectable γ rays originate from high energy inter-band transitions between the β-vibrational band and ground state band. These transitions can seen as E2 γ transitions [Cas00]. In a γ-ray spectrum these inter-band transitions from a β-vibrational band to the ground state band would create peaks side-by-side as a comb-like structure where the transition energy roughly correspond to the energy difference between the bandheads. Such a dense concentration of peaks can be observed in ^{252}No spectrum in the 600 keV region as seen in figures 6.15 and 6.16.

Another possibility is the γ vibrational band. Like in β vibrational band the γ vibrational band is a collective structure. The γ vibration couples with rotation to form

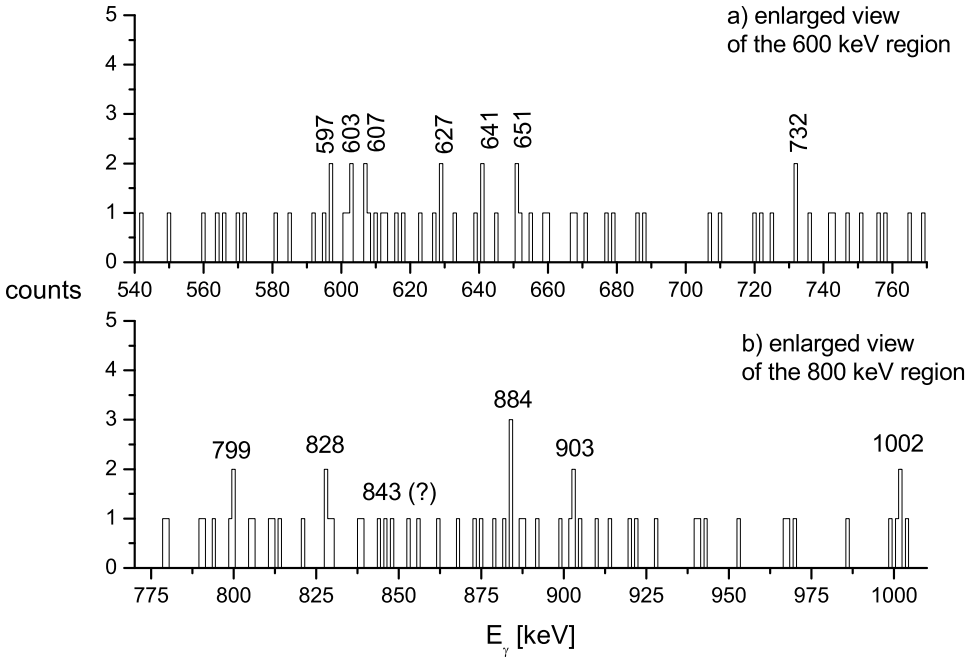

Figure **6.17**: Enlarged view of the peaks around 600 and 800 keV regions

a rotational band with $I^{\pi}=2^{+},3^{+},4^{+}\ldots$. The level spacing in the γ vibrational band does not mimic the level spacings of the ground-state band. This causes scattering of the inter-band transition energies and a clear comb-like structure would not be visible. The γ-ray transitions seen in the spectrum at the 600 keV region would then represent the inter-band transitions to the ground state band. The transitions between the β and γ bands are not allowed due to the annihilation of a phonon in one band and creation in another [Cas00].

The weak γ peaks seen in the 800-1000 keV region are probably from a similar band as seen in ^{254}No which presumably do not originate from β or γ vibrations. The isotones ^{248}Cf and ^{246}Cm have been studied extensively and level schemes have been established [Yat75] [Mul76]. In ^{248}Cf there is a sideband with negative parity where the band head is located around 600 keV. In ^{246}Cm there is also a similar negative parity sideband with the band head located at 840 keV. The peaks in ^{252}No may belong to a similar band to those negative parity bands found in ^{246}Cm and ^{248}Cf. In the recent studies of ^{254}No the transitions with 841 keV and 943 keV decay energies were assigned to be decays from a K=3 sideband [Eec05]. In the case of ^{252}No the situation is more complex and more peaks are visible. The predicted energy difference between the 4^{+} and the 2^{+} states is 107 keV. The energy difference between the 799 keV and 903 keV peaks is 104$\pm$2 keV, only 3 keV lower than the prediction. This would support

the assumption that the situation is similar to that of ^{254}No. Figure 6.18 displays a partial potential level scheme of ^{252}No. The high energy transitions which decay to the ground state band are marked with black arrows. The open arrows represent the ground state band. The dashed arrows represent converted transitions.

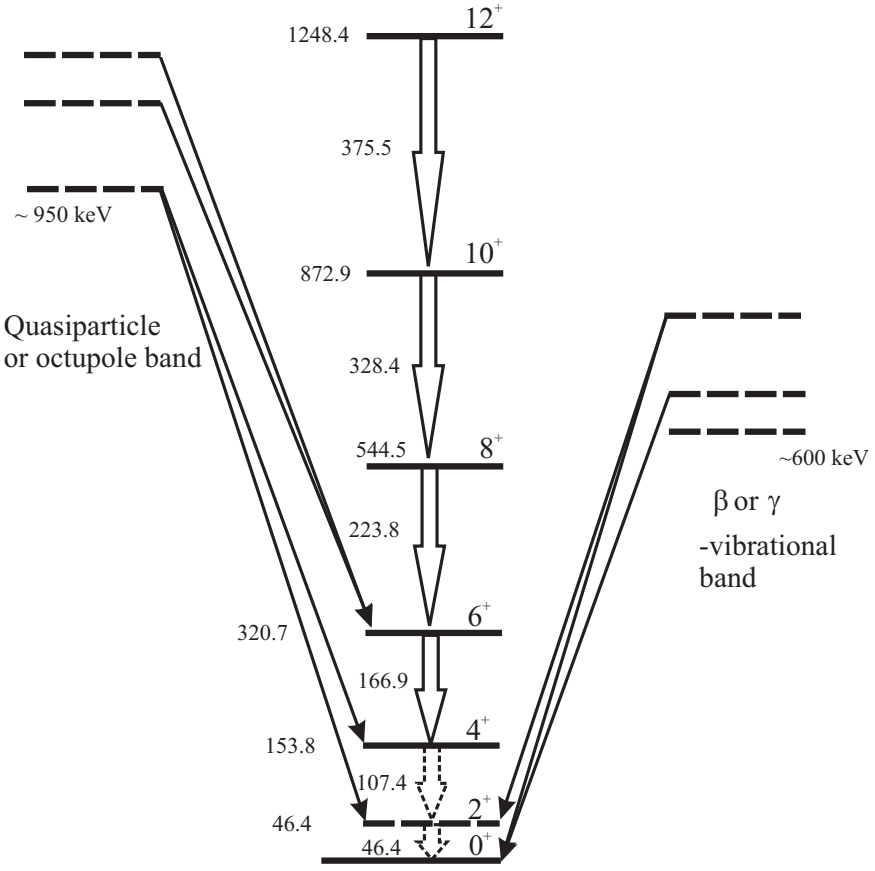

Figure **6.18**: Partial potential level scheme of the ^{252}No.

Definite assignments cannot be made due to the lack of statistics and γ-γ coincidences. Further experiments are needed to solve this puzzle. The GREAT spectrometer with it's TDR data acquisition and the JUROGAM array might be sufficiently efficient to obtain statistics required in order to make definite assignment on each transition. The structures are very weak and can only be probed with powerful spectroscopic tools.

6.5 Discussion

Fission events detected at the focal plane of RITU were analyzed for the first time. The recoil fission tagging method was employed to obtain tagged γ-ray data. The results of the analysis proved the feasibility of the method. The fission events were detected

simultaneously with α decay which gives direct access to relative branching ratios. The measured spectra showed that fission originates from the same initial state as the α decay does. In the figure 6.2c, the 3-4 highest transitions are barely distinguishable. The weakest transitions in the rotational spectrum published in Ref. [Her01] were confirmed. In addition new peaks were found but the origin of the peaks could not be determined due to low statistics. In the future, fission events may be utilized in tagging experiments of super-heavy nuclei.

These peaks are labelled as members of the rotational band and it is important to verify these peaks. In the spectra published in Ref. [Her01] only recoil α tagging method was used. In the second analysis both α decay and fission events were used to obtain tagged γ spectrum. The proof of feasibility of the fission tagging method was achieved. Analysis of the high energy part of the γ spectrum show signs of similar structure as observed in ^{250}Fm and in ^{254}No, it can be speculated that the observed transitions are from different vibrational bands or quasiparticle structures.

6.6 Future prospects

The recoil-fission tagging method developed in this work opens new possibilities in heavy element nuclear structure studies (see section 6.1). The transfermium nuclides with fission branches close to 100 % have never been studied via in-beam γ-ray spectroscopy. The only available information for these nuclei are from studies of decay half-life and branching ratios. Recoil-fission tagging provides an important tool to study the structure of these nuclei with in-beam methods. A natural way to proceed further is to study a heavier even-even nucleus with Z=104. Experimentally this is very challenging since the production cross section becomes extremely low, reaching the nanobarn level.

6.6.1 The ^{256}Rf experiment

The chart of the nuclides has been explored widely including the heavy element region where progress has been made also with in-beam spectroscopy of the transfermium nuclides. The current detection system has allowed us to measure rotational spectra of different heavy elements and their various isotopes. Currently the heaviest isotope which has been successfully studied via in-beam spectroscopy is ^{255}Lr [Gre05]. The next interesting case is the even-even isotope ^{256}Rf (Z=104) which lies on the N=152 closed neutron shell. Previously ^{256}Rf has been studied via α spectroscopy with high precision and the half-life, decay energy, α-decay branch and the production cross section are known [Heß97]. The general prediction in this region of the chart of the

nuclides is strong prolate ground state deformation with β_2 ≈0.25 [Ćwi94]. Thus a rotational band is expected in the experimental γ-ray spectrum. Another general feature in this region is that the transitions from the lowest excited states are strongly converted where the decay proceeds via internal conversion. The lowest transitions visible in the γ-ray spectrum of ^{254}No and ^{250}Fm are the $6^+ \rightarrow 4^+$ transition and similar behaviour can be expected in ^{256}Rf.

The experiment would be performed using the ^{50}Ti(^{208}Pb,2n)^{256}Rf reaction with a beam energy of E_{MOT}=237 MeV. The cross section for this reaction is 12 nb which is at the detection limit for in-beam studies. ^{256}Rf decays mainly via fission with a half-life of $T_{1/2}$=6.2±0.2 ms [Heß97]. The measured α branch is only b_α=0.0032±0.0017, thus the fission branch is b_{SF}>99.5 % [Heß97]. In the ^{252}No experiment the total production cross section was 220 nb and from this the fission branch was 23 %, thus the effective spontaneous fission cross section was approximately 50 nb. The production cross section of ^{256}Rf is 4 times smaller, around 12 nb, which puts it right at the detection limit. Since the ^{252}No experiment RITU has gone through a series of upgrades as discussed in Chapter 3. The γ detection efficiency has gone up from 1.7 % to 4.3 % with the JUROGAM detector array. The RITU beam suppression has improved significantly due to the new dipole chamber, and scattering of the primary beam has been reduced due to the differential pumping system. Although the production cross section for ^{256}Rf is only approximately 25 % of the effective ^{252}No fission cross section the spectrum quality is expected to be better and the detection efficiency higher. In a two week experiment the spectrum expected from a ^{256}Rf experiment would be similar to the recoil-fission tagged spectrum shown in figure 6.14 but with less background. The rotational structure of the nucleus should be visible with about 15 counts in the most intense peak, which in the ^{252}No case was the $8^+ \rightarrow 6^+$ transition.

The most challenging part in this experiment is the identification of a fission event. The GREAT spectrometer was never designed to detect fission and α decay events simultaneously. The gains would have to be lowered so that high energy signals from fission events will not saturate in the amplifier resulting in the loss of the low-energy α-decay signals. This is, however, not crucial since the α decay branch in ^{256}Rf is very weak at only <0,5 %. As discussed in section 2.2.2, a fission event is a very energetic decay where the nucleus is split into two lighter nuclei. These particles fly roughly in opposite directions. In the GREAT spectrometer a fission event would be characterized as a high decay energy, an anti-coincidence with the MWPC and, optimally, a PIN diode detecting the fission fragment.

The ^{256}Rf experiment requires an intense ^{50}Ti beam and a rotating target system. The newly-commissioned target chamber by IReS allows us to do in-beam spectroscopy with rotating targets. At present, the major problem is the low intensity of the beam. The current MIVOC system where gaseous titanocene has been used is based on natural titanium. The abundance of ^{50}Ti is only 5.2 % out of natural titanium. The

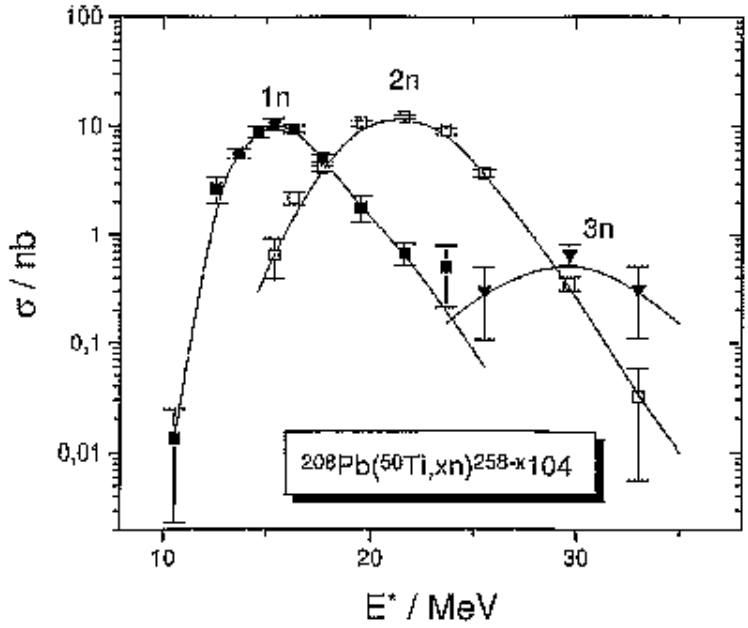

Figure **6.19**: Excitation function of ^{50}Ti beam irradiated on ^{208}Pb. The figure adapted from [Heß97].

situation can be improved if an oven system is used where enriched metallic titanium can be used. The oven is expensive due to the exotic materials which can stand temperatures above the titanium melting point (1660 °C). In addition the oven can only be used once.

At the moment the maximum beam intensity is around 30 pnA before the maximum germanium detector counting rate is exceeded. There is ongoing development of digital data acquisition electronics. The digital data acquisition electronics will allow higher counting rates for germanium detectors and thus higher beam intensities can be used and smaller cross sections can be reached via in-beam studies.

7 The low cross section experiment of ^{255}Db

Synthesis of the heaviest elements has been a quest ever since the first artificial transuranium isotopes were produced in 1940. Theoretical calculations predict the next major proton shell closure between Z=114 or Z=120 or Z=126, depending on the model. Before the heaviest elements can be synthesized the behaviour and structure of these nuclei should be understood. This requires thorough mapping of the chart of nuclides by studying decay properties of various isotopes of the heavy elements. Increasing the number of super-heavy elements that can be synthesized and provides stringent constraints on nuclear structure calculations.

7.1 Motivation

The ^{255}Db (Z=105) experiment was the first test at JYFL in the field of low cross section studies in the region of very heavy elements. Claims that ^{255}Db had been synthesized were made by the Dubna group in the mid-1970's [Fle76]. However, the reported cross section and half-life do not agree with the systematics of the dubnium, rutherfordium and lawrencium isotopes. From more recent chart of nuclides the ^{255}Db has been removed and therefore it is classified as undiscovered. The study of the heaviest man-made elements (Z=114-118) has progressed in recent years. All of the isotopes of new elements have been observed in low-yield experiments with cross sections of the order of picobarn or lower. The synthesis of new isotopes in this region is a demanding task. Very high beam intensities are required combined with high demands on target technology. Rotating targets must be used to prevent the target from melting and the separator efficiency has to be high in order to minimize fusion product losses.

The excitation functions in cold fusion reactions where only 1-2 neutrons are evaporated, are typically very narrow. Thus, the middle of target energy must be well defined. The beam energy has to be well tuned and all the energy losses before and in the target have to be taken into account. This introduces the problem of stopping powers of heavy elements in different media which has been discussed in Section 4.3.1.

The isotope ^{255}Db should have a sufficiently high cross section in order to gain expe-

rience in the synthesis of very heavy elements. It will provide valuable information on the physics of the nuclei under extreme conditions and experience in the field of low cross section studies.

7.2 Experimental details

The isotope ^{255}Db can be synthesized with the reaction ^{209}Bi(^{48}Ti,2n)^{255}Db. The estimated cross section for this reaction was calculated to be 360 pb by Heßberger [Heß01] with the HIVAP code. The improvements in the ECR ion source and the development of the MIVOC method has allowed the use of high intensity metallic beams [Koi94]. The beam of ^{48}Ti was used to bombard a ^{209}Bi target with a thickness of 450 μg/cm^2. The excitation energy of the compound nucleus ^{257}Db was E*=21.8-25.1 MeV with two different bombarding energies of E$_{beam}$=242 MeV and E$_{beam}$=246 MeV. The total dose of beam to the target was 2.1×10^{17} particles and the duration of the experiment was 8 days. All these experimental details are summarized in table 7.1.

Table **7.1**: Summary of the experimental details

Beam	^{48}Ti^{10+}
Beam energy (E$_{lab}$)	242-246 MeV
Excitation energy (E*)	21.8-25.1 MeV
Target	^{209}Bi
Target thickness	450 μg/cm^2
Irradiation time	109 h
Total dose	2.1×10^{17} part.

The reaction ^{209}Bi(^{48}Ti,2n)^{255}Db is a so called cold fusion reaction where a heavy stable target was bombarded with metallic ions. The name cold fusion refers to low excitation energy of the compound nucleus where the excitation energy is 10-25 MeV and only 1-2 neutrons are evaporated. Towards the heavier elements fissility increases and the survival probability becomes of increasingly important. Cold compound systems are expected to have an enhanced survival probability. When synthesizing very heavy elements the beam ions have barely enough energy to overcome the Coulomb repulsion. In cold fusion the projectile is selected to be fairly heavy but close to the magic numbers 20 and 28. In the ^{255}Db experiment the projectile proton number was 22 and the neutron number was 26.

Since the predicted cross section was low, RITU had to be tuned to close to the optimum settings at the beginning of the experiment. The required magnetic rigidity Bρ was determined beforehand according to the method presented in Chapter 4. During the experiment magnetic field values were changed from 1.112 T to 1.179 T to scan through the range of possible magnetic field values.

7.2.1 Target wheel

The target foils were mounted on a rotating target wheel in order to prevent the targets from melting. Figure 7.1 shows the rotating target wheel where the target foils are placed on the circumference of the wheel.

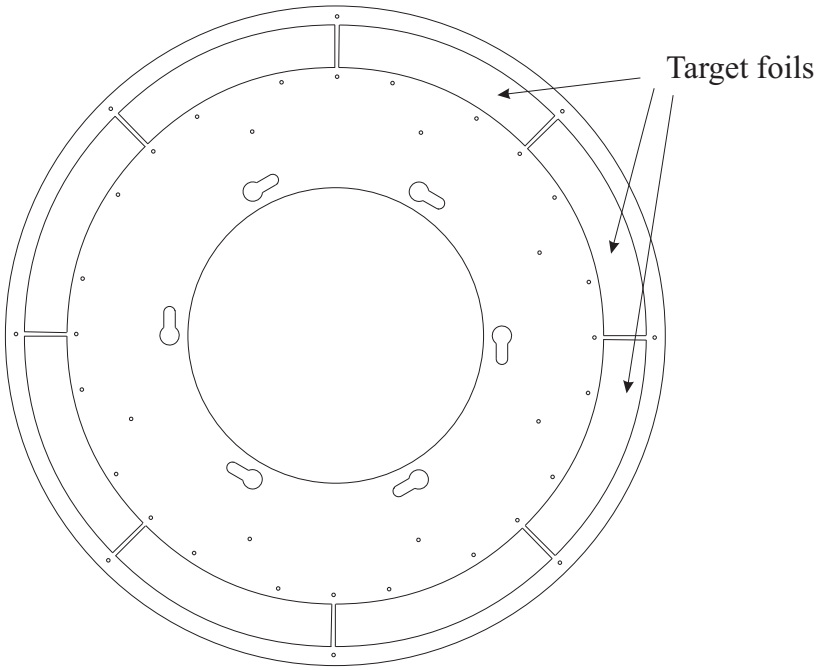

Figure **7.1**: Schematic diagram of the target wheel used in the low cross section experiments.

The wheel can house 8 targets of 11×100 mm^2 in size. The target wheel rotates at approximately 100 rpm. The diameter of the wheel is 37.5 cm and thus it cannot be fitted into any of the conventional target chambers and it requires a separate target chamber. The target chamber is connected to the RITU gas volume containing 0.6 mbar pressure of helium gas. The helium is essential in order to cool down the target via convection. During the experiment the chamber was separated from the beam line with a thin gas window. The windows were made either of nickel of thickness 450 μg/cm^2 or carbon of thickness 70-100 μg/cm^2. During the experiment the gas windows were the main limiting factor for beam intensity. Today RITU has a differential pumping system and the gas windows have become obsolete.

7.2.2 Calibration

Before the experiment the high amplification side of the PIPS detector was calibrated with an internal calibration. A beam of ^{48}Ti was used to bombard ^{112}Sn and ^{170}Er

targets. The α decays from the fusion products were used to calibrate the PIPS detector. Figure 7.2 shows the α spectrum from the calibration runs. The peaks of ^{152}Er and ^{155,155m}Lu were used to calibrate the high amplification channel of the PIPS detector. In figure 7.2 the peaks used in calibration are marked with arrows.

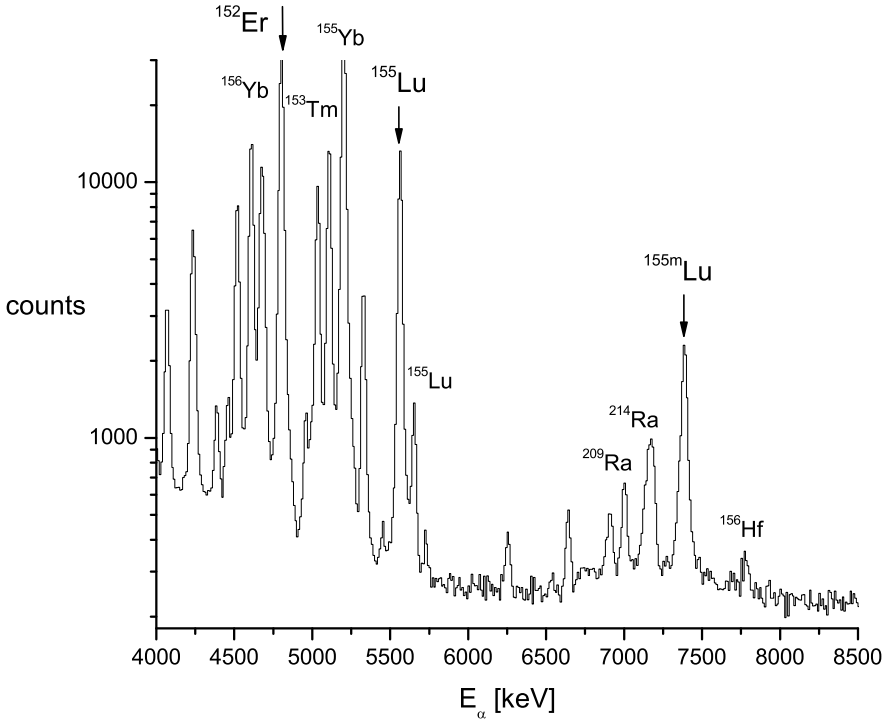

Figure **7.2**: Alpha spectrum obtained from the calibration runs. The peaks used to calibrate the high amplification side of the PIPS detector are marked with arrows.

A rough calibration for the low amplification channel can be obtained by using the transfer products ejected at 0°. Calibrating with transfer products is not an accurate calibration but it gives an energy scale appropriate for identifying fission events. From kinematics, the energy of the transfer products can be calculated. Taking all the energy losses into account the transfer products have an energy of the order of 70 MeV when hitting the PIPS detector. Figure 7.3 shows the gas-vetoed recoil spectrum obtained from the calibration runs where RITU was tuned to collect transfer products. In figure 7.3 the transfer products peak at around the channel number 1400.

The total kinetic energy release (TKE) of the fission of ^{255}Db was calculated to be 214 MeV using equation 2.15. The fission energy measured should be of the same order as in the ^{252}No experiment. In the ^{252}No experiment the fission events were 1.5-3 times higher in energy than the transfer products (see figure 6.11). Initially the

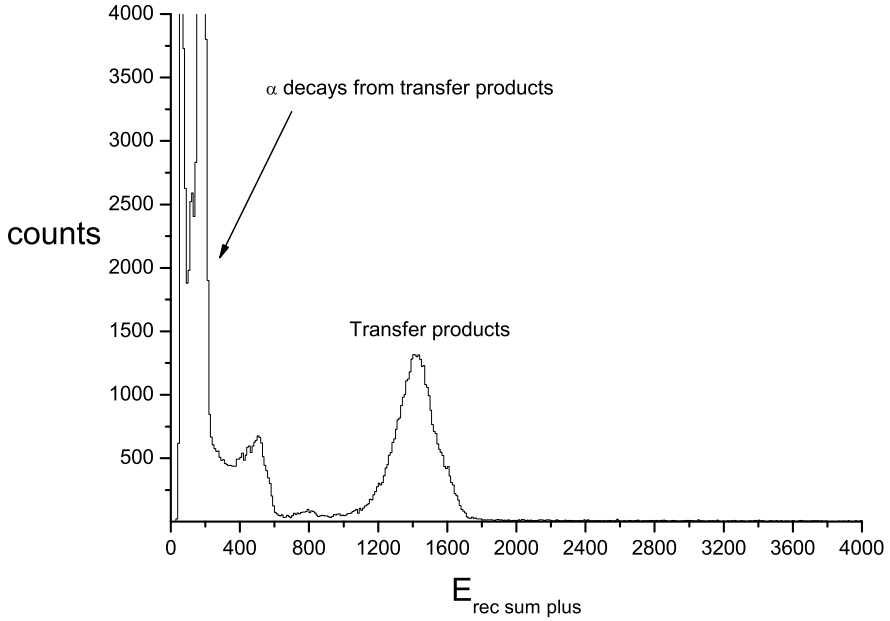

Figure **7.3**: MWPC vetoed low amplification side energy spectrum. The broad distribution around channel 1400 represents transfer products.

target-like products have an energy on the order of 140 MeV, but when taking all the energy losses into account, the target-like products have an energy of the order of 70 MeV when hitting the PIPS detector. Thus, if the channel number 1400 in Figure 7.3 corresponds to the target-like product energy of 70 MeV, the fission events have minimum energies of around 100 MeV. The fission events should lie in the channel numbers 2500 to 4500. The pulse height defect might cause distortions to the energy scale. This causes non-linearity to the energy scale but the degree of non-linearity is not clear. The pulse height defect is a function of energy and mass: the target-like product is massive but less energetic while the fission fragment is less massive but more energetic.

The calibration runs have a significant meaning in the low cross section experiments. In low cross section studies only a few fusion evaporation residues are produced. The calibration data not only give the energy calibrations for the main detector but also the gate limits for the ^{255}Db can be determined. In calibration runs the fusion recoils are abundant and an accurate identification of fusion products in the ΔE and TOF spectra provides initial gate limits for the ^{255}Db recoils. For correlation analysis, the gates in the ΔE, TOF and in the recoil spectrum must be set accurately to minimize the number of accidental correlations. The production cross section is so low that the possible ^{255}Db recoils are lost in the background without effective rejection of

scattered beam and target-like particles.

7.3 Analysis

In the online analysis no decays of ^{255}Db were observed. From the systematics the possible decay properties of ^{255}Db and the daughter ^{251}Lr were deduced. The deduced α decay properties for ^{255}Db were E_α=9.45 MeV with a half-life of $T_{1/2}$=20 ms and for the daughter nucleus ^{251}Lr E_α=9.02 MeV with a half-life of $T_{1/2}$=80 ms, respectively [Heß01]. The estimates were obtained when an unhindered decay was assumed. Since the isotopes were unknown before and spontaneous fission is the dominant decay mode in this region, it was unclear if the ^{255}Db or ^{251}Lr have α-decay branches at all. The data analysis was performed with the sort code written with C-programming language described in Section 3.6.1.

Gates for a ^{255}Db recoil were determined from the calibration runs using the slightly modified gates set to ^{155}Lu recoils. It was realized that these gates are far too wide since the ^{255}Db are slower and more massive than recoils detected in the calibration runs. Since the lutetium recoils are faster and more energetic than ^{255}Db recoils they are found in higher channel numbers. The real ^{255}Db recoils would require tighter gates but the risk of losing real recoils in a low cross section experiments was too high. The low counting rate at the focal plane and the high granularity of the PIPS detector allowed the use of wide recoil gates without significantly increasing the number of accidental correlations. Figure 7.4 shows the position of the correlated lutetium recoils in the recoil energy versus TOF plot. The energy gates for ^{255}Db recoils were obtained from this plot. Figure 7.4 also compares the position of the correlated lutetium recoils obtained from calibration runs with the position of the correlated ^{255}Db events which are marked with open circles.

7.3.1 Recoil-fission correlation

The gas-vetoed fission spectrum did not show any clear signs of fission events. The events were buried in the background caused by scattered particles. This can be seen in figure 7.5.

The definition of a fission event is of paramount importance in this respect. Fission were defined as energetic events in the PIPS with no coincidence with either of the MWPCs. The second MWPC was placed only 1.5 cm upstream from the PIPS detector. In the case of fission, the fragments share the fission energy according to their masses. The angle between the fragments is determined by conservation of momen-

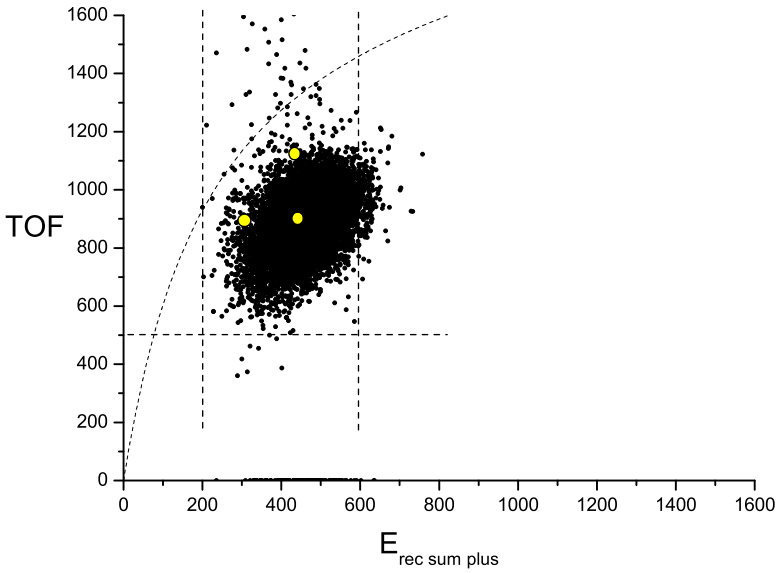

Figure **7.4**: The correlated recoil energy versus TOF plot from the calibration runs. The lutetium recoils are visible as a cluster. The positions of correlated ^{255}Db recoils are marked with light circles. The limits for recoil gates are indicated. The beam was cut off in software by fitting a function to the lower limit of the beam.

tum. In binary fission the fragments are ejected at a 180° angle with respect to each other. In this respect it is very likely that the other fission fragment trajectory goes through at least the MWPC closest to the PIPS detector triggering it. Tight gates were chosen even if real events could possibly be vetoed. The lower limit for the fission gate was determined based on the experience gained from the ^{252}No experiment. These two experiments were done with fairly similar beam and target combinations and with a similar bombarding energy. In the ^{252}No experiment the lower limit of fission energy range was about 1.6 times higher than the peak of the transfer products. In the ^{255}Db experiment the peak of the transfer products was at 1400 and thus the lower limit for fission event energy was set to 2200. The lowering of the gate limits would increase the number accidental events and it would be hard to distinguish between real and accidental correlations. Figure 7.5 shows the uncorrelated spectrum of events which passed through the fission gates.

Figure 7.6 shows the correlated fission spectrum. The fission events were correlated with recoils within a one second time window and a 1.3 mm position window. Only two events were found with lifetimes of τ=4 ms and τ=99 ms, respectively.

The correlation was solely between recoils and fission events. Most likely the ^{251}Lr also has a spontaneous fission branch. In this study the distinction between ^{251}Lr and

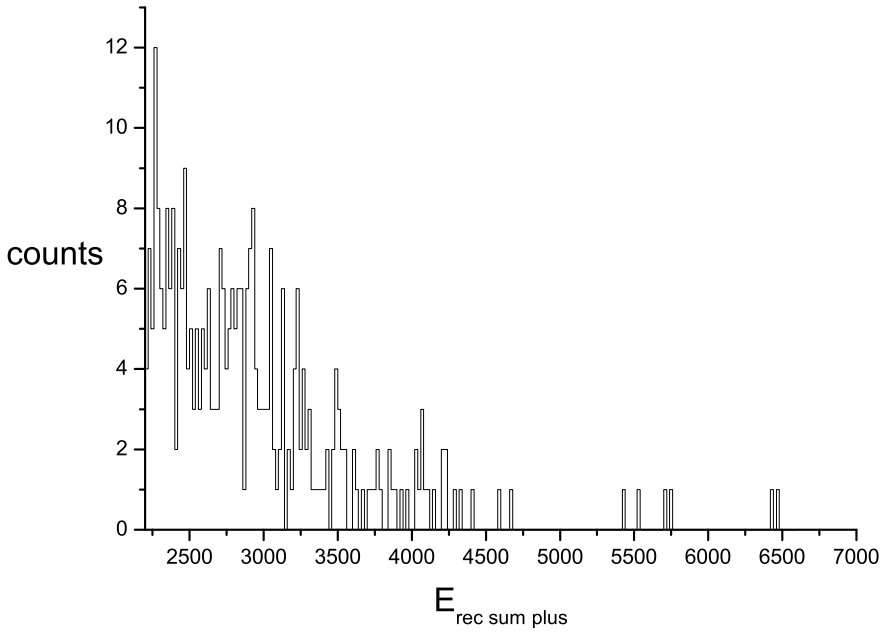

Figure **7.5**: Events which passed through the fission gate. The lower limit of the fission gates was set to channel 2200 while no higher limit was set.

^{255}Db fission events is impossible. Thus it is possible that the fission events are from ^{251}Lr. This would require an α decay before the fission event. Possible recoil-α-fission and recoil-escape α-fission chains were also checked event-by-event for these two types of events. Such decay chains were not found in either case.

7.3.2 Recoil-α correlations

The α-decay branch of the ^{255}Db isotope was unknown. The estimates presented in the Section 7.2 were based on systematic studies by F. Heßberger [Heß01]. The α-decay energy range seen in figure 7.7 shows no clear α-decay peak above 9000 keV.

The α-decay peaks from transfer reaction products are clearly visible in figure 7.7a, especially ^{211}Po and ^{211}At which correspond to 2p and 1p1n transfer reactions. In figure 7.7b the α spectrum from the production runs is presented. In the lower spectra the peaks from transfer products are small except for two strong peaks from ^{211}Po and ^{211}At. These isotopes are the main transfer products which scatter to the focal plane during the production runs when RITU was tuned for ^{255}Db. In addition, a lot of ^{211}Po and ^{211}At was implanted into the PIPS detector during the calibration runs with transfer products. Despite the contaminants from transfer products the energy

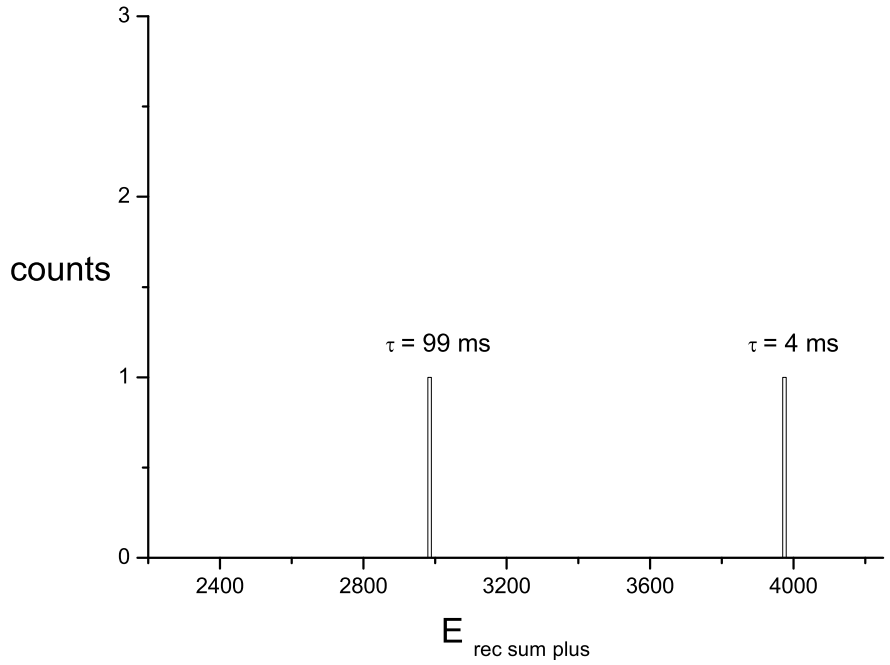

Figure **7.6**: Correlated recoil-fission spectrum within one second time window. The lower limit for the fission gate was set to channel 2200.

region where possible ^{255}Db α decays are expected is very clean. In figure 7.7a the transfer products with decay energies above 9000 keV are very scarce thus this energy region should contain very few contaminants. In figure 7.7b the high energy part above 9000 keV does not show any clear α decay peaks, but rather a steady background from scattered beam. The possible α-decay peaks are lost in the background.

The correlation analysis was done in order to pinpoint the ^{255}Db α-decay peak. The α-decays were correlated with a recoil event within one second time and within a 0.85 mm position window. The correlated α spectrum can be seen in the figure 7.8. The spectrum shows some correlated events from the decay of ^{214m}Fr. The energy window used to find the ^{255}Db alpha decay was set to 8500-10500 keV covering all the possible ^{255}Db α-candidate energies in case the estimated α-decay energy was not accurate. In figure 7.8 all the events are labelled with lifetimes.

The only candidate, which satisfies the expected energy and lifetime requirements of a ^{255}Db α decay, is the event at E_α=9564 keV and with a lifetime of τ=56 ms. This event is labelled in figure 7.8. This recoil-α correlation is significant since as mentioned previously this energy region was free from contaminants. Any isotopes which have similar decay energies and could have been produced in a transfer reaction have half-

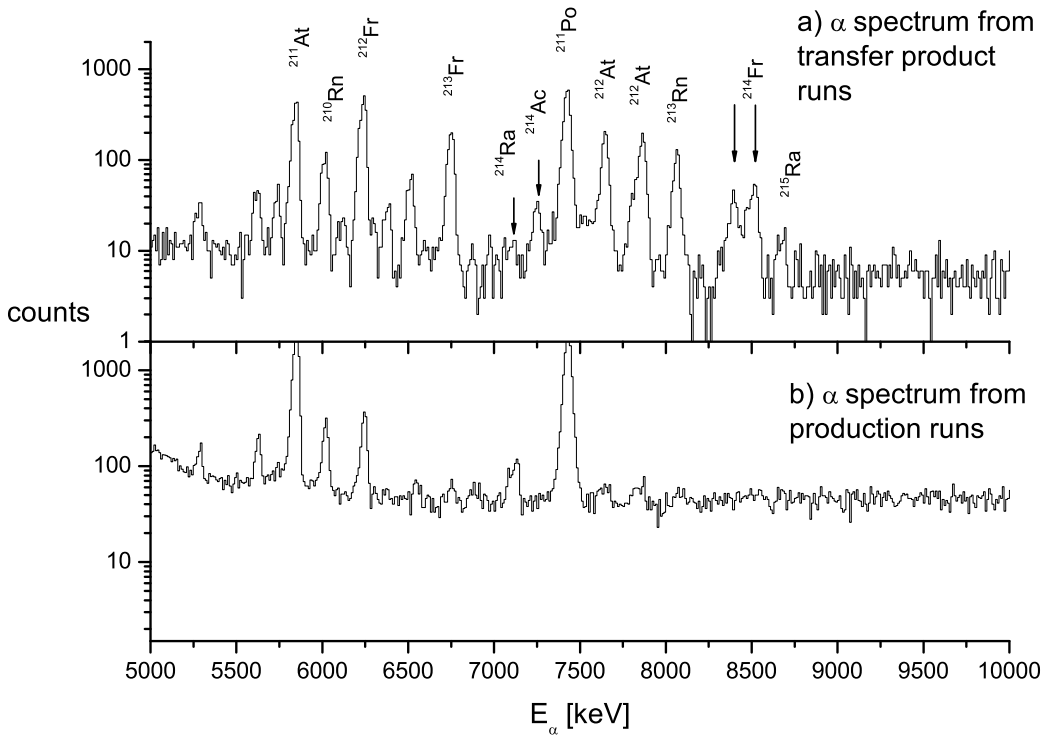

Figure **7.7**: Two different MWPC vetoed α spectra. Figure a) represents the α-decay spectrum obtained when RITU was tuned for transfer products and figure b) represents the α-decay spectrum obtained when RITU was tuned for ^{255}Db. RITU was tuned to collect transfer products twice, in the middle and at the end of the experiment.

lives of the order of 1 ms and below. Unfortunately, this event does not correlate further with a full-energy daughter α decay thus making the identification of the event uncertain. The possible recoil-α-α-α chain with a known ^{247}Md α decay as a grand-daughter would give undisputed evidence for a detection of an ^{255}Db α decay.

There is a possibility that the daughter of the ^{255}Db α decay has escaped the detector and the observed event would be followed by an escape α particles. Another possibility is that the ^{255}Db α decay is followed by a fission of ^{251}Lr.

Recoil-α-^{251}Lr fission correlation

The daughter nucleus of ^{255}Db is ^{251}Lr and the decay properties of ^{251}Lr were unknown prior to this experiment. Generally, nuclei in this region have significant spontaneous fission branches and thus it is possible that ^{251}Lr decays via fission. Since there was

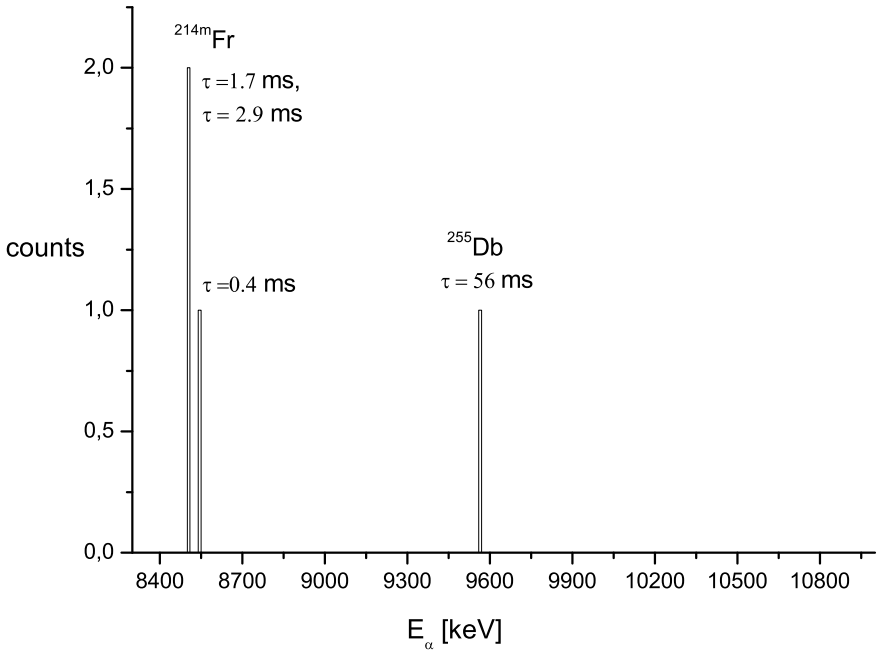

Figure **7.8**: Correlated α spectrum within 1 s search time and with an energy window of 8500-10500 keV. The lifetime of each event is indicated. The event labelled as ^{255}Db was the only one which correlated with a fission event.

only one recoil-α chain to be checked, a search for the possible recoil-α-fission and recoil-α-escape α chains were performed event-by-event. The events following the correlated α decay within a five second time window and in the same pixel were printed out. The 9564 keV α decay was followed by a fission event candidate which satisfied all the requirements set for a fission event in the Section 7.3.1. The energy of the event in the arbitrary units used for the low amplification side was 3334. Determined from the top and bottom signals of a PIPS strip, this energy satisfies the requirements set for a fission event in the section 7.2.2. The lifetime of the fission event was within acceptable limits since the predicted half-life for ^{251}Lr was 80 ms while the experimental half-life for this event was 27 ms. Some of the transfer-α decay events were checked in a similar manner including the isomeric α decays of ^{214m}Fr. The behaviour observed following the 9564 keV α decay was unique and it was not found anywhere else. Another possibility is that the produced decay chain is a real chain but it does not originate from ^{255}Db. For example, a transfer reaction can produce uranium or protactium isotopes with similar decay energies. The products produced in transfer reactions do not have known spontaneous fission branches. In addition, the half-lives of the isotopes produced in transfer reactions are of the order of 1 ms or faster which are too fast compared to the measured lifetime of 56 ms. Thus the chain was labelled as recoil-α-fission chain belonging to ^{255}Db.

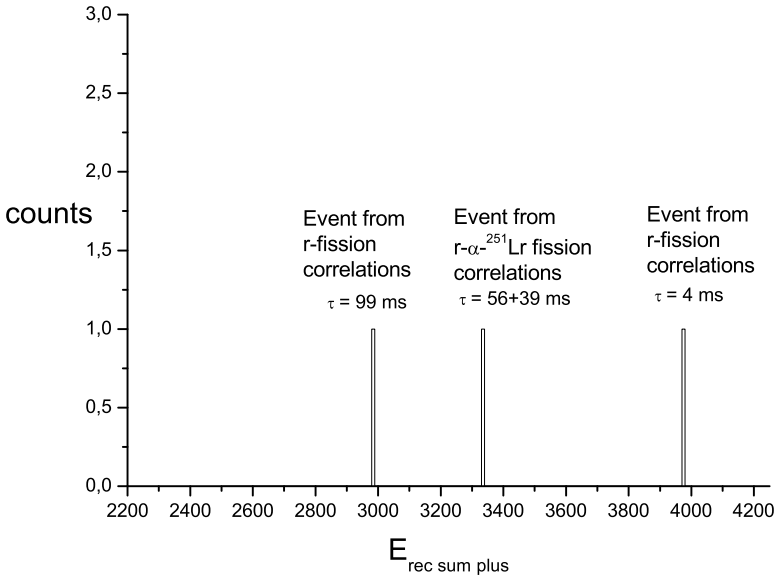

Figure **7.9**: All the correlated fission events observed in the experiment. Individual events labelled according to their origin.

A case of special interest is if the super-heavy element experiments are done with actinide targets. Transfer products from these targets have spontaneous fission branches which could be mixed with fission events of interest. The current experiment was performed with a stable target where transfer products do not have spontaneous fission branches and thus the only possible source for fission events is fusion products.

7.4 The error analysis

In low cross section studies, accidental correlations can play a significant role. Since the detector system measures the effect of radiation on matter, not the decay directly, the origin of the radiation cannot be stated. Random fluctuations of the background radiation can produce events or correlation chains which look like real events. In high cross section studies where the statistics of the decay peaks are much higher than the background the number of random correlations compared to the number of real events is practically non-existent. In low cross section studies usually only few events are collected and the number of random correlations can become comparable to the number of real events. Thus in low cross section studies before an event or decay chain can be stated as a real chain the probability of accidental chain or event has to be much lower than the number of observed chains or events.

By using equation 3.5 the expected number of accidental recoil-fission correlations can be determined. The error probability for the calculated number of accidental correlations can be determined with equation 3.6. The values needed for the equations are given in table 7.2. The energy range for fission events was from 2200 to 4500.

Table **7.2**: The details needed to estimate the probability of accidental recoil-fission correlation.

Number of fission candidates	324
Number of recoil candidates	79500
Measurement time	391000 s
Search time	1 s
Effective pixel number	300
Number of accidental recoil-fission correlations (N_{acc}^{r-f})	0.22
Error probability ($P_{err}(N_{obs}=2)$)	2.8 %

The expected number of accidental recoil-fission correlations is 0.22 and the number of observed correlations is 2. The number of expected accidental correlations is clearly lower than the number of observed events. The error probability, or the probability for observing two accidental recoil-fission chains, is 2.8 %.

Similarly the expected number of accidental recoil-α-fission correlations can be calculated. The necessary parameters and values are given in table 7.3. The energy range for fission events was from 2200 to 4500 and the energy range for an α event was 9000-10 000 keV.

Table **7.3**: The details needed to estimate the probability of accidental recoil-α-fission correlations.

Number of recoil candidates	79500
Number of fission candidates	324
Number of α-decay candidates	1646
Measurement time	391000 s
Search time for α-decay events	1 s
Search time for fission events	5 s
Effective pixel number	300
Number of accidental recoil-α-fission correlations ($N_{acc}^{r-\alpha-f}$)	1.5×10^{-5}
Error probability ($P_{err}(N_{obs}=1)$)	1.5×10^{-3} %

According to the error analysis the probability that the recoil-α-fission chain observed is produced by random fluctuation of the background is very small. The number of expected accidental correlation chains is several orders of magnitude smaller than the number of observed decay chains. In light of this study, it can be stated that all of the observed decay chains are statistically meaningful.

7.5 Discussion

A total of three events of ^{255}Db isotopes were detected. The total production cross section was estimated to be as low as 40 pb. Most likely this does not represent the maximum production cross section for this reaction since no excitation function was available. The bombardment energy was based on HIVAP calculations [Heß01]. In addition, this cross section is fairly tentative since the fission detection efficiency could not be determined. Nevertheless the cross section was much lower than anticipated, roughly by an order of magnitude.

Taking into account escaped α particles, a 50 % α branch can be deduced. This value was used in the hindrance factor calculations. The fission detection efficiency could not be determined and it is likely some fission events were lost due to the triggering of the second gas counter. Thus the real branching ratio cannot be determined accurately but rather a statement can be made that ^{255}Db has an α-decay branch of approximately 50 % with a decay energy and half-life as given in table 7.4. A confidence interval of 68 % was used in the error limits of the decay half-life.

Table **7.4**: Summary of the experimental results. For ^{255}Db two fission events and one α decay event were seen. The error bars refer to 68% confidence levels.

Nucleus	$T_{1/2}$ [ms]	Cross section [pb]	α decay energy [keV]
^{255}Db	37^{+51}_{-14}	40	9564(27)
^{251}Lr	27^{+118}_{-13}		(fission)

Table 7.5 shows a comparison of calculated hindrance factors between the closest known isotope ^{257}Db and the isotone ^{253}Lr. The reduced widths shown the table were calculated with the Rasmussen method using the known half-lives and branching ratios. The even-even isotopes around ^{255}Db tend to decay via fission, the closest even-even isotopes which have an α decay branch are ^{254}No and ^{260}Sg (Z=106). They were chosen to be the reference decays in this region in the chart of nuclei. The average nucleus is needed to calculate hindrance factors with the Rasmussen method. Since both of them are quite far away from ^{255}Db both of them were used as references. Table 7.5 shows a variety of nuclei around ^{255}Db and their calculated hindrance factors and reduced widths. In table 7.5 the hindrance factor comparison to ^{254}No is labelled with No and comparison to ^{260}Sg is labelled with Sg. The experimental half-lives and branching ratios needed for the hindrance and reduced width calculations for ^{253}Lr and ^{257}Db were adopted from Ref. [Heß01]. Similar values for ^{261}Db were adopted from Ref. [Ghi71], ^{261}Bh from Ref. [Mün89] and ^{255}Lr from Ref. [Esk71]. If more than one α-decay energy had been identified, the transitions were labelled as e1 and e2 as decays to the first or second excited state in the daughter nucleus, respectively.

The hindrance factor and reduced width study presented in table 7.5 indicates that

Table **7.5**: Comparison of hindrance factors of an alpha decay from ground state to an excited stated in daughter nucleus. The α decay reduced widths δ^2 and hindrance factors were calculated according to Ref. [Ras59]. In the case of ^{255}Db α branch of 50 % was used.

Nucleus	HF (No)	HF (Sg)	δ^2 [keV]
^{261}Bh	8.6	14	5
^{263}Db	0.8	1.3	48
^{261}Db	3.0	4.9	13
^{257e2}Db	4.0	6.5	10
^{257e1}Db	11	17	4
^{257}Db	20	32	2
^{255}Db	3.2	5.2	12
^{259}Lr	1.1	1.8	35
^{257e2}Lr	5.6	9.2	7
^{257e1}Lr	19	32	20
^{255e2}Lr	4.7	7.6	8
^{255e1}Lr	2.1	3.5	18
^{253e1}Lr	2.3	3.8	17
^{253}Lr	3.0	4.9	13

the favoured decay seen in ^{255}Db agrees quite well with the systematics in this region. There is a correlation between the reduced width and the hindrance factor of the observed ^{255}Db α decay and those of the known α decays from a ground state to the excited state in the daughter nucleus. Based on this the decay of ^{255}Db is a similar process as the favoured decays in ^{261}Bh, ^{257}Db and in ^{253}Lr. In an odd system it is common that the α decay from ground state decays to an excited state in the daughter nucleus. Thus, indicating that the ^{255}Db α decay is a favoured decay.

The spins and parities of dubnium, lawrencium and mendelevium isotopes are shown in table 7.6. Unfortunately there are no predictions available for the ground state and excited states spins and parities for ^{251}Lr. The recent in-beam studies on ^{251}Md [The04], ^{255}Lr [Gre05] support Ćwiok et als. predictions for ground state spins and parities in these nuclei.

The predicted ground state, first excited and the second excited state spins and parities for the ^{259}Db, ^{257}Db and ^{255}Db isotopes are $9/2^+$, $7/2^-$ and $5/2^-$ [Ćwi94]. The ground state and excited states spins and parities of ^{251}Lr were not available. An assumption was made, based on the systematics of the lowest levels in the dubnium, lawrencium and mendelevium isotopes, that there is no major structural change between the isotopes ^{251}Lr and ^{253}Lr. Therefore, the spins and parities of ground state, first and second excited states in ^{251}Lr and ^{253}Lr was assummed to be similar. The ground-state spins and parities of the dubnium isotopes can be found as a first or a second excited

Table **7.6**: Predicted ground state, 1^{st} excited state and 2^{nd} excited state spins and parities of dubnium, lawrencium and mendelevium isotopes according to Ref. [Ćwi94].

Nucleus	ground state	1^{st} excited state	2^{nd} excited state
^{261}Db	$9/2^+$	$5/2^-$	$1/2^-$
^{259}Db	$9/2^+$	$7/2^-$	$5/2-$
^{257}Db	$9/2^+$	$7/2^-$	$5/2-$
^{255}Db	$9/2^+$	$7/2^-$	$5/2-$
^{257}Lr	$7/2^-$	$9/2^+$	$1/2^-$
^{255}Lr	$7/2^-$	$9/2^+$	$1/2^-$
^{253}Lr	$7/2^-$	$1/2^-$	$9/2^+$
^{251}Lr	-	-	-
^{251}Md	$1/2^-$	$7/2^-$	$7/2^+$
^{249}Md	$1/2^-$	$7/2^-$	$7/2^+$
^{247}Md	$1/2^-$	$7/2^-$	$7/2^+$

state in the lawrencium isotopes. Thus, the possible unhindered α decay would decay from ground state of the mother nucleus to an excited state in daughter nucleus.

In fusion-evaporation reactions the high-spin yrast states are more likely to be populated than the low-spin non-yrast states. According to this the $9/2^+$ ground state in ^{255}Db is more likely to be populated than the $7/2^-$ and $5/2^-$ excited states. Thus based on the proposed level scheme by Ćwiok et al. the observed unhindered α decay in ^{255}Db is possibly a decay from the ground state to an excited state of ^{251}Lr with identical spin and parity of $9/2^+$.

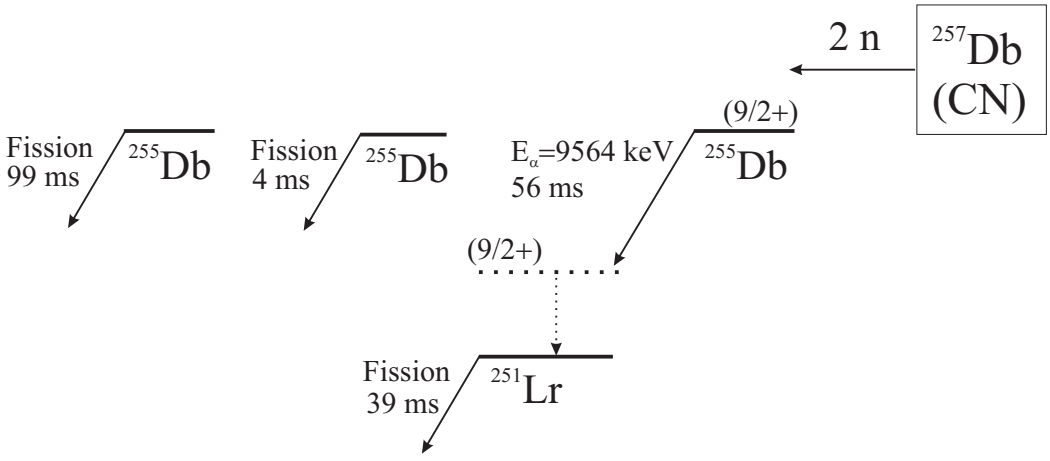

Figure **7.10**: All three events presented as a block diagram.

In figure 7.10 the observed decay chains are presented as a block diagram. The search time for recoils was one second. All of the events were checked for escape α particles.

Each event is labelled by its decay properties.

7.6 Future prospects

A rerun of the ^{255}Db experiment would be instructive since more statistics are necessary to confirm the results presented in this work. In order to acquire more statistics a 14 day experiment is needed. During the last run one of the "bottle necks" was the gas window before the target which has now been replaced by a differential pumping system, thus allowing more intense beams to be impinged on the targets. Unfortunately, the ^{48}Ti beam intensity has not improved significantly over the years. A new oven system for ECR ion source may improve the beam intensity to some extent. The main problem with the oven is that at the moment it is expensive due to the exotic materials which are required to withstand temperatures above the titanium melting of 1660 °C. Based on the experience gained in the present experiment the rotating target system can withstand beam intensities of at least 100-120 pnA for long periods of time.

The upgrades (see Section 3.3) of RITU since the ^{255}Db experiment have lowered the background from scattered beam considerably. The GREAT spectrometer at the RITU focal plane provides a higher selectivity of fusion recoils making the number of accidental correlations even less. The GREAT spectrometer only has sufficient readout channels for one amplification to be used for a single DSSD strip; hence the simultaneous collection of α-decay and fission fragment is not straightforward. It is possible to use two different gain ranges on the front and the back faces of the detector allowing both the fission fragment and α-particle to be identified in a single pixel.

This method has been successfully used to detect α-particles, electrons and internal conversion electrons but has never been used to detect α-particles and fission events. The method is feasible and referring these experiments would provide a good proof of principle.

8 Summary

It has been shown in this work that the RITU separator combined with a sensitive focal plane detector setup is a powerful tool for studying heavy exotic nuclei. The experiments were carried out in a four year time period when RITU and the detector systems went through a series of upgrades. These upgrades improved the background suppression and detection efficiency significantly. The nuclei of interest were produced in fusion evaporation reactions with very low cross sections. Each of the studied cases presented different challenges. The experimental methods used were α-decay spectroscopy, recoil-decay tagging (RDT) and fission-decay tagging.

The experimental results obtained from these three experiments gave new insight and information on nuclear structure in these exotic nuclei. In the ^{218}U experiment a new α-decaying isomeric state was found to decay to the ground state of ^{214}Th. The existence of this state does not support theoretical predictions of a sub-shell closure at Z=92. In addition the ground state properties of ^{218}U and ^{219}U were measured with improved statistics.

In the ^{252}No study, a new method of recoil-fission tagging was employed to obtain more tagged γ-decay data. This work marks the first time this technique has been used. The method used in the ^{252}No case increased the statistics by approximately 50 %, enabling new weak peaks to be discerned from the background. These peaks lie higher in energy than the peaks belonging to the ground state band. Possibly two separate non-yrast or quasiparticle bands were seen.

The ^{255}Db experiment was the first low cross section experiment performed with RITU. The experiment required high beam intensity and a rotating target. The measured cross section in the experiment was as low as 40 picobarns. The ^{255}Db isotope was a previously unknown isotope of dubnium, in addition the daughter nucleus ^{251}Lr was also an unknown isotope of lawrencium. A total of three decay chains were observed; two of the chains decayed via fission and one chain via α-delayed fission. Little information on the nuclear structure of ^{255}Db could be extracted, but information on the decay properties of ^{255}Db was obtained. The observed α decay of ^{255}Db is an unhindered transition. In an odd-A system the ground state quite often decays to an excited state in the daughter nucleus. An unhindered decay refers to a decay to an excited state in ^{251}Lr with a similar structure. The calculations by Ćwiok et al. support this picture.

The experiments carried out at the JYFL cyclotron laboratory and each experiment was a pioneering one. In each experiment new information on each of the nuclei was obtained. Many of the results obtained raised new questions and interest in these nuclei. In all of the cases new experiments and further study of the nuclei is needed to fully understand the structure of these nuclei. The study of these nuclei will help us to better understand the behaviour of the atomic nucleus under extreme conditions. The results obtained will contribute to untangling the mysteries of the atomic nucleus. Many of the fundamental questions about the atomic nucleus presented almost 100 years ago still remain unanswered. The studies in this thesis contribute a tiny portion to the sea of knowledge bringing the answers a little bit closer.

Bibliography

[Alp69] M. Alpsten and G. Astner, Nucl. Phys. A **134**, (1969) 407.

[And92] A.N. Andreyev, D.D. Bogdanov, V.I. Chepigin, A.P. Kabachenko, O.N. Malyshev, R.N. Sagaidak, G.M. Ter-Akopian, and A.V. Yeremin, Z.Phys. A **342**, (1992) 123.

[And93a] A.N. Andreyev, D.D. Bogdanov, V.I. Chepigin, A.P. Kabachenko, O.N. Malyshev, R.N. Sagaidak, G.M. Ter-Akopian, M. Veselsky, and A.V. Yeremin, Z. Phys. A **345**, (1993) 247.

[And93b] A.N. Andreyev, D.D. Bogdanov, V.I. Chepigin, A.P. Kabachenko, O.N. Malyshev, R.N. Sagaidak, L.I. Salamatin, G.M. Ter-Akopian, and A.V. Yeremin, Z. Phys. A **345**, (1993) 389.

[Bas74] R. Bass, Nuclear Physics A **231**, (1974) 45.

[Bea92] C.W. Beausang, S.A. Forbes, P. Fallon, P.J. Nolan, P.J. Twin, J.N. Mo, J.C. Lisle, M.A. Bentley, J. Simpson, F.A. Beck, D. Curien, G. de France, G. Duchône, and D. Popescu, Nucl. Instrum. Methd. Phys. Res. **A313**, (1992) 37.

[Bem77] C.E. Bemis Jr., R.L. Ferguson, F. Plasil, R.J. Silva, F. Pleasonton, and R.L. Hahn, Phys. Rev. C **15**, (1977) 705.

[Bel03] A.V. Belozerov, M.I. Chelnokov, V.I. Chepigin, T.P. Dropina, V.A. Gorshkov, A.P. Kabachenko, O.N. Malyshev, I.M. Merkin, Yu.Ts. Oganessian, A.G. Popeko, R.N. Sagaidak, A.I. Svirikhin, A.V. Yeremin, G. Berek, I. Brida, and Š. Šáro, Eur. Phys. J. **16**, (2003) 447.

[Bet72] H.D. Betz, Rev. Mod. Phys. **44**, (1972) 465.

[Bra82] W. Brandt and M. Kitagawa, Phys. Rev. B **25**, (1982) 5631.

[Cas00] Richard F. Casten, *Nuclear structure from a simple perspective*, 2. ed., Oxford University Press, New York 2000

[Cau03] E. Caurier, M. Rejmund and H. Grawe, Phys. Rev. C **67**, 054310 (2003).

[Cau05] E. Caurier, IReS, Strasbourg, private communication (2005).

[Coh58] B.L. Cohen and C.B. Fulmer, Nucl. Phys. **6**, (1958) 547.

[Ćwi94] S. Ćwiok, S. Hofmann, and W. Nazarewicz, Nucl. Phys. A **573**, (1994) 356.

[Dud02] J. Dudek, A. Gozdz, N. Schunck, and M. Miskiewicz, Phys.Rev.Lett. **88** (2002) 252502.

[Ebe97] J. Eberth, H.G. Thomas, D. Weisshaar, F. Becker, B. Fiedler, S. Skoda, P. v. Brentano, C. Gund, L. Palafox, P. Reiter, D. Schwalm, D. Habs, R. Servene, R. Schwengner, H. Schnare, W. Schulze, H. Prade, G. Winter, A. Jungclaus, C. Lingk, C. Teich, K.P. Lieb, and the Euroball Collaboration, Prog. Part. Nucl. Phys **38**, (1997) 29.

[Eec05] S. Eeckhaudt, P.T. Greenlees, N. Amzal, J.E. Bastin, E. Bouchez, P.A. Butler, A. Chatillon, K. Eskola, J. Gerl, T. Grahn, A. Görgen, R.-D. Herzberg, F.P. Heßberger, A. Hürstel, P.J.C. Ikin, G.D. Jones, P. Jones, R. Julin, S. Juutinen, H. Kettunen, T.L. Khoo, W. Korten, P. Kuusiniemi, Y. Le Coz, M. Leino, A.-P. Leppänen, P. Nieminen, J. Pakarinen, J. Perkowski, A. Pritchard, P. Reiter, P. Rahkila, C. Scholey, Ch. Theisen, J. Uusitalo, K. Van de Vel, and J. Wilson, ENAM '04 conference proceedings, Eur. Phys. J. A direct (2005).

[Esk71] K. Eskola, P. Eskola, M. Nurmia and A. Ghiorso, Phys. Rev. C **4**, (1971) 632.

[Fir96] R.B. Firestone and V.S. Shirley, *Table of isotopes*, 8th edition, John Wiley & Sons, Inc., New York, 1996 .

[Fle76] G.N. Flerov, JINR-E7-10128, (1976).

[Gam28] G. Gamow, Z. Phys. **51** (1928) 204.

[Ghi71] A. Ghiorso, M. Nurmia, K. Eskola and P. Eskola, Phys. Rev. C **4**, (1971) 1850.

[Ghi88] A. Ghiorso, S. Yashita, M. Leino, L. Frank, J. Kalnins, P. Armbruster, J.-P. Dufour, and P.K. Lemmertz, Nucl. Inst. Meth. in Phys. Res. A **269**, (1988) 192.

[Gre05] P.T. Greelees et al., University of Jyväskylä, to be published.

[Gur29] R.W. Gurney and E. U. Condon, Phys. Rev. **33**, (1929) 127.

[Hau01] K. Hauschild, M. Rejmund, H. Grawe, E. Caurier, F. Nowacki, F. Becker, Y. Le Coz, W. Korten, J. Döring, M. Górska, K. Schmidt, O. Dorvaux, K. Helariutta, P. Jones, R. Julin, S. Juutinen, H. Kettunen, M. Leino, M. Muikku, P. Nieminen, P. Rahkila, J. Uusitalo, F. Azaiez, and M. Belleguic, Phys. Rev. Lett **87**, (2001) 072501-1.

[Hei95] P. Heikkinen and E. Liukkonen, 14$^{\text{th}}$ International Conference on Cyclotrons and their Applications, Cape Town, October 8-13 (1995).

[Her85] B. Herskind, Nucl. Phys. **A447**, (1985) 395.

[Her01] R.-D. Herzberg, N. Amzal, F. Becker, P.A. Butler, A.J.C. Chewter, J.F.C. Cocks, O. Dorvaux, K. Eskola, J. Gerl, P.T. Greenlees, N.J. Hammond, K. Hauschild, K. Helariutta, F.P. Heßberger, M. Houry, G.D. Jones, P.M. Jones, R. Julin, S. Juutinen, H. Kankaanpää, H. Kettunen, T.L. Khoo, W. Korten, P. Kuusiniemi, Y. Le Coz, M. Leino, C.J. Lister, R. Lucas, M. Muikku, P. Nieminen, R.D. Page, P. Rahkila, P. Reiter, C. Schlegel, C. Scholey, O. Stezowski, C. Theisen, W.H. Trzaska, J. Uusitalo, and H.J. Wollersheim, Phys. Rev. C **65**, (2001) 014303.

[Heß97] F.P. Heßberger, S. Hofmann, V. Ninov, P. Armbuster, H. Folger, G. Münzenberg, H.J. Schött, A.G. Popeko, A.V. Yeremin, A.N. Andreyev, and S. Saro, Z. Phys. A **359**, (1997) 415.

[Heß01] F.P. Heßberger, S. Hofmann, D. Ackermann, V. Ninov, M. Leino, G. Münzenberg, S. Saro, A. Lavrentev, A.G. Popeko, A.V. Yeremin, and C. Stodel, Eur. Phys. J. A **12**, (2001) 57.

[Heß01] F.P. Heßberger, Gesellschaft für Schwerionenforschung, Darmstadt, Germany, private communication (2001).

[Heß02] F.P. Heßberger, S. Hofmann, I. Kojouharov, D. Ackermann, S. Antalic, P. Cagarda, B. Kindler, B. Lommel, R. Mann, A.G. Popeko, S. Saro, J. Uusitalo, and A.V. Yeremin, Eur. Phys. J. A **15**, (2002) 335.

[Hul94] E.K. Hulet, Sov. J. Nucl. Phys. **57**, (1994) 1165.

[Iku98] T. Ikuta, H. Ikezoe, S. Mitsuoka, I. Nishinaka, K. Tsukada, Y. Nagame, and J. Lu, Phys. Rev. C **57**, (1998) R2804.

[Ket01] H. Kettunen, P.T. Greenlees, K. Helariutta, P. Jones, R. Julin, S. Juutinen, P. Kuusiniemi, M. Leino, M. Muikku, P. Nieminen, and J. Uusitalo, Acta Phys. Pol. B **32** 3, (2001) 989.

[Ket02] H. Kettunen, JYFL, private communication, 2002.

[Koi94] H. Koivisto, J. Ärje and M. Nurmia, Metal Ion Beams from an ECR Ion Source Using Volatile Compounds, Nucl. Instr. and Meth. **B94** (1994) 291-296.

[Koi05] H. Koivisto, JYFL, private communication, 2005.

[Kos05] T.A. Kosonen, Master of Science thesis, JYFL, Jyväskylä, Finland 2005.

[Kra88] Kenneth S. Krane, *Introductory nuclear physics*, John Wiley & Sons, New York, 1988

[Kuu04] P. Kuusiniemi, F.P. Heßberger, D. Ackermann, S. Hofmann and I. Kojouharov, Eur. Phys. J. A **22**, (2004) 429.

[Laz01] I.H. Lazarus, D.E. Appelbe, P.A. Butler, P.J. Coleman-Smith, J.R. Cresswell, S.J. Freeman, R.-D. Herzberg, I. Hibbert, D.T. Joss, S.C. Letts, R.D. Page, V.F.E. Pucknell, P.H. Regan, J. Sampson, J. Simpson, J. Thornhill, and R. Wadsworth, IEEE Transactions on Nuclear Science **48**, NO. 3 June (2001) 567

[Lei81] M. Leino, S. Yashita and A. Ghiorso, Phys. Rev. C **24**, (1981) 2370.

[Lei95] M. Leino, J. Äystö, T. Enqvist, P. Heikkinen, A. Jokinen, M. Nurmia, A. Ostrowski, W.H. Trzaska, J. Uusitalo, K. Eskola, P. Armbruster, and V. Ninov, Nucl. Instr. and Meth. B **99**, (1995) 653.

[Lep05] A.-P. Leppänen, J. Uusitalo, M. Leino, S. Eeckhaudt, T. Enqvist, K. Eskola, T. Grahn, F.P. Heßberger, P.T. Greenlees, P. Jones, R. Julin, S. Juutinen, H. Kettunen, P. Kuusiniemi, P. Nieminen, J. Pakarinen, J. Perkowski, P. Rahkila, C. Scholey, and G. Sletten, to be published (2005).

[Lin63] J. Linhard, M. Scharff, and H.E. Schiøtt Mat. Fys. Medd. Dan. Vid. Selsk., **33**, no. 14 (1963).

[Mal00] O.N. Malyshev, A.V Belozerov, M.L. Chelnokov, V.I. Chepigin, V.A. Gorshkov, A.P. Kabachenko, A.G. Popeko, J. Rohach, R.N. Sagaidak, A.V. Yeremin, S.I. Mulgin, and S.V. Zhdanov, Eur. Phys. J. A **8**, (2000) 295.

[Mul76] L.G. Multhauf, K.G. Tirsell and R.A. Meyer, Phys. Rev. C **13**, (1976) 771.

[Mün89] G. Münzenberg, P. Armbruster, S. Hofmann, F.P. Heßberger, H. Folger, J. Keller, V. Ninov, K. Poppensieker, A.B. Quint, W. Reisdorf, K.-H. Schmidt, J.R.H. Schneider, H.J. Schött, K. Sümmerer, I. Zychor, M.E. Leino, D. Ackermann, U. Gollerthan, E. Hanelt, W. Morawek, D. Vermeulen, Y. Fujita, and T. Schwab, Z. Phys. A **333**, (1989) 163.

[Mye66] W.D. Myers and W.J. Swiatecki, Nucl. Phys. **81**, (1966) 1.

[Möl97] P. Möller, J.R. Nix and K.-L. Kratz, At. Data and Nucl. Data Tables **66**, (1997)

[Nik68] V.S. Nikolaev and I.S. Dmitriev, Phys. Lett. **28 A** 4, (1968) 278.

[Nol85] P.J. Nolan, D.W Gifford, and P.J. Twin, Nucl. Instrum. Methd. Phys. Res. **A236**, (1985) 95.

[Nor70] L.C. Northcliffe and R.F. Schilling, Nucl. Data Tabl. A **7**, (1970) 233.

[Nuc75] Nucl. Data Sheets. A **15**, No. 2, VI (1975).

[Oga91] Yu.Ts. Oganessian, Yu.V. Lobanov, A.G. Popeko, F.Sh. Abdullin, Yu.P. Kharitonov, A.A. Ledovskoy, and Yu.S. Tsyganov, Z. Phys. D **21**, (1991) 357.

[Oga01] Yu.Ts. Oganessian, V.K. Utyonkov, Yu.V. Lobanov, F.Sh. Abdullin, A.N. Polyakov, I.V. Shirokovsky, Yu.Ts. Tsyganov, A.N. Mezentsev, S. Iliev, V.G. Subbotin, A.M. Sukhov, G.V. Buklanov, K. Subotic, and Yu.A. Lazarev, Phys. Rev. C **64**, (2001) 064309.

[Oga02] Yu.Ts. Oganessian, V.K. Utyonkov, Yu.V. Lobanov, F.Sh. Abdullin, A.N. Polyakov, I.V. Shirokovsky, Yu.Ts. Tsyganov, A.N. Mezentsev, S. Iliev, V.G. Subbotin, A.M. Sukhov, O.V. Ivanov, A.A. Voinov, K. Subotic, V.I. Zagrebaev, M.G. Itkis, K.J. Moody, J.F. Wild, M.A. Stoyer, N.J. Stoyer, C.A. Laue, D.A. Shaughnessy, J.B. Patin, and R.W. Lougheed, "JINR Preprints and Communications", D-7-2002-287, (2002).

[Pag03] R.D. Page, Nucl. Inst. Meth. Phys. Res. **B204**, (2003) 634.

[Pau95] E.S. Paul, P.J. Woods, T. Davinson, R.D. Page, P.J. Sellin, C.W. Beausang, R.M. Clark, R.A. Cunningham, S.A. Forbes, D.B. Fossan, A. Gizon, J. Gizon, K. Hauschild, I.M. Hibbert, A.N. James, D.R. LaFosse, I. Lazarus, H. Schnare, J. Simpson, R. Wadsworth, and M.P. Waring, Phys. Rev. C **51**, (1995) 78.

[Pri05] A. Prichard, University of Liverpool, Ph.D. thesis in preparation.

[Rah05] P. Rahkila, University of Jyväskylä, to be published in Nucl. Instrum. Methods A (2005).

[Ras59] J.O. Rasmussen, Phys. Rev. **113**, (1959) 1593.

[Rut98] K. Rutz, M. Bender, P.-G. Reinhard, J.A. Maruhn and W. Greiner, Nucl. Phys. A **634**, (1998) 67.

[Sch01] G. Schiwietz and P.L. Grande, Nucl. Instr. and Meth. in Phys. Res. B **175-177**, (2001) 125-131.

[Sch84] K.-H. Schmidt, C.-C. Sahm, K. Pielenz, and H.-G. Clerc, Z. Phys. A **316**, (1984) 19.

[Seg65] E. Segré, *Nuclei and Particles, An Introduction to Nuclear and Sub-nuclear Physics*, W.A. Benjamin, Inc., New York (1965).

[Sim86] R.S. Simon, K.-H. Schmidt, F.P. Heßberger, S. Hlavac, M. Honusek, G. Münzenberg, H.-G. Clerc, U. Gollerthan, and W. Schwab, Z. Phys. A **325**, (1986) 197.

[SRI03] J.F. Ziegler, SRIM website http://www.srim.org/SRIM/SRIM2003.htm

[The04] Ch. Theisen et al., EXON 2004 Conference, 5.-12.7.2004, Peterhof, Russia. Conference Proceedings, to be published.

[Trz90] W.H. Trzaska, Nucl. Instrum. Meth. Phys. Res. **A297**, (1990) 223.

[Uus05] J. Uusitalo, University of Jyväskylä, private communication, 2005.

[Vio85] V.E. Viola, K. Kwiatkowski, and M. Walker, Phys. Rev. C **31**, (1985) 1550.

[Yat75] S.W. Yates, R.R. Chasman, A.M. Friedman, I. Ahmad, and K. Katori, Phys. Rev. C **12**, (1975) 442.

[Yer04] A. Yeremin, Decay spectroscopy at VASSILISSA, talk at Midwinter workshop on Tagging Methods and Experiments, Jyväskylä, Finland 2004.

[Zie05] J.F. Ziegler, Yale University, developer of SRIM code, private communication, 2005.